AD-A083 127 TEXAS UNIV AT AUSTIN APPLIED RESEARCH LABS F/G 17/1
SUMMARY OF RECENT RESULTS IN ACOUSTIC BOTTOM INTERACTION.(U)
FEB 80 P J VIDMAR, S R RUTHERFORD, K E HAWKER N00014-78-C-0113
UNCLASSIFIED ARL-TR-80-6 NL

1 OF 2
AD
A083127

UNCLASSIFIED

(9) Annual rept. 1 Jan-31 Dec 79

SECURITY CLASSIFICATION OF THIS PAGE *(When Data Entered)*

REPORT DOCUMENTATION PAGE

READ INSTRUCTIONS BEFORE COMPLETING FORM

1. REPORT NUMBER

2. GOVT ACCESSION NO.

3. RECIPIENT'S CATALOG NUMBER

(6) 4. TITLE *(and Subtitle)*
A SUMMARY OF SOME RECENT RESULTS IN ACOUSTIC BOTTOM INTERACTION

5. TYPE OF REPORT & PERIOD COVERED
annual report
1 Jan - 31 Dec 79

6. PERFORMING ORG. REPORT NUMBER
19 February 1980

(10) 7. AUTHOR(s)
Paul J. Vidmar, Steven R. Rutherford, Kenneth E. Hawker

(15) 8. CONTRACT OR GRANT NUMBER(s)
N00014-78-C-0113

9. PERFORMING ORGANIZATION NAME AND ADDRESS
Applied Research Laboratories
The University of Texas at Austin
Austin, Texas 78712

(12) 10. PROGRAM ELEMENT, PROJECT, TASK AREA & WORK UNIT NUMBERS
(11) 1 3 4

11. CONTROLLING OFFICE NAME AND ADDRESS
Naval Ocean Research an Development Activity
NSTL Station, Mississip, i 39529

12. REPORT DATE
19 Febr[illegible]980

13. NUMBER OF PAGES
152

14. MONITORING AGENCY NAME & ADDRESS *(if different from Controlling Office)*
(14) ARL-TR-79-6

15. SECURITY CLASS. *(of this report)*
UNCLASSIFIED

15a. DECLASSIFICATION/DOWNGRADING SCHEDULE

16. DISTRIBUTION STATEMENT *(of this Report)*

Approved for public release; distribution unlimited.

17. DISTRIBUTION STATEMENT *(of the abstract entered in Block 20, if different from Report)*

18. SUPPLEMENTARY NOTES

19. KEY WORDS *(Continue on reverse side if necessary and identify by block number)*
bottom interaction
geoacoustics
mode-mode coupling
shear waves

20. ABSTRACT *(Continue on reverse side if necessary and identify by block number)*

This report summarizes research carried out during 1979 at Applied Research Laboratories, The University of Texas at Austin (ARL:UT), on acoustic interaction with the sea floor. Major topics considered are propagation in a range variable environment using mode-mode coupling methods and the effect of sediment rigidity on bottom reflection loss. Additional topics are the coherence of bottom interacting energy and the effects of bottom roughness (scattering).

DD FORM 1 JAN 73 1473 EDITION OF 1 NOV 65 IS OBSOLETE

1/(4/34

UNCLASSIFIED

SECURITY CLASSIFICATION OF THIS PAGE *(When Data Entered)*

JCE

TABLE OF CONTENTS

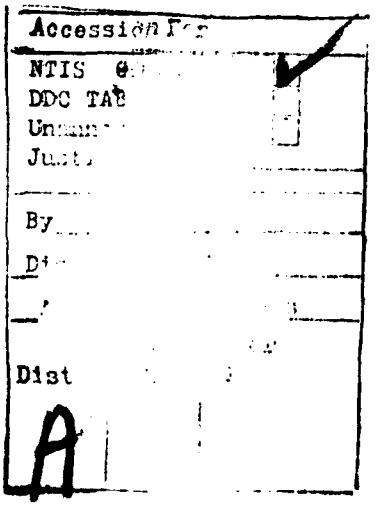

I. INTRODUCTION

For the past several years exploratory development bottom interaction studies at ARL:UT have concentrated on the acoustic mechanisms of bottom interaction. Substantial effort has been directed toward the study of reflection, refraction, and absorption within realistic models of marine sediments. These studies have had as their principal technical goals the identification of all processes important to low frequency acoustic propagation, and the quantification of the relative importance of these processes. These studies included theoretical investigations complemented by close interaction with data analyses carried out in concurrent advanced development programs at ARL:UT.

During the past contract year (FY79) there have been four lines of investigation: (1) lateral subbottom variations, (2) sloping bottom effects, (3) subbottom roughness scattering loss, and (4) bottom interaction sensitivity. The first two topics have been grouped together for reporting purposes under the heading of range variable environment studies. Of these four study areas, the first two are expected to continue into the next year, whereas the second two are terminated with the work reported here.

This year's research has resulted in extensive documentation, primarily in the form of journal articles, some of which have only recently been submitted for publication. Because of this extensive reporting the present report contains only a summary of the principal results together with references to the papers and reports where complete documentation is to be found. Three of the most recent papers are included as appendices to this report since their appearance in the literature will occur long after this contract year is terminated. In

addition to summarizing the work carried out during the past year, this report also contains bibliographies of the complete documentation for the contract year as well as complete project documentation to date.

II. PROPAGATION IN A RANGE VARIABLE ENVIRONMENT

The work concerning propagation in a range dependent environment is summarized in this section. This work is subdivided into sloping bottom and subbottom lateral variability problem areas.

The primary goal of the work on lateral variability has been to determine whether lateral subbottom variability that might reasonably be expected to occur in marine sediments is a significant factor influencing acoustic propagation. In long range acoustic propagation some degree of lateral subbottom variability is always present. The sources of this variability are differential sediment depositional processes and/or propagation over differing geophysical provinces. The prime focus of the the lateral variability work is to determine whether range variability of the bottom is likely to be significant, and if so, how best to include it in the description of acoustic propagation, possibly through average bottom loss or average geoacoustic model descriptions.

The main goal of the work on sloping bottoms is to determine how best to describe acoustic propagation in these areas and what level of detail is required to adequately characterize the acoustic propagation. Sloping bottom problems of particular interest concern propagation over continental slopes and seamounts. Another goal is to determine the role of the bottom properties of the slope. In other words, are the geometrical properties of the sloping bottom the driving mechanism influencing sound propagation, or do the geoacoustic properties of the bottom play an important role?

A. Review of Previous Work

1. Lateral Variability

At the beginning of this contract year the work on lateral subbottom variability had progressed to the point of being able to estimate the importance of mode-mode coupling effects as a function of subbottom sediment type and range-rate of change of sediment sound speed. The bulk of this work is summarized in Ref. 1. One outgrowth of this work was that the adiabatic approximation to coupled mode theory is probably sufficient to address propagation problems concerning realistic lateral subbottom variability. This clearly established the need for the capability to calculate propagation loss using the adiabatic approximation as a tool in investigating lateral variations.

2. Sloping Bottom

In the previous contract year investigations of the importance of mode-mode coupling effects and how they depend on bottom slope and sediment type were begun and essentially completed (see Ref. 1). The results of this work indicated that mode coupling effects are likely to manifest themselves for bottom slopes characteristic of typical continental rise and slope areas. This conclusion gave rise to an investigation, begun in FY78 and completed in FY79, concerning the presence or absence of multipath conversion effects in the adiabatic approximation when applied to problems with sloping boundaries. The intent of this investigation was to determine exactly what information was being eliminated by neglecting mode coupling effects in the adiabatic approximation. Since this work was completed in FY79 it is included in this report. To summarize, at the beginning of FY79 the sloping bottom work had reached a point where (1) it was determined that mode conversion effects are likely to be important for slopes of interest, and (2) more theoretical study of coupled mode theory[2,3] and its various approximations (adiabatic and boundary condition approximations) with respect to sloping bottom problems was called for.

B. Results of FY79 Research

1. Lateral Variability

In FY78, the need for the capability to compute propagation loss in the adiabatic approximation was established; the bulk of this year's work has been to build the numerical modeling tools necessary to attain this capability. A result of this work is a numerical modeling tool, ADIAB, which calculates transmission loss in the adiabatic approximation for a general waveguide having range variable bathymetry, sound speed, attenuation, etc. Another result has been the selection of useful power transport quantities for examining the effects of lateral subbottom variations. These quantities are the power transported via waterborne and bottom interacting modes of propagation, and their ratios. Additional software to be used in conjunction with ADIAB computes the power transport quantities as a function of range along with additional modeling components that permit estimates of the validity of the adiabatic approximation. The modeling capabilities developed in FY79 will be used extensively in the work on lateral variability and sloping bottoms to be carried out in FY80.

2. Sloping Bottom

The FY79 work on sloping bottom problems has focused on a theoretical examination of the mode coupling process as it occurs in acoustic propagation over a sloping bottom. The two issues that were examined are: (1) when one employs the adiabatic approximation in sloping bottom propagation problems, is multipath conversion present or has it been eliminated with the neglect of mode coupling? and (2) what are the implications of a boundary condition approximation inherent to coupled mode theory and can the induced errors be corrected for?

Concerning issue 1, it has been determined that the adiabatic approximation does indeed contain multipath conversion effects. This conclusion was reached through the use and extension of the work by Tindle and Guthrie[4] on the analogy between ray theory and mode theory. This

conclusion is significant in that the adiabatic approximation to coupled mode theory is substantially easier to implement than the full mode coupling formulation. It is clearly important therefore to understand the implications of the approximation so that it might be exploited whenever valid and appropriate. The work concerning issue 1 is summarized in Ref. 5.

Regarding issue 2, it was determined that the result of the boundary condition approximation inherent to coupled mode theory in sloping bottom applications is that the field given by conventional coupled mode theory[2,3] does not conserve energy. The boundary condition approximation in question involves the substitution of continuity of the z (depth) derivative of the acoustic field for the physically correct boundary condition of continuity of the normal derivative of the field at sloping interfaces. This boundary condition approximation was thought to be necessary to carry out the partial separation of depth and range variables employed in the mathematical formulation of the theory. A significant conclusion of the work reported here is that if one wishes to use coupled mode theory on sloping bottom problems, the adiabatic approximation is the only consistent form of the theory that can be used. The adiabatic approximation is consistent because the boundary condition approximation is of the same order as the adiabatic approximation, whereas the inclusion of mode coupling effects is not. Therefore, if one wishes to include mode coupling effects, the original formulation of coupled mode theory must be altered. The FY79 work on sloping bottoms concluded with the development of a corrected coupled mode theory which includes mode coupling effects consistent with the boundary conditions satisfied by the field. The FY79 work on issue 2 is summarized in Ref. 6 (see also Appendix A). Reference 7 contains a more detailed account of the work on the boundary condition approximation as well as more detailed versions of the work summarized in Refs. 1 and 5.

C. Future Directions

With regard to lateral subbottom variability, the procedure of range averaging geoacoustic parameters should be investigated. This investigation should explore the relation between a range averaged geoacoustic bottom model and range averaging the acoustic field. Another important problem concerns the relation between bottom loss obtained from multibounce measurements over a laterally variable ocean bottom and that obtained from a range averaged geoacoustic model.

A problem area involving sloping bottoms is the partitioning of energy for upslope and downslope propagation over continental slope type bathymetries. The change in the amount of bottom interacting and waterborne energy as a function of bottom slope, frequency, and bottom composition needs to be determined. In particular, one could investigate (1) whether acoustic energy traveling through the bottom and "popping out" on the slope is energetically feasible, and (2) the relative amounts of energy reaching an array position via water and bottom interacting paths as a function of the "geoacoustics" of the slope.

REFERENCES

CHAPTER II

1. S. R. Rutherford and K. E. Hawker, "An examination of the influence of the range dependence of the ocean bottom on the adiabatic approximation", J. Acoust. Soc. Am. 66, 1145-1151 (1979).

2. A. D. Pierce, "Extension of the method of normal modes to sound propagation in an almost-stratified medium", J. Acoust. Soc. Am. 37, 19-27 (1965).

3. D. M. Milder, "Ray and wave invariants for SOFAR channel propagation", J. Acoust. Soc. Am. 46, 1259-1263 (1969).

4. C. T. Tindle and K. M. Guthrie, "Rays as interfering modes in underwater acoustics", J. Sound Vib. 34, 291-295 (1974).

5. S. R. Rutherford, "An examination of multipath processes in a range dependent ocean environment within the context of adiabatic mode theory", J. Acoust. Soc. Am. 66, 1482-1486 (1979).

6. S. R. Rutherford and K. E. Hawker, "A consistent coupled mode theory of sound propagation of a class of nonseparable problems", submitted to The Journal of The Acoustical Society of America (see Appendix A).

7. S. R. Rutherford, "An Examination of Coupled Mode Theory as Applied to Underwater Sound Propagation", Applied Research Laboratories Technical Report No. 79-44 (ARL-TR-79-44), Applied Research Laboratories, The University of Texas at Austin, 26 July 1979.

III. BOTTOM ROUGHNESS STUDIES

The problem of accounting for the effects of bottom roughness on sound propagation is a very difficult one that has received the attention of many researchers over a period of years. Since the inception of the ARL:UT bottom interaction program a small continuous effort has been devoted to this specific problem. The goals of this work have been to assess the usefulness of existing methods for accounting for bottom roughness and then to carry out sensitivity studies using the most promising of these methods. The goals of the sensitivity studies are (1) to determine the required level of detail of description of subbottom roughness, and (2) to assess the impact of bottom roughness effects on propagation problems relating to surveillance.

A. Review of Previous Work

Initial efforts were directed toward understanding the effects of roughness at the water-sediment interface within the context of ARL:UT bottom loss and normal mode models, which treat the sediment as a fluid. The best available method for treating a randomly rough two-fluid interface was found to be a smoothed or averaged boundary condition approach.[1,3] This approach was implemented in FY77; sensitivity studies[3] suggested that the roughness of the water-sediment interface is not important at low frequencies for high porosity sediments (clays and silts) such as those found in deep ocean basins (abyssal plains).

In FY78 it was suggested that, for regions of thin sediment cover, such as the Northeast Pacific, the most important roughness effects might occur at the sediment-substrate interface. Application of the two-fluid theory was not attempted because it was recognized that the solid (shear wave) properties of the substrate were important. Work to develop an

average boundary condition approach to describe a randomly rough fluid-solid interface was initiated and completed to the stage of equations suitable for numerical computation.[4]

B. Results of FY79 Research

Computer software to implement the average boundary condition approach to a randomly rough fluid-solid interface was developed and tested. The computer program calculates the reflection and transmission coefficients of the coherent component of the sound field. Techniques were also developed to use these coefficients to modify the ARL:UT fluid sediment bottom reflection loss model[5] to include the effects of substrate roughness. Results of the sensitivity studies carried out under this task will appear in a future publication.

REFERENCES

CHAPTER III

1. W. A. Kuperman, "Coherent component of specular reflection and transmission at a randomly rough two-fluid interface", J. Acoust. Soc. Am. 61, 365-370 (1975).

2. W. A. Kuperman and F. Ingenito, "Attenuation of the coherent component of sound propagating in shallow water with rough boundaries", J. Acoust. Soc. Am. 61, 1178-1187 (1977).

3. S. R. Rutherford, K. E. Hawker, and S. G. Payne, "A study of the effects of ocean bottom roughness on low frequency sound propagation", J. Acoust. Soc. Am. 65. 381-386 (1979).

4. P. J. Vidmar, "Coherent component of reflection and transmission at a randomly rough fluid-solid interface", in preparation.

5. K. E. Hawker and T. L. Foreman, "A plane wave reflection loss model based on numerical integration", J. Acoust. Soc. Am. 64, 1470-1477 (1978).

IV. BOTTOM INTERACTION SENSITIVITY STUDIES

A continuing aspect of the bottom interaction studies at ARL:UT has been the use of various "measures" of bottom interaction as vehicles to test the importance of one or more parameter variations or uncertainties. Initially a commonly used measure was propagation loss, and work was carried out to determine the sensitivity of propagation loss to variations in bottom loss. More recent studies have explored the acoustical importance of various sea floor parameters such as density, sound speed, and absorption gradient using bottom reflection loss as a measure of bottom interaction.

In FY76 a study of the sensitivity of bottom reflection loss to subbottom parameter variations began. Initially the work concentrated on the properties of a fluid sediment and was carried out using a sophisticated bottom reflection loss model[1] developed at ARL:UT for this purpose. Various sea floor parameters such as density gradient,[2] sound speed[3] and absorption gradients,[4] and substrate rigidity[3,6] have been successfully studied.

A. Review of Previous Work

In FY78 the direction of these studies turned toward the inclusion of sediment rigidity (shear waves) in the bottom reflection loss model. The necessary theoretical work to develop a numerical bottom reflection loss model for use in studying the acoustic properties of solid sediments was initiated, completed, and implemented.[7] The assumptions underlying this model restrict its validity to frequencies above about 10 Hz. Theoretical work to extend the frequency range to lower frequencies was also completed.

Initial studies of a hypothetical turbidite layer showed that sediment shear waves were more important than heretofore thought, particularly for regions of thin sediment cover. Preliminary results suggested that the major mechanism for sediment shear wave excitation is compressional wave conversion at the sediment-substrate interface and that the water-sediment interface can be accurately represented as a fluid-fluid interface.

B. Results of FY79 Research

During FY79 computer software was developed to be used in preliminary studies of bottom interaction effects on coherence. The procedure followed uses the ARL:UT normal mode model to calculate the sound field for realistic environmental and subbottom acoustic properties. The coherence between two receivers at the same range but different depths is then computed. The averaging procedure simulates a time average of the received signal. Doppler effects are not included at this time so that multipath and bottom interaction effects could be isolated.

The major effort in FY79 concentrated on the effect of sediment rigidity on bottom reflection loss. This work is reported in detail in Ref. 8, which is being segmented into several smaller reports (Refs. 9-12) for journal publication. References 9 and 10 appear as Appendices B and C of this report. The results of FY79 work are summarized below.

1. The Effect of Sediment Rigidity on Bottom Reflection Loss in a Typical Deep Sea Sediment

A study of the effect of sediment rigidity on bottom reflection loss (RL) from typical deep sea sediment types shows that sediment shear (S) wave excitation is important for thin sediment layers but is negligible for thick layers. The major mechanism for S wave excitation is compressional (P) wave conversion at the sediment-substrate interface. Little energy is coupled into S waves at the water-sediment interface.

The mechanism for S wave excitation provides a means for quantifying the categories of thick and thin layers. It is the amplitude of the P wave at the substrate interface that matters. If the P wave amplitude at the substrate interface is significant, the layer is thin; if it is small, the layer is thick. The categories of thick and thin, then, will depend upon the wave frequency (through P wave attenuation), grazing angle (through the depth of the turning point), and the sediment thickness.

For physically thin sediment layers the dependence of RL on frequency (at a given grazing angle) exhibits high and low frequency regimes with strikingly different properties. The existence of these frequency regimes is the result of interference effects related to S wave propagation within the sediment. At low frequencies sediment shear wave attenuation is small and interference effects dominate the dependence of RL on frequency. Large peaks in RL ($\simeq$20 dB) occur with a separation in frequency related to changes in S wave phase of 2π. At higher frequencies the increased shear wave attenuation decreases the magnitude of this peak structure. At high frequencies the oscillatory structure disappears as S waves excited at the sediment-substrate interface are totally absorbed within the sediment, resulting in an almost constant additional loss compared to the RL of a fluid sediment.

The total attenuation of the S wave traveling one way through the sediment provides a quantitative means of separating these frequency regimes. For total S wave attenuation greater than 20 dB an S wave generated at the substrate interface is essentially absorbed within the sediment before striking the other interface. Since attenuation is proportional to frequency, this defines[5] a high frequency regime in which the propagation of sediment S waves can be neglected; however, their excitation is still an important loss mechanism. At low frequencies S wave attenuation is less than 20 dB across the layer and the additional interference effects due to the propagation of S waves through the sediment are important.

2. A Ray Path Analysis of Sediment Shear Wave Effects on Bottom Reflection Loss

A theoretical treatment of the reflection and transmission coefficients at the water and substrate interfaces by means of an expansion in the small sediment S wave velocity provides a basis for developing a ray path model of the effect of sediment rigidity on bottom reflection loss. The basic mechanism for S wave excitation emerges as P wave conversion at the substrate interface. The dependence on S wave velocity and attenuation, and P wave attenuation, are predicted by the ray model and verified in detail by results obtained from the computational bottom reflection loss model.[7]

The bottom reflection loss is found to be due to the interference of three waves in the water: the A_o wave, similar to that generated by a fluid sediment, the A_1 wave, whose amplitude depends on the S wave velocity to the first power, and the smaller A_2 wave, whose amplitude depends on the S wave velocity to the second power. The interference between the A_o and A_1 waves produces the large interference peaks in the low frequency regime of RL noted above. The A_2 wave provides an additional modulation to the peak structure. At high frequencies the A_1 and A_2 waves become negligible as the attenuation of the shear wave increases. The A_o wave, however, remains and carries the effect of shear waves excited at the substrate and absorbed within the sediment. The A_o wave describes the increased loss in the high frequency regime of RL.

3. Sensitivity Studies

Studies to identify significant parameters determining bottom reflection loss in thin sediment layers were completed in FY79. For homogeneous sediment layers, at high frequencies, the sediment S wave and P wave velocities, sediment P wave attenuation, and substrate P and S wave velocities are important parameters. Varying these parameters through their geophysically allowed ranges produces a change in bottom reflection loss of more than 0.5 dB relative to that calculated using the value at

the center of their range attenuation. At lower frequencies S wave propagation within the sediment becomes important and the sediment S wave attenuation also becomes an important parameter. Studies of thin sediment layers with gradients show that gradients of compressional and shear wave velocity and shear wave attenuation are also important parameters.

Studies indicating the accuracy required in specifying the geoacoustic parameters of thin sediment layers were also completed. Bottom reflection loss from solid sediments was found to be particularly sensitive to water sound speed, sediment thickness, sediment surficial density, sediment surficial compressional wave speed, and substrate shear velocity. Fractional changes of these parameters induced much larger fractional changes in the magnitude of the reflection coefficient of the ocean bottom. Several parameters induced negligible changes in bottom reflection loss when varied over their geophysically expected ranges. These very low sensitivity parameters were: all attenuations, the gradients of all attenuations, the gradients of sediment density, and the gradient of the sediment compressional wave velocity. The remaining parameters fell between these limits of sensitivity, producing fractional changes in the reflection coefficient of the same size as the fractional change in the parameter.

4. Effect of Sediment Rigidity on Interface Wave Excitation

Sediment rigidity was also found to influence the energy lost to interface waves. The Stoneley wave peak, generated in the fluid sediment case, merges into the generally increased bottom reflection loss in the solid sediment case. The characteristic peak in the dependence of bottom reflection loss on grazing angle, seen in the fluid sediment case, cannot be unambiguously identified in the case of a solid sediment with realistic geophysical parameter values. This work goes some way toward explaining why the previously predicted Stoneley wave reflection loss peaks have not been observed, and to clarify the true role of these interface waves in the reflection loss process.

REFERENCES

CHAPTER IV

1. K. E. Hawker and T. L. Foreman, "A plane wave reflection loss model based on numerical integration", J. Acoust. Soc. Am. 64, 1470-1477 (1978).

2. S. R. Rutherford and K. E. Hawker, "The effects of density gradients on bottom reflection loss for a class of marine sediments", J. Acoust. Soc. Am. 63, 750-757 (1978).

3. K. E. Hawker, W. E. Williams, and T. L. Foreman, "A study of the acoustical effects of subbottom absorption profiles", J. Acoust. Soc. Am. 65, 360-367 (1979).

4. K. E. Hawker, K. C. Focke, and A. L. Anderson, "A Sensitivity Study of Underwater Sound Propagation Loss and Bottom Loss", Applied Research Laboratories Technical Report No. 77-17 (ARL-TR-77-17), Applied Research Laboratories, The University of Texas at Austin, 28 February 1977.

5. K. E. Hawker, "The influence of Stoneley waves on plane wave reflection coefficients: Characteristics of bottom reflection loss", J. Acoust. Soc. Am. 64, 548-555 (1978).

6. K. E. Hawker, "Existence of Stoneley waves as a loss mechanism in plane wave reflection problems", J. Acoust. Soc. Am. 65, 682-686 (1979).

7. P. J. Vidmar and T. L. Foreman, "A plane-wave reflection loss model including sediment rigidity", J. Acoust. Soc. Am. 66, 1830-1835 (1979).

8. P. J. Vidmar, "The Effect of Sediment Rigidity on Bottom Reflection Loss", Applied Research Laboratories Technical Report No. 79-49 (ARL-TR-79-49), Applied Research Laboratories, The University of Texas at Austin, 19 September 1979.

9. P. J. Vidmar, "The effect of sediment rigidity on bottom reflection loss in a typical deep sea sediment", submitted to The Journal of The Acoustical Society of America for publication (see Appendix B).

10. P. J. Vidmar, "A ray path analysis of sediment shear wave effects on bottom reflection loss," accepted for publication in The Journal of The Acoustical Society of America (see Appendix B).

11. P. J. Vidmar, "The dependence of bottom reflection loss on the geoacoustic parameters of deep sea (solid) sediments", in preparation.

12. P. J. Vidmar, "The influence of sediment rigidity on interference wave excitation", in preparation.

ACKNOWLEDGMENTS

The authors wish to acknowledge the work of Susan Payne, Terry Foreman, and Ruth Gonzalez in developing the extensive and sophisticated computer software required for carrying out the computations central to this research.

The authors also wish to acknowledge the many useful and detailed conversations with Drs. Steve Mitchell and Claude Horton of ARL:UT, the former, especially, for the stimulus provided by other bottom interaction research carried out under his direction.

V. BIBLIOGRAPHY

A. DOCUMENTATION OF FY79 RESEARCH

1. S. R. Rutherford and K. E. Hawker, "An examination of the influence of the range dependence of the ocean bottom on the adiabatic approximation," J. Acoust. Soc. Am. 66, 1145-1151 (1979).

2. S. R. Rutherford, "An examination of multipath processes in a range dependent ocean environment within the context of adiabatic mode theory," J. Acoust. Soc. Am. 66, 1482-1486 (1979).

3. S. R. Rutherford and K. E. Hawker, "A consistent coupled mode theory of sound propagation of a class of nonseparable problems," submitted to The Journal of The Acoustical Society of America for publication (see Appendix A).

4. S. R. Rutherford, "An examination of coupled mode theory as applied to underwater sound propagation," Applied Research Laboratories Technical Report No. 79-44 (ARL-TR-79-44), Applied Research Laboratories, The University of Texas at Austin, 26 July 1979.

5. P. J. Vidmar, "Coherent component of reflection and transmission at a randomly rough fluid-solid interface," in preparation.

6. P. J. Vidmar, "The effect of sediment rigidity on bottom reflection loss," Applied Research Laboratories Technical Report No. 79-49 (ARL-TR-79-49), Applied Research Laboratories, The University of Texas at Austin, 19 September 1979.

7. P. J. Vidmar, "The effect of sediment rigidity on bottom reflection loss in a typical deep sea sediment," submitted to The Journal of The Acoustical Society of America for publication (see Appendix B).

8. P. J. Vidmar, "A ray path analysis of sediment shear wave effects on bottom reflection loss," accepted for publication in The Journal of The Acoustical Society of America (see Appendix C).

9. P. J. Vidmar, "The dependence of bottom reflection loss on the geoacoustic parameters of deep sea (solid) sediments," in preparation.

10. P. J. Vidmar, "The influence of sediment rigidity on interface wave excitation," in preparation.

V. BIBLIOGRAPHY

B. COMPREHENSIVE BOTTOM INTERACTION PROGRAM DOCUMENTATION

A.L. Anderson, "Influence of the Ocean Bottom on Long Range Propagation," International Workshop on Low Frequency Propagation and Noise, Vol. I, Woods Hole, Massachusetts, 1974.

A.L. Anderson, "Use of Bottom Properties in Long Range Propagation Predictions," Applied Research Laboratories Technical Memorandum No. 74-5 (ARL-TM-74-5), Applied Research Laboratories, The University of Texas at Austin, February 1974.

A.L. Anderson and K.C. Focke, "Model Sensitivity Studies: Relation Between Ambient Noise Depth Dependence and Propagation Loss Sensitivity to Bottom Loss (U)," presented at the 31st U.S. Navy Symposium on Underwater Acoustics, San Diego, California, November 1976. (CONFIDENTIAL)

A.L. Anderson and K.C. Focke, "Model Sensitivity Studies: Ambient Noise Depth Dependence Related to Propagation Loss (U)," U.S. Navy Journal of Underwater Acoustics 28, 219-228, April 1978. (ARL-TP-77-21, May 1977). (CONFIDENTIAL)

K.E. Cumella and S.G. Payne, "Implementation of the NOSC Random Ambient Noise Model, RANDI," Applied Research Laboratories Technical Letter No. 79-5 (TL-EV-79-5), Applied Research Laboratories, The University of Texas at Austin, May 1979.

K.C. Focke and D.E. Weston, "Problem of the Caustics in Range-Averaged Ocean Sound Channels," presented at the 96th Meeting of the Acoustical Society of America, Honolulu, Hawaii, 26 November - 1 December 1978.

T.L. Foreman, "Acoustic Ray Models Based on Eigenrays," Applied Research Laboratories Technical Report No. 77-1 (ARL-TR-77-1), Applied Research Laboratories, The University of Texas at Austin, January 1977.

L.D. Hampton, "Acoustic Bottom Interaction System Implications (U)," presented at the Laboratory Technical Exchange Meeting, NORDA, Bay St. Louis, Mississippi, 8 February 1978. (CONFIDENTIAL)

L.D. Hampton, "Acoustic Bottom Interaction System Implications (U)," Proceedings of the NSTL NORDA Laboratory Technical Exchange Meeting, Bay St. Louis, Mississippi, 8-9 February 1978. (CONFIDENTIAL)

L.D. Hampton, "Acoustic Bottom Interaction Program at ARL:UT," presented to Admiral Waller, Office of Chief of Naval Operations, 14 September 1978.

L.D. Hampton, S.K. Mitchell and R.R. Gardner, "Acoustic Bottom Loss Measurements Using Multipath Resolution," presented at the EASCON '78, IEEE Electronics and Aerospace Systems Conference, Arlington, Virginia, 24-27 September 1978.

L.D. Hampton, S.K. Mitchell and R.R. Gardner, "Acoustic Bottom Loss Measurement Using Multipath Resolution," EASCON '78 Record, IEEE Electronics and Aerospace Systems Conference, Arlington, Virginia, 25-27 September 1978.

L.D. Hampton and J.A. Shooter, "Merchant Ship Acoustic Data from Deep Moored Receivers (U)," for presentation at the 33rd Navy Symposium on Underwater Acoustics to be held in Gaithersburg, Maryland, 3-5 December 1979. (CONFIDENTIAL)

K.E. Hawker, "The Influence of Surface Waves on Plane Wave Bottom Reflection Loss for Realistic Ocean Sediments," presented at the 92nd Meeting of the Acoustical Society of America, San Diego, California, 16-19 November 1979.

K.E. Hawker, "An Introduction to the Acoustic Processes of Bottom Interaction with Application to Surveillance (U)," Applied Research Laboratories Technical Report No. 77-20 (ARL-TR-77-20), Applied Research Laboratories, The University of Texas at Austin, April 1977. (CONFIDENTIAL)

K.E. Hawker, "Acoustic Field Generated by a Moving Source (U)," presented at the ARPA/ELEX 320 Undersea Surveillance Symposium, Naval Postgraduate School, Monterey, California, 6-8 June 1978. (CONFIDENTIAL)

K.E. Hawker, "The Acoustic Bottom Interaction Problem," presented at the ONR Earth Physics Program Workshop, Washington, D.C., 6-7 July 1978.

K.E. Hawker, "The Influence of Stoneley Waves on Plane-Wave Reflection Coefficients: Characteristics of Bottom Reflection Loss," J. Acoust. Soc. Am. 64, 548-555 (1978). (ARL-TP-77-44, December 1977)

K.E. Hawker, "Calculation of the Acoustic Field Generated by a Moving Source," presented at the 96th Meeting of the Acoustical Society of America, Honolulu, Hawaii, 26 November - 1 December 1978.

K.E. Hawker, "Aspects of the Acoustic Bottom Interaction Problem," Applied Research Laboratories Technical Report No. 78-49 (ARL-TR-78-49), Applied Research Laboratories, The University of Texas at Austin, December 1978.

K.E. Hawker, "A Normal Mode Theory of Acoustic Doppler Effects in the Oceanic Waveguide," J. Acoust. Soc. Am. 65, 675-681 (1979). (ARL-TP-78-17, May 1978)

K.E. Hawker, "The Existence of Stoneley Waves as a Loss Mechanism in Plane Wave Reflection Problems," J. Acoust. Soc. Am. 65, 682-686 (1979). (ARL-TP-77-45, December 1977)

K.E. Hawker, "The Role of Bottom Interaction in Source Motion-Induced Doppler Broadening Processes," presented at the Seminar on Bottom Effects in Underwater Sound Propagation, Miami, Florida, April 1979.

K.E. Hawker, A.L. Anderson, K.C. Focke and T.L. Foreman, "Initial Phase of a Study of Bottom Interaction of Low Frequency Underwater Sound," Applied Research Laboratories Technical Report No. 76-14 (ARL-TR-76-14), Applied Research Laboratories, The University of Texas at Austin, April 1976.

K.E. Hawker, K.C. Focke and A.L. Anderson, "A Preliminary Sensitivity Study of Underwater Sound Propagation Loss and Bottom Loss," Applied Research Laboratories Technical Report No. 77-17 (ARL-TR-77-17), Applied Research Laboratories, The University of Texas at Austin, February 1977.

K.E. Hawker, K.C. Focke, S.R. Rutherford, W.E. Williams, T.L. Foreman and R. Gonzalez, "Results of a Study of the Bottom Interaction of Underwater Sound," Applied Research Laboratories Technical Report No. 77-27 (ARL-TR-77-27), Applied Research Laboratories, The University of Texas at Austin, October 1977.

K.E. Hawker and T.L. Foreman, "A Plane Wave Reflection Coefficient Model Based on Numerical Integration: Formulation, Implementation, and Application," Applied Research Laboratories Technical Report No. 76-23 (ARL-TR-76-23), Applied Research Laboratories, The University of Texas at Austin, June 1976.

K.E. Hawker and T.L. Foreman, "A Plane Wave Reflection Loss Model Based on Numerical Integration," J. Acoust. Soc. Am. 64, 1470-1477 (1978). (ARL-TP-78-11, March 1978)

K.E. Hawker, T.L. Foreman and K.C. Focke, "A Status Report on Propagation and Bottom Loss Models in Use at ARL:UT," Applied Research Laboratories Technical Memorandum No. 77-1 (ARL-TM-77-1), Applied Research Laboratories, The University of Texas at Austin, January 1977.

K.E. Hawker and S.G. Payne, "Interpolation of Normal Mode Eigenvalues in the Frequency Domain," presented at the 95th Meeting of the Acoustical Society of America, Providence, Rhode Island, 16-19 May 1978.

K.E. Hawker, S.R. Rutherford and P.J. Vidmar, "A Summary of the Results of a Study of Acoustic Interaction with the Sea Floor," Applied Research Laboratories Technical Report No. 79-2 (ARL-TR-79-2), Applied Research Laboratories, The University of Texas at Austin, March 1979.

K.E. Hawker and J.A. Shooter, "The Roles of Integration Time and Acoustic Multipaths in Determining the Structure of cw Line Spectra," Proceedings of the IEEE Conference on Acoustics, Speech and Signal Processing, Washington, D.C., 2-4 April 1979. (ARL-TP-78-50, December 1978)

K.E. Hawker, W.E. Williams and T.L. Foreman, "A Study of the Acoustical Effects of Subbottom Absorption Profiles," J. Acoust. Soc. Am. 65, 360-367 (1979). (ARL-TP-78-16, May 1978)

C.W. Horton, Sr., "The Influence of Biot's Second Dilatational Wave on the Reflection Coefficient of Ocean Sediments," presented at the 95th Meeting of the Acoustical Society of America, Providence, Rhode Island, 16-19 May 1978.

A.C. Kibblewhite, A.L. Anderson and G.E. Ellis, "Factors Controlling the Ambient Noise Field Below the Deep Sound Channel (U)," U.S. Navy Journal of Underwater Acoustics 27, 551-568, July 1977. (ARL-TR-77-54, September 1977) (CONFIDENTIAL)

S.R. Rutherford, "Analytical Techniques for Determining Subbottom Sound Velocity Profiles in Unconsolidated Sediments," Applied Research Laboratories Technical Report No. 76-58 (ARL-TR-76-58), Applied Research Laboratories, The University of Texas at Austin, December 1976.

S.R. Rutherford, "An Examination of Multipath Processes in a Range Dependent Environment Within the Context of Adiabatic Mode Theory," presented at the 97th Meeting of the Acoustical Society of America, Cambridge, Massachusetts, 11-15 June 1979.

S.R. Rutherford, "An Examination of Multipath Processes in a Range Dependent Ocean Environment Within the Context of Adiabatic Mode Theory," J. Acoust. Soc. Am. 66, 1482-1486 (1979). (ARL-TP-79-18, February 1979)

S.R. Rutherford, "An Examination of Coupled Mode Theory as Applied to Underwater Sound Propagation," Ph.D. Dissertation awarded by The University of Texas at Austin, August 1979. Also Applied Research Laboratories Technical Report No. 79-44 (ARL-TR-79-44), Applied Research Laboratories, The University of Texas at Austin, July 1979.

S.R. Rutherford and K.E. Hawker, "Effects of Density Gradients on Bottom Reflection Loss for a Class of Marine Sediments," J. Acoust. Soc. Am. 63, 750-757 (1978). (ARL-TP-77-22, May 1977)

S.R. Rutherford and K.E. Hawker, "An Examination of the Influence of the Range Dependence of the Ocean Bottom on the Adiabatic Approximation," scheduled to appear in The Journal of the Acoustical Society of America, October 1979. (ARL-TP-79-8, January 1979)

S.R. Rutherford and K.E. Hawker, "A consistent coupled mode theory of sound propagation for a class of nonseparable problems," submitted to The Journal of the Acoustical Society of America for publication. (ARL-TP-79-65, October 1979)

S.R. Rutherford and K.E. Hawker, "The Effects of Boundary Condition Approximations on Coupled Mode Theory," presented at the 98th Meeting of the Acoustical Society of America, Salt Lake City, Utah, 26-30 November 1979.

S.R. Rutherford and K.E. Hawker, "An Examination of the Coupling Coefficients of a Coupled Mode Theory," presented at the Fall 1978 Meeting of the American Geophysical Union, San Francisco, California, 4-8 December 1978.

S.R. Rutherford, K.E. Hawker and S.G. Payne, "A Sensitivity Study of the Effects of Bottom Roughness on Low Frequency Sound Propagation," presented at the 95th Meeting of the Acoustical Society of America, Providence, Rhode Island, 16-19 May 1978.

S.R. Rutherford, K.E. Hawker and S.G. Payne, "A Study of the Effects of Ocean Bottom Roughness on Low Frequency Sound Propagation," J. Acoust. Soc. Am. 65, 381-386 (1979). (ARL-TP-78-14, May 1978)

J.A. Shooter, K.E. Hawker and L.D. Hampton, "An Introduction to the Characteristics and Acoustic Mechanisms of the Deep Ocean Ambient Noise Field (U)," Applied Research Laboratories Technical Report No. 77-55 (ARL-TR-77-55), Applied Research Laboratories, The University of Texas at Austin, September 1977. (CONFIDENTIAL)

C.T. Tindle, "Frequency Dependence and Detection of Individual Normal Modes in Shallow Water," presented at the 95th Meeting of the Acoustical Society of America, Providence, Rhode Island, 16-19 May 1978.

C.T. Tindle, "Reflection from a Structured Ocean Bottom," presented at the Underwater Acoustics Session of the ANZAAS '79 Conference, Auckland, New Zealand, January 1979.

C.T. Tindle, "Virtual Modes and Mode Amplitudes Near Cutoff," J. Acoust. Soc. Am. 65, 1423-1428 (1979). (ARL-TP-78-25, May 1978)

C.T. Tindle, "The Equivalence of Bottom Loss and Mode Attenuation per Cycle in Underwater Acoustics," J. Acoust. Soc. Am. 66, 250-255 (1979). (ARL-TP-78-42, October 1978)

P.J. Vidmar, "The Effect of Sediment Rigidity on Bottom Reflection Loss," presented at the Workshop on Interpretative Modeling of Deep-Ocean Sediments and Their Physical Properties, NORDA, Bay St. Louis, Mississippi, September 1979.

P.J. Vidmar, "The Effect of Sediment Rigidity on Bottom Reflection Loss in a Typical Deep Sea Sediment," submitted to The Journal of the Acoustical Society of America for publication. (ARL-TP-79-59, September 1979)

P.J. Vidmar, "A ray path analysis of sediment shear wave effects on bottom reflection loss," submitted to The Journal of the Acoustical Society of America for publication. (ARL-TP-79-67, November 1979)

P.J. Vidmar, "The Effect of Sediment Rigidity on Bottom Reflection Loss," presented at the 98th Meeting of the Acoustical Society of America, Salt Lake City, Utah, 26-30 November 1979.

P.J. Vidmar and T.L. Foreman, "The Effect of Sediment Rigidity on the Acoustic Reflectivity of the Ocean Bottom," presented at the Fall 1978 Meeting of the American Geophysical Union, San Francisco, California, 4-8 December 1978.

P.J. Vidmar and T.L. Foreman, "A Plane Wave Reflection Loss Model Including Sediment Rigidity," presented at the 97th Meeting of the Acoustical Society of America, Cambridge, Massachusetts, 11-15 June 1979.

P.J. Vidmar and T.L. Foreman, "A Plane Wave Reflection Loss Model Including Sediment Rigidity," scheduled to appear in The Journal of the Acoustical Society of America, December 1979. (ARL-TP-79-20, March 1979)

D.E. Weston, "Acoustic Flux Formulae for Range-Dependent Ocean Ducts," submitted to The Journal of the Acoustical Society of America for publication. (ARL-TP-78-36, September 1978)

D.E. Weston, "Shallow Water Sound Propagation," presented at the EASCON '78, IEEE Electronics and Aerospace Systems Conference, Arlington, Virginia, 24-27 September 1978.

D.E. Weston, "Shallow Water Sound Propagation," EASCON '78 Record, Proceedings of the IEEE Electronics and Aerospace Systems Conference, Arlington, Virginia, 25-27 September 1978, pp. 252-255.

D.E. Weston, "Nature of the Caustics in Range-Averaged Ocean Sound Channels, presented at the 96th Meeting of the Acoustical Society of America, Honolulu, Hawaii, 26 November - 1 December 1978.

D.E. Weston, "Wave-Theory Peaks in Range-Averaged Channels of Uniform Sound Velocity," submitted to The Journal of the Acoustical Society of America for publication. (ARL-TP-79-5, January 1979)

D.E. Weston, "Acoustic Flux Methods for Oceanic Guided Waves," submitted to The Journal of the Acoustical Society of America for publication. (ARL-TP-79-14, January 1979)

D.E. Weston, "Thermoviscous Regions for the Principal and Higher Sound Propagation Modes in Tubes," submitted to The Journal of the Acoustical Society of America for publication. (ARL-TP-79-31, April 1979)

D.E. Weston, "Deep Ambient Noise Field and Volume Scattering (U)," scheduled to appear as a Letter to the Editor in the U.S. Navy Journal of Underwater Acoustics, October 1979. (ARL-TP-79-25, March 1979) (CONFIDENTIAL)

D.E. Weston, "Ambient Noise Depth-Dependence Models and Their Relation to Low Frequency Attenuation," scheduled to appear in The Journal of the Acoustical Society of America, January 1980. (ARL-TP-79-30, April 1979)

D.E. Weston and C.T. Tindle, "Reflection Loss and Mode Attenuation in a Pekeris Model," J. Acoust. Soc. Am. 66, 872-879 (1979). (ARL-TP-79-4, January 1979)

D.E. Weston and C.T. Tindle, "Connection of Acoustic Beam Displacement, Cycle Distances and Attenuations for Rays and Normal Modes," submitted to The Journal of the Acoustical Society of America for publication. (ARL-TP-79-15, January 1979)

A.O. Williams, Jr., "Use of Plane-Wave Expansions in Acoustic Propagation - Two Examples," Applied Research Laboratories Technical Memorandum No. 75-14 (ARL-TM-75-14), Applied Research Laboratories, The University of Texas at Austin, May 1975.

A.O. Williams, Jr., "Acoustic Reflection from a Structured Sea Bottom," presented at the 90th Meeting of the Acoustical Society of America, San Francisco, California, 4-7 November 1975.

A.O. Williams, Jr., "Hidden Depths: Acceptable Ignorance About Ocean Bottoms," presented at the 90th Meeting of the Acoustical Society of America, San Francisco, California, 4-7 November 1975.

A.O. Williams, Jr., "Comments on Propagation of Normal Mode in the Parabolic Approximation (Suzanne T. McDaniel, J. Acoust. Soc. Am. 57, 307-311, February 1975)," J. Acoust. Soc. Am. 58, 1320-1321 (1975).

A.O. Williams, Jr., "Acoustic Reflection from a Structured Sea Bottom," J. Acoust. Soc. Am. 59, 62-68 (1976). (ARL-TP-75-23, July 1975).

A.O. Williams, Jr., "Hidden Depths: Acceptable Ignorance About Ocean Bottoms," J. Acoust. Soc. Am. 59, 1175-1179 (1976). (ARL-TP-75-46)

A.O. Williams, Jr., "Discrete, Continuous, and Virtual Modes in Underwater Sound Propagation," Applied Research Laboratories Technical Report No. 76-40 (ARL-TR-76-40), Applied Research Laboratories, The University of Texas at Austin, August 1976.

A.O. Williams, Jr., "Pseudoresonances and Virtual Modes in Underwater Sound Propagation," J. Acoust. Soc. Am. 64, 1487-1491 (1978). (ARL-TP-78-1 January 1978)

A.O. Williams, Jr., "Mode Interactions in an Isovelocity Ocean of Uniformly Varying Depth," scheduled to appear in The Journal of the Acoustical Society of America, October 1979. (ARL-TP-78-28, August 1978)

A.O. Williams, Jr. and D.R. MacAyeal, "Acoustic Reflection from a Sea Bottom with Linearly Increasing Sound Speed," accepted for publication in The Journal of the Acoustical Society of America. (ARL-TP-79-16, February 1979)

A.O. Williams, Jr. and D.R. MacAyeal, "Acoustic Reflection from Sea Bottom with Linearly Increasing Sound Speed," presented at the 92nd Meeting of The Acoustical Society of America, San Diego, California, 16-17 November 1976.

W.E. Williams and K.E. Hawker, "Effects of Variation of Attenuation with Depth in the Sediment on the Bottom Reflection Coefficient," presented at the 95th Meeting of the Acoustical Society of America, Providence, Rhode Island, 16-19 May 1978.

APPENDIX A

A CONSISTENT COUPLED MODE THEORY OF SOUND PROPAGATION FOR A CLASS OF NONSEPARABLE PROBLEMS

by

Steven R. Rutherford
Kenneth E. Hawker

Paper submitted to The Journal of The Acoustical Society of America for publication

A consistent coupled mode theory of sound propagation for a class of non-separable problems[a)]

Steven R. Rutherford and Kenneth E. Hawker

Applied Research Laboratories, The University of Texas at Austin,

Austin, Texas 78712

(Received

This article examines the effects of boundary condition approximations that arise whenever the coupled mode theories of Pierce and Milder are applied to propagation problems involving range dependent boundaries. This boundary condition approximation requires that the depth derivative, rather than the normal derivative of the field, be continuous across a sloping interface. The approximation is necessary in order to carry out the partial separation of depth and range variables effected in the mathematical formulation of the theory. This article will show that a consequence of this approximation is that conventional coupled mode theory applied to dissipationless media with nonhorizontal boundaries does not conserve energy. It is shown that a correction to coupled mode theory can be derived such that the proper boundary conditions are satisfied and energy is conserved to first order in the local bottom slope. Moreover, the corrections are not prohibitive in terms of added computational complexity. Numerical examples are presented which illustrate the nonconservation of energy effect and the corrections to the theory.

PACS numbers:

INTRODUCTION

In the coupled mode theory of underwater sound propagation proposed independently by Pierce[1] and Milder,[2] a certain form of the boundary conditions satisfied by the field was assumed, namely, continuity of pressure and vertical component of particle velocity. This assumption allowed a partial separation of the depth and radial variables and resulted in a workable theory. In range dependent media having horizontal boundaries and interfaces, the assumed form of the boundary conditions was physically correct; however, when applied to problems having range variable boundaries and interfaces, the assumed boundary conditions were approximations to the proper ones to be satisfied by the field at fluid-fluid interfaces (continuity of normal stress and displacement). The intent of this article is to explore the consequences of this approximation to the physically correct boundary conditions. It is shown that one consequence of the approximation is nonconservation of energy within the original formalism of coupled mode theory. It is also shown that a consistent correction to the theory can be made such that the field so obtained satisfies both the proper boundary conditions and conserves energy to first order in the slopes of nonhorizontal boundaries and interfaces that are present in the problem.

Of the recent applications of coupled mode theory,[3-8] most involved media with horizontal boundaries; hence, as shall be shown, the issue of nonconservation of energy did not arise. The adiabatic approximation to coupled mode theory (see Refs. 9-12) has been applied to many types of acoustic propagation problems. The nonconservation of energy effect does not arise in adiabatic mode theory (see Ref. 9) because the assumed, approximate boundary conditions are consistent with the assumption of adiabacity.

I. BACKGROUND

In the coupled mode theories of Pierce and Milder, the acoustic velocity potential in a range dependent, fluid medium is expressed as

$$\psi(r,z) = \sum_n R_n(r)\ \phi_n(z;r) \tag{1}$$

with $R_n(r)$ and $\phi_n(z;r)$ satisfying

$$\frac{d^2}{dr^2}\ R_m(r) + \frac{1}{r}\ \frac{d}{dr}\ R_m(r) + k_m^2\ (r)\ R_m(r) =$$

$$-\sum_n \left[A_{mn}\ R_n + B_{mn} \left(\frac{R_n}{r} + \frac{2dR_n}{dr} \right) \right] \tag{2}$$

$$\left[\frac{\partial^2}{\partial z^2} + k^2(r;z) - k_n^2(r) \right] \phi_n(z;r) = 0. \tag{3}$$

The summation in Eq. (1) extends over all discrete modes. In Eqs. (1) through (3) a cylindrical coordinate system has been assumed and the azimuthal symmetry of the medium used to reduce the problem to two dimensions. The velocity potential ψ satisfies the following partial differential equation

$$\nabla^2\psi + k^2(r,z)\ \psi = 0 \quad , \tag{4}$$

with $k(r,z)$ being the wave number of the medium ($k(r,z)=\omega/c(r,z)$). As indicated by Eq. (4) the developments of this article will consider acoustic propagation in a source free region of space. The extension to include a source is straightforward. The boundary conditions on ϕ_n are that $\rho\phi_n$ and $\partial\phi_n/\partial z$ be continuous across any interfaces. The functions ϕ_n are assumed to form an orthonormal, complete set of functions such that

$$\int_0^\infty \rho\phi_n\ (z;r)\ \phi_m\ (z;r)\ dz = \delta_{n,m} \quad , \tag{5}$$

where ρ is the density of the medium, assumed to have step function discontinuities at boundary interfaces. If the eigenfunctions corresponding

to the discrete spectrum do not form a complete set (due to the presence of a continuous spectrum), the results throughout this paper remain correct but only approximate. The A_{mn} and B_{mn} in Eq. (2) are range-dependent coupling coefficient matrices defined by

$$B_{mn}(r) = \int_0^\infty \rho\phi_m \frac{\partial\phi_n}{\partial r}\, dz \tag{6}$$

$$A_{mn}(r) = \int_0^\infty \rho\phi_m \frac{\partial^2\phi_n}{\partial r^2}\, dz \quad . \tag{7}$$

Implicit in the partial separation of variables described by Eqs. (1) through (4) is that the field ψ satisfies boundary conditions such that $\rho\psi$ and $\partial\psi/\partial z$ are continuous throughout the waveguide. These boundary conditions are equivalent to requiring that the pressure and z-component of particle velocity be continuous functions of depth and range. These boundary conditions are the physically correct ones for range dependent waveguides having horizontally stratified boundaries. However, if one wishes to consider nonstratified boundaries, the correct conditions for ψ to satisfy at surfaces of discontinuity are continuity of $\rho\psi$ and $\partial\psi/\partial n$, where $\partial/\partial n$ is the normal derivative operator given by

$$\frac{\partial}{\partial n} = \frac{1}{\sqrt{1+\dot{H}^2(r)}}\left(\frac{\partial}{\partial z} - \dot{H}(r)\,\frac{\partial}{\partial r}\right) \quad . \tag{8}$$

In Eq. (8), $\dot{H}(r)$ is the local slope of a surface of discontinuity defined by $z=H(r)$ with $\dot{H}(r)=dH/dr$; $H(r)$ might, for example, be the water depth at range r.

Of course, if ψ is required to satisfy boundary conditions given by Eq. (8), the partial separation of the range and depth variables implied

by Eq. (1) is not possible. In this situation the variables are not separable and an exact solution to Eq. (4) having the assumed form of ψ given in Eq. (1) cannot be obtained. A natural approximation to make when applying coupled mode theory to problems involving range dependent boundaries is to approximate the normal derivative of the field at the boundary with the z derivative, i.e.,

$$\frac{\partial}{\partial n}\psi\Big|_{z=H(r)} \approx \frac{\partial\psi}{\partial z}\Big|_{z=H(r)} . \tag{9}$$

Under this approximation, the coupled mode theory formalism summarized by Eqs. (1) through (4) can be applied to problems having nonhorizontal boundaries. It is usually reasoned that, for small boundary slopes, the errors incurred from the approximation of Eq. (9) will be negligible. It is the purpose of this paper to explore the implications of the approximation of Eq. (9) and to show that a correction to coupled mode theory must be applied whenever nonhorizontal boundaries are present.

The coupling coefficients of Eqs. (6) and (7) are quantities that depend on the radial rates of change of the medium. It will be shown that B_{mn} and A_{mn} have components of order $\dot{H}$ and $\dot{H}^2$, respectively. Therefore, the inconsistency of the approximation in Eq. (9) is immediately apparent since terms of order $\dot{H}$ and higher are being neglected in Eq. (9) while they are being retained in Eq. (2) with the coupling coefficients. An implication of this inconsistency is that if one insists on satisfying the boundary conditions on ψ only to zero order in $\dot{H}$, as given by Eq. (9), then the only consistent treatment of the radial equation is one in which mode coupling effects are ignored (i.e., the adiabatic approximation).

In the next section of this article it will be shown that a consequence of the inconsistent use of Eq. (9) is a nonconservation of energy within

the conventional coupled mode theory formalism. This inconsistency problem has not arisen until now because previous applications of coupled mode theory were ones in which boundary conditions involving the normal derivative either did not appear, or else the subsequent assumption of adiabatic propagation avoided the question.

II. CONSIDERATIONS OF ENERGY TRANSPORT

In this section we shall examine energy transport, and the question of energy conservation in dissipationless media, using the form of coupled mode theory outlined in the previous section.

It is of course recognized that preservation of an intact fluid-fluid interface requires continuity of both displacement and normal stress, leading, in the time harmonic problem considered here, to continuity of $\partial\psi/\partial n$ and ψ. In this sense, then, it is required that $\partial\psi/\partial n$ be continuous and it should not be surprising that inconsistencies develop when this requirement is not met. However, in as much as coupled mode theory has been developed for the approximate continuity condition, it becomes necessary to explore the consequences of this requirement. Moreover, it is not <u>a priori</u> obvious to what order in $\dot{H}(r)$, the local interface slope, inconsistencies may develop or whether the inclusion of mode coupling at all is consistent with the approximation $\partial\psi/\partial n \simeq \partial\psi/\partial z$.

Following Ref. 9, we consider the time averaged (rms) radial energy flux J_r given by[13]

$$J_r = \frac{1}{2}\,\mathrm{Re}(pv_r^*) = -\frac{1}{2}\,\omega\rho\,\mathrm{Im}\left(\psi\frac{\partial\psi^*}{\partial r}\right) \quad , \tag{10}$$

where v_r is the radial velocity and p the pressure. Also of interest will be the total power transported through a cylindrical surface of radius

r, centered at the origin and extending from the sea surface (z=0) to infinity. This quantity P is given by

$$P = \int_0^{2\pi} d\theta \int_0^{\infty} dz\ rJ_r = 2\pi r \int_0^{\infty} dz\ J_r(r,z) \quad , \tag{11}$$

where it must be remembered that integrals of the form $\int_0^{\infty} dz(\cdot)$ are abbreviated notation for a sum of integrals over the contiguous layers $\int_0^{H_1} dz(\cdot)+\int_{H_1}^{H_2} dz(\cdot)\ldots$. Upon differentiating with respect to r and using Eq. (10) we have for the single interface (water-sediment) problem

$$\frac{\partial P}{\partial r} = -\pi\omega\ \mathrm{Im}\left\{\int_0^{\infty} dz\ \rho\left[\psi\frac{\partial\psi^*}{\partial r} + r\left|\frac{\partial\psi}{\partial r}\right|^2 + r\psi\frac{\partial^2\psi^*}{\partial r^2}\right]\right\}$$

$$-\pi\omega\ \mathrm{Im}\left\{r\dot{H}\left(\left[\rho\psi\frac{\partial\psi^*}{\partial r}\right]_{H^-} - \left[\rho\psi\frac{\partial\psi^*}{\partial r}\right]_{H^+}\right)\right\} \quad , \tag{12}$$

where H^- and H^+ refer to limits approaching the water-sediment interface (z=H(r)) from above and below, respectively. The wave equation can now be used to substitute for $\partial^2\psi^*/\partial r^2$, and after routine manipulations one obtains

$$\frac{\partial P}{\partial r} = -\pi\omega r\dot{H}\ \mathrm{Im}\left\{\rho_1\psi_1\left(\dot{\psi}_1^* - \dot{\psi}_2^*\right)\right\}$$

$$+\pi\omega r\ \mathrm{Im}\left\{\int_0^{\infty} dz\left(\rho\psi\frac{\partial^2\psi^*}{\partial z^2}\right)\right\} \quad , \tag{13}$$

with $\dot{H}=dH/dr$ and $\dot{\psi}_1=(\partial\psi/\partial r)\big|_{z\to H^-}$, etc.

In passing from Eq. (12) to Eq. (13) it has been assumed that $\rho\psi$ is continuous across the interface z=H(r). Without further assumptions, for the moment, as to the continuity of $\partial\psi/\partial z$, one has, from Eq. (13) upon integration by parts in the second term, the result

$$\frac{\partial P}{\partial r} = -\pi\omega r\mathrm{Im}\left\{\rho_1\psi_1\left[\dot{H}(\dot{\psi}_1^* - \dot{\psi}_2^*) - (\psi_1^{*\prime} - \psi_2^{*\prime})\right]\right\} \quad , \tag{14}$$

where $\psi'_1 = [\partial\psi(z,r)/\partial z]_{z\to H^-}$, etc.

If, as has been assumed in conventional coupled mode theory, $\partial\psi/\partial z$ is taken to be continuous at all interfaces, the last term in Eq. (14) vanishes

and one has the result,

$$\frac{\partial P}{\partial r} = -\pi\omega r \, \mathrm{Im}\left\{\rho_1\psi_1 \, \dot{H}(\dot{\psi}_1^* - \dot{\psi}_2^*)\right\} \quad . \tag{15}$$

At this stage it will be useful to introduce the partially separated solution given by Eq. (1). After carrying out some straightforward manipulations, as described in Appendix A, one obtains

$$\frac{\partial P}{\partial r} = \frac{1}{2} \, i\pi\omega \sum_{m,n} \left\{\left(\dot{B}_{nm} - A_{nm}\right)^A r \, Q_{nm}(r) + r \, B_{nm}^S \, P_{nm}(r)\right\} \quad , \tag{16}$$

where the superscripts A and S refer to the antisymmetric and symmetric parts of the matrices. The range dependent factors Q_{nm} and P_{nm} are defined as

$$Q_{nm} = 2i\,\mathrm{Im}(R_n R_m^*) \tag{17}$$

$$P_{nm} = 2i\,\mathrm{Im}(\dot{R}_n R_m^* + \dot{R}_m R_n^*) \quad , \tag{18}$$

while, as shown in Appendix A, the matrices in Eq. (16) are given by

$$(\dot{B}_{nm} - A_{nm})^A = \frac{1}{2} \dot{H}\rho_1 \left\{\phi_n^{(1)}(\dot{\phi}_m^{(1)} - \dot{\phi}_m^{(2)}) - \phi_m^{(1)}(\dot{\phi}_n^{(1)} - \dot{\phi}_n^{(2)})\right\} \tag{19}$$

$$B_{nm}^S = -\frac{1}{2} \dot{H}\rho_1 \left(1 - \frac{\rho_1}{\rho_2}\right) \phi_n^{(1)} \, \phi_m^{(1)} \quad , \tag{20}$$

for the waveguide geometry of Fig. 1.

In a general problem where $\dot{H} \neq 0$ there is clearly no reason to expect the right-hand side of Eq. (16) to vanish. Thus, in general, $\partial P/\partial r \neq 0$ and the (radial) energy flux passing through a semiinfinite cylindrical surface is not independent of range. Of course, in the horizontally stratified case $\dot{H}$ vanishes identically and energy is properly conserved. Similarly, in the adiabatic approximation to a nonhorizontally stratified problem, all mode coupling terms are ignored and once again energy is conserved.

Even though we have not yet presented a coupled mode theory which satisfies the proper continuity relations at a fluid-fluid interface, the presence of (only) boundary terms on the right-hand side of Eq. (16) leads one to inquire as to the respective roles of the continuity of $\partial\psi/\partial z$ and $\partial\psi/\partial n$ at the boundary. Returning to Eq. (14) and using Eq. (8) one has,

$$\dot{H}(\dot{\psi}_1^* - \dot{\psi}_2^*) - (\psi_1'^* - \psi_2'^*) = \sqrt{1+\dot{H}^2}\left\{\left.\frac{\partial\psi^*}{\partial n}\right|_{H^+} - \left.\frac{\partial\psi^*}{\partial n}\right|_{H^-}\right\} \quad . \tag{21}$$

Thus, when $\partial\psi/\partial n$ is assumed continuous at $z=H(r)$, we have at once that $\partial P/\partial r=0$ and energy is conserved. The motivation for developing a coupled mode theory based on continuity of $\partial\psi/\partial n$ rather than $\partial\psi/\partial z$ is therefore clearly established.

As a final point we shall clarify the role of the water-sediment interface, and the continuity of $\partial\psi/\partial z$ imposed there, in determining the overall flow of acoustic energy. It is easily verified by direct computation that $\nabla\cdot\underset{\sim}{J}=0$, where $\underset{\sim}{J}$ is the time averaged energy flux vector, the radial component of which is given by Eq. (10). Hence, by Gauss' theorem the surface integral of the normal component of $\underset{\sim}{J}$, integrated over a closed surface, vanishes. We now choose as the surface a cylinder of radius r, centered at the origin, and extending from the surface (z=0) to infinity. Since only at the boundary z=H(r) can any component of $\underset{\sim}{J}$ be discontinuous, and because $\underset{\sim}{J}$ vanishes at z=0, and as $z\to\infty$, we have

$$\int_0^{2\pi} d\theta \int_0^{\infty} dz\ rJ_r + \int_S \left[J_\perp^- - J_\perp^+\right] dA = 0 \quad , \tag{22}$$

where $J_\perp$ is the energy flux normal to the surface defined by the water-sediment interface, and the $\left(\pm\right)$ superscripts refer to the fluxes normal to the interface as approached from above and below.

Using area element $dA = r\sqrt{1+\dot{H}^2}\, dr d\theta$, one finds,

$$P(r) + 2\pi \int_0^r dr'\, r' \sqrt{1+\dot{H}^2(r')} \left[J_\perp^- - J_\perp^+ \right] = 0 \quad , \tag{23}$$

and thus we must have,

$$\frac{\partial P}{\partial r} + 2\pi r \sqrt{1+\dot{H}^2} \left[J_\perp^- - J_\perp^+ \right] = 0 \quad . \tag{24}$$

The energy flux normal to $z=H(r)$, $J_\perp$, is given by

$$J_\perp = -\frac{1}{2} \omega \rho \, \mathrm{Im}\left(\psi \frac{\partial \psi^*}{\partial n}\right) \quad , \tag{25}$$

where the normal derivative is given by Eq. (8). Direct computation yields at once the result for the normal flux

$$J_\perp = -\frac{1}{2} \omega \rho \left(1+\dot{H}^2\right)^{-1/2} \mathrm{Im}\left\{ \sum_{m,n} \left[R_n^* R_m \phi_m \phi_n' - \dot{H}\left(\dot{R}_n^* R_m \phi_n \phi_m + R_n^* R_m \phi_n \phi_m\right) \right] \right\} \quad . \tag{26}$$

After straightforward computation, the net energy flux across the water-sediment interface, $J_\perp^- - J_\perp^+$, is found to be

$$J_\perp^- - J_\perp^+ = \frac{-i\omega r}{4\sqrt{1+\dot{H}^2}} \sum_{m,n} \left| \left(\dot{B}_{nm} - A_{nm}\right)^A Q_{nm} + B_{nm}^S P_{nm} \right| \quad . \tag{27}$$

Upon introducing Eq. (27) into Eq. (24), the expression for the radial rate of change of total power transmitted through the cylindrical surface must obey the conservation equation,

$$\frac{\partial P}{\partial r} - \frac{i\omega\pi}{2} \sum_{m,n} \left| \left(\dot{B}_{nm} - A_{nm}\right)^A r\, Q_{nm} + r B_{nm}^S P_{nm} \right| = 0 \quad . \tag{28}$$

However, as previously shown in Eq. (16), the second term in Eq. (28) is simply $-\partial P/\partial r$ so the total energy balance equation is satisfied identically.

It is appreciated that the conventional coupled mode theory outlined in Section I, the energy considerations given here, and the consistent

coupled mode theory to be developed in Section II, have all been restricted to lossless media. In practice when significant acoustic energy interacts with the sea floor, the volume absorption within the sediments must be taken into account. In horizontally stratified situations this is accomplished most easily by letting wave numbers take on an imaginary part, $k \to k+i\alpha$, and obtaining the corresponding imaginary correction to the eigenvalues, $k_n \to k_n + i\delta n$, by first order perturbation theory. It is not difficult to convince oneself that a similar result will hold for a coupled mode theory when absorption is small. This subject will be addressed in a later paper.

In summary, we have shown in this section that (1) conventional coupled mode theory, employing continuity of $\partial\psi/\partial z$ at all interfaces, does not properly conserve total radial energy flux in a dissipationless problem, (2) the anomalous energy loss (right-hand side of Eq. (16)) can be expressed in terms of mode coupling coefficients and radial functions R_n, together with the interface slope $\dot{H}$, (3) total energy is conserved if one includes energy lost into the bottom as a result of the application of the incorrect boundary condition, and (4) if $\partial\psi/\partial n$ is assumed continuous at the interface, the total radial energy flux is correctly conserved.

Finally, we wish to remark that as a consequence of the use of continuity conditions on $\partial\psi/\partial z$, resulting in a theory which fails to conserve energy to order $\dot{H}$, when one is concerned with small but finite slopes, it will be manifestly inconsistent to use conventional coupled mode theory (wherein the coupling coefficients are corrections of order $\dot{H}$) except in the adiabatic approximation. In this theory, we can already see that the first order corrections to the adiabatic theory will be proportional to B_{nm} and thence at least to $\dot{H}$. Thus retaining mode coupling as the conventional theory

will entail retaining some terms of order $\dot{H}$ while ignoring other terms of the same order (arising through the continuity conditions imposed at sloping interfaces). Of course in range variable problems not involving sloping interfaces this inconsistency does not arise.

III. FIRST ORDER CORRECTIONS TO COUPLED MODE THEORY

In this section a first order correction to coupled mode theory is proposed and derived. It will be shown that with an improvement on the theories of Pierce and Milder, the field can be obtained in terms of coupled modes so that the proper boundary conditions are satisfied and energy is conserved (both to first order in the boundary slope $\dot{H}$) and a consistent theory is obtained.

To derive the appropriate corrections to the theory, Eq. (1) is replaced by

$$\psi(r,z) = \sum_n X_n(r)\ \Phi_n\ (z;r) \quad . \tag{29}$$

When ψ is required to satisfy the proper boundary conditions (continuity of normal stress and displacement) to first order in $\dot{H}$, the appropriate conditions on Φ_n and its z derivative at a sloping interface defined by $z=H(r)$ are found to be that

$$\rho\Phi_n \quad ,$$

and (30)

$$\Phi'_n - \frac{\dot{H}\dot{X}_n}{X_n}\ \Phi_n \quad ,$$

be continuous across $z=H(r)$. In these expressions the dot and prime symbols denote differentiation with respect to range and depth, respectively. The second of Eqs. (30) follows from the fact that $\dot{\Phi}_n$ is first order in $\dot{H}$.

Now, assume that the depth equation Φ_n satisfies the following differential equation.

$$\left[\frac{\partial^2}{\partial z^2} + k^2\ (r,z) - \sigma_n^2\ (r)\right] \Phi_n\ (z;r) = 0 \tag{31}$$

Equation (31) is of the same form as the differential equation assumed in the developments of Ref. 1, the only difference being that it satisfies the modified boundary conditions of Eqs. (30).

If Eqs. (29) and (31) are used in Eq. (4), one obtains the following equation

$$\sum_n \left(\ddot{X}_n + \frac{\dot{X}_n}{r} + \sigma_n^2 X_n \right) \Phi_n = -\sum_n \left[\left(2\dot{X}_n + \frac{X_n}{r} \right) \dot{\Phi}_n - X_n \ddot{\Phi}_n \right] \quad . \tag{32}$$

It is now convenient to express Φ_n as

$$\Phi_n = \phi_n + \delta\phi_n \quad , \tag{33}$$

where ϕ_n satisfies Eq. (3) with ϕ_n' and $\rho\phi_n$ continuous at $z=H(r)$. The $\delta\phi_n$ is a function of order $\dot{H}$ that vanishes in the limit of horizontally stratified boundaries. Equations (3) and (33) in Eq. (31) yield a differential equation for $\delta\phi_n$.

$$\left(\frac{\partial^2}{\partial z^2} + k^2 - \sigma_n^2 \right) \delta\phi_n = \left(\sigma_n^2 - k_n^2 \right) \phi_n \quad . \tag{34}$$

The boundary conditions on $\delta\phi_n$ are obtained by using Eq. (33) in Eqs. (30) and retaining only terms of order $\dot{H}$. For a nonhorizontal boundary defined by $z=H(r)$ separating two fluids of densities ρ_1 and ρ_2, as shown in Fig. 1, the boundary conditions on $\delta\phi_n$ are found to be

$$\begin{aligned} \rho_1 \delta\phi_n^{(1)} &= \rho_2 \delta\phi_n^{(2)} \quad z=H(r) \\ \delta\phi_n'^{(1)} - \delta\phi_n'^{(2)} &= \frac{\dot{X}_n}{X_n} \dot{H}\, \phi_n^{(1)} \left(1 - \frac{\rho_1}{\rho_2} \right) \quad z=H(r) \end{aligned} \quad . \tag{35}$$

In Eq. (35) the superscripts 1 and 2 mean values of the function approached from above and below the interface at $z=H(r)$, respectively.

Equations (34) and (3) can be combined to give

$$\phi_m \, \delta\phi_n'' - \delta\phi_n \, \phi_m'' = \left(\sigma_n^2 - k_m^2 \right) \phi_m \, \delta\phi_n + \left(\sigma_n^2 - k_n^2 \right) \phi_n \, \phi_m \quad . \tag{36}$$

If Eq. (36) is multiplied by ρ and integrated over depth, the resulting equation is

$$\sum_i \rho_i \phi_m^{(i)} \left[\delta\phi_n'^{(i)} - \delta\phi_n'^{(i+1)} \right]_{z=H_i} = (\sigma_n^2 - k_m^2)\, I_{mn} + (\sigma_n^2 - k_n^2)\delta_{n,m} \quad . \tag{37}$$

where

$$I_{mn} = \int_0^\infty \rho\phi_m\, \delta\phi_n\, dz \quad . \tag{38}$$

In Eq. (37) the summation is over all sloping interfaces in the waveguide defined by $z=H_i(r)$. The superscripts i and i+1 denote values of the functions approached from above and below the interface $z=H_i(r)$. If Eq. (35) is used in Eq. (37), one obtains

$$\frac{\dot{X}_n}{X_n} \sum_i \dot{H}_i \rho_i \phi_m^{(i)}\, \phi_n^{(i)} \left(1 - \frac{\rho_i}{\rho_{i+1}}\right) \Big|_{z=H_i} = (\sigma_n^2 - k_m^2)\, I_{mn} + (\sigma_n^2 - k_n^2)\delta_{n,m} \quad . \tag{39}$$

The left-hand side of Eq. (39) can be simplified with the following expression

$$B_{mn}^S = -\frac{1}{2} \sum_i \dot{H}_i\, \rho_i \phi_m^{(i)}\, \phi_n^{(i)} \left(1 - \frac{\rho_i}{\rho_{i+1}}\right) \Big|_{z=H_i} \quad . \tag{40}$$

The function B_{mn}^S is the symmetric part of the coupling coefficient defined in Eq. (6). Equation (40) is a generalization to multiple interfaces of the result given in Appendix A. The use of Eq. (40) in Eq. (39) yields the result,

$$-2 \frac{\dot{X}_n}{X_n} B_{mn}^S = (\sigma_n^2 - k_m^2) I_{mn} + (\sigma_n^2 - k_n^2)\delta_{n,m} \quad . \tag{41}$$

For m=n Eq. (41) gives

$$\sigma_n^2 - k_n^2 = -2 \frac{\dot{X}_n}{X_n} B_{nm} + O(\dot{H}^2) \quad , \tag{42}$$

since $I_{mn} \propto O(\dot{H})$. For $m \neq n$ Eq. (41) gives

$$I_{mn} = \frac{-2\dot{X}_n B_{mn}^S}{X_n (k_n^2 - k_m^2)} \quad . \tag{43}$$

(In obtaining Eq. (43), $\sigma_n^2 = k_n^2 + O(\dot{H})$ was employed.)

Now return to Eq. (32) and use Eq. (33) to get

$$\sum_n \left(\ddot{X}_n + \frac{\dot{X}_n}{r} + \sigma_n^2 X_n\right)\phi_n = -\sum_n \left[\left(\ddot{X}_n + \frac{\dot{X}_n}{r} + \sigma_n^2 X_n\right)\delta\phi_n + \left(2\dot{X}_n + \frac{X_n}{r}\right)\left(\dot{\phi}_n + \delta\dot{\phi}_n\right) + X_n\left(\ddot{\phi}_n + \delta\ddot{\phi}_n\right)\right] \quad . \tag{44}$$

If Eq. (44) is multiplied by $\rho\phi_m$ and integrated over depth, one obtains

$$\ddot{X}_m + \frac{\dot{X}_m}{r} + \sigma_m^2 X_m = -\sum_n \left\{\left(2\dot{X}_n + \frac{X_n}{r}\right) B_{mn} + X_n A_{mn} + \left(\ddot{X}_n + \frac{\dot{X}_n}{r} + \sigma_n^2 X_n\right) I_{mn}\right\} \quad . \tag{45}$$

In obtaining Eq. (45), terms involving $\delta\dot{\phi}_n$ and $\delta\ddot{\phi}_n$ have been dropped since they are of order $\dot{H}^2$ and $\dot{H}^3$, respectively. Since a first order treatment of the field is desired, Eq. (45) may be further simplified by dropping some additional terms of order $\dot{H}^2$ and higher. To do this note that

$$\ddot{X}_n + \frac{\dot{X}_n}{r} + \sigma_n^2 X_n = 0 + O(\dot{H}) \quad ,$$

and

$$I_{mn} = O(\dot{H}) \quad . \tag{46}$$

With Eq. (46), Eq. (45) becomes

$$\ddot{X}_m + \frac{\dot{X}_m}{r} + k_m^2 X_m = (k_m^2 - \sigma_m^2) X_m - \sum_n \left\{\left(2\dot{X}_n + \frac{X_n}{r}\right) B_{mn} + X_n A_{mn}\right\} \quad . \tag{47}$$

If Eq. (42) is used in Eq. (47), the result is

$$\ddot{X}_m + \frac{\dot{X}_m}{r} + k_m^2 X_m = -\sum_{n\neq m} B_{mn}\left(\frac{X_n}{r} + 2\dot{X}_n\right) \tag{48}$$

where $X_n/r << 2\dot{X}_n$ has been assumed.

In Eq. (48) the coupling coefficient A_{mn} defined by Eq. (7) has been dropped. In situations in which the only range dependence of the medium is through sloping boundaries, A_{mn} is directly proportional to $\dot{H}^2$ and should be dropped in Eq. (47). If the medium has range dependent sound speed, for example, A_{mn} will have terms of order $\dot{c}^2$, $\dot{c}\dot{H}$, and $\dot{H}^2$. In this case

one is in principle entitled to retain the terms of order $\dot{c}^2$ and $\ddot{c}H$ in Eq. (48). Since values of $\dot{c}/c$ that one might expect for the ocean are of the same size or less than typical values of $\dot{H}/H$ on continental slopes, it is asserted that Eq. (48) is adequate even when there is range variation of the geoacoustic parameters of the waveguide.

It is interesting to note that the effect of requiring the boundary conditions to be satisfied to order $\dot{H}$ is to remove the diagonal elements of B_{mn} (compare with Eq. (2)). Equation (40) reveals that B_{mn} is completely off-diagonal only when $\dot{H}=0$ or when the sloping interfaces are pressure release with $\phi_n^{(i)}[z=H_i(r)]=0$. These two situations correspond to cases in which conventional coupled mode theory is capable of exactly satisfying the imposed boundary conditions. The occurrence of the diagonal elements of B_{mn} is therefore directly linked to the use of improper boundary conditions at sloping interfaces.

Return now to the equation for $\delta\phi_n$. Equation (42) when used in Eq. (34) yields

$$\left(\frac{\partial^2}{\partial z^2} + k^2 - \sigma_n^2\right)\delta\phi_n = -2\frac{\dot{X}_n}{X_n} B_{nn}\phi_n \quad . \tag{49}$$

Only the particular solution to Eq. (49) is desired since it is the one that vanishes as $\dot{H}$ goes to zero.

To summarize, a coupled mode theory expression for the field which satisfies the physically correct boundary conditions to first order in the bottom slope is given by the following

$$\psi(r,z) = \sum_n X_n(r)\ \Phi_n(z;r) \quad , \tag{50}$$

where X_n satisfies Eq. (48) and Φ_n, Eq. (31). Computation of the field using Eq. (50) as opposed to Eq. (1) is only slightly more complicated.

Solving for X_m is no more involved than solving for the R_m of conventional coupled mode theory. An added complication arises in the calculation of Φ_n since it entails the computation of two sets of functions ϕ_n and $\delta\phi_n$. However, the additional effort to calculate the $\delta\phi_n$ may not be as great as it first appears. An approximation to Eq. (49) may be obtained by ignoring the first order part of σ_n^2 and using a WKB approximation for $\dot{X}_n$ ($\dot{X}_n \simeq ik_n X_n$) to obtain

$$\left[\frac{\partial^2}{\partial z^2} + k^2 - k_n^2\right]\delta\phi_n = -2ik_n B_{nn}\phi_n \quad . \tag{51}$$

Once the ϕ_n and k_n are known, the $\delta\phi_n$ may be obtained by a routine integration of Eq. (51). The only eigenvalue problems to be solved will be for $\{k_n, \phi_n\}$ at whatever range values are required in the solution of Eq. (48).

A final point concerning calculation of the field using Eq. (50) is one of energy conservation. In Appendix B it is shown that the time rate of energy flow in the radial direction is a constant to first order in $\dot{H}$ for the field given by Eq. (50). Thus, the introduction of the corrections proposed here not only result in a theory which is valid to a specified order in $\dot{H}$, and in which the physically correct boundary conditions are satisfied, but also in a theory which properly conserves energy in the case of zero volume absorption.

IV. NUMERICAL CALCULATIONS

In this section some numerical calculations illustrating the major points of this paper are presented. The range variable waveguide model chosen for these calculations is the isovelocity wedge shown in Fig. 2. The surface at z=0 is taken as pressure release and the sloping bottom as a rigid reflector. For this waveguide structure the normalized depth functions of Eq. (3) are given by

$$\phi_n(z;r) = \sqrt{\frac{2}{H(r)}}\ \sin\left[\frac{\left(n + \frac{1}{2}\right)\pi z}{H(r)}\right] \quad . \tag{52}$$

For an initial depth of H_o = 500 m, a sound speed of 1.5 km/sec, and a frequency of 20 Hz, there are 13 propagating modes present at the source location.

Since the mode functions and coupling coefficients are known analytically, the main part of the numerical calculation involves computation of the radial functions of Eq. (48). To solve Eq. (48) an iterative procedure was employed in which Eq. (48) is replaced with

$$\ddot{X}_m^{(o)} + \frac{\dot{X}_m^{(o)}}{r} + k_m^2 X_m^{(o)} = 0 \tag{53}$$

$$\ddot{X}_m^{(i+1)} + \frac{\dot{X}_m^{(i+1)}}{r} + k_m^2 X_m^{(i+1)} = -\sum_{n \neq m} B_{mn} \left[\frac{X_n^{(i)}}{r} + 2\dot{X}_n^{(i)} \right] . \tag{54}$$

Equation (53) is the adiabatic approximation[9-12] to the set of coupled radial equations and Eq. (54) is an approximation to Eq. (48) in which the right-hand side is formed from the previous iterate. The iterative process of Eq. (54) is continued until the difference between two successive iterations is less than some specified tolerance. In the calculations presented here, convergence to four significant figures was required. The iterative procedure just described is very similar to one used in atomic physics applications to calculate quantum mechanical bound state[14] and scattering state[15] atomic wave functions.

In solving for the radial functions, the initial conditions for the X_m were obtained by matching to the known horizontally stratified radial functions at $r=r_s$ in Fig. 2. The field at the source was approximated as having only outgoing waves, and the radial functions are found to be proportional to Hankel functions of the first kind (for $e^{-i\omega t}$ time dependence).

$$X_m (r_s) \sim H_o^{(1)} \left(k_m (r_s)\, r_s \right) .$$

Figure 3 shows the result of a computation of the time rate of change of the total energy in the radial direction as a function of range using Eq. (B8). Also shown in Fig. 3 is the same calculation performed within the formalism of conventional coupled mode theory, employing the vanishing of $\partial\psi/\partial z$ at $z=H(r)$. The stair-step nature of the top curve in Fig. 3 is a consequence of the neglect of backscattered energy in solving for the radial functions. The abrupt drops in the top curve correspond to ranges at which a given mode reaches cutoff. With the neglect of the backscattered field one is examining only the time rate of change of energy flowing away from the source and this quantity abruptly changes whenever a mode drops out. The flat portion of the top curve in Fig. 3 between successive mode cutoff ranges indicates a constant rate of energy transport over regions having the same number of propagating modes. The small ripples in the top curve between successive mode cutoff ranges arise because of second and higher order terms that are retained through the use of Eq. (B8). Although the radial functions contain only zero and first order terms, the products of radial functions in Eq. (B8) give rise to terms of order $\dot{H}^2$ and $\dot{H}^3$ which cannot easily be removed. The dotted curve in Fig. 3 is a conventional coupled mode theory version of the solid curve. The nonconservation of energy effect is readily apparent.

Figure 4 shows the time rate of change of energy in the radial direction associated with mode No. 1. This was obtained from Eq. (B8) by eliminating the summation over n and taking n to be 1. In Fig. 4 the lower curve is a conventional coupled mode theory evaluation of the same quantity. Again, the nonconservation of energy is easily observed.

Figure 5 shows a comparison between the radial functions obtained from Eq. (48) and the adiabatic approximation to Eq. (48) for mode No. 0. In Fig. 5 the $1/\sqrt{r}$ range dependence has been removed. Note the changes in amplitude of the solid curve arising from energy interchange between modes, a process not present in adiabatic mode theory.

Figure 6 shows a comparison of ϕ_n and $\delta\phi_n$ for n=3. The curve for $\delta\phi_n$ was obtained from the approximation of Eq. (51) whose solution can be found analytically,

$$\delta\phi_n = i\sqrt{\frac{2}{H}}\frac{k_n B_{nn}}{\kappa_n}\left\{z\cos\kappa_n z - \frac{\sin\kappa_n z}{\kappa_n}\right\}$$

$$\kappa_n = \frac{\left(n+\frac{1}{2}\right)\pi}{H(r)} \quad .$$

The range at which the computations shown in Fig. 6 were performed was $r=r_s$ (see Fig. 2) which was taken to be 1.0 km.

Figure 7 depicts the absolute square of the velocity potential, which is proportional to the intensity, computed from Eq. (50) for the waveguide structure of Fig. 2. For this calculation the bottom slope was 5.0° and the source and receiver depths were 200 m and 100 m, respectively. Note the differences between the adiabatic and coupled mode descriptions of $\psi^*\psi$. Figure 8 shows the differences between the two curves in Fig. 7 plotted versus range. Though large differences between the two curves exist, the mean difference over the range of Fig. 8 is +0.083. This leads one to suspect that if a range averaged description of acoustic propagation is desired, then mode-mode coupling effects might become much less important or even insignificant.

Figure 9 shows the phases associated with the two velocity potentials used to generate Fig. 7. It should be noted that the adiabatic phase accurately

follows the phase of the field computed including mode-mode coupling. The approximate agreement of the two phases tends to support the conclusion of a previous publication[16] that the phase structure of the acoustic field is given quite accurately by the adiabatic approximation.

V. CONCLUSIONS

Two major conclusions may be drawn from this work. First, the conventional theory of sound propagation via coupled normal modes involves approximations that are inconsistent when the theory is applied to multiple fluid media having range variable boundaries. A consequence of this inconsistency is nonconservation of energy. Second, a correction to the conventional theory can be derived such that the field so obtained satisfies the physically proper boundary conditions to first order in the slope of range variable boundaries that are present. With these first order corrections, energy also becomes conserved to first order. For a more detailed account of some aspects of the work presented in this article, see Ref. 17.

The most important difference between the conventional theory and the corrected theory is the additional quantity $\delta\phi_n$ that must be computed. Depending on the type of application, the added computational difficulty imposed by the $\delta\phi_n$ may be negligible compared to the other calculations that must be performed, e.g., solving Eq. (48). The $\delta\phi_n$ are not needed until the field is to be constructed from the three components X_n, ϕ_n, and $\delta\phi_n$. This is not true of the ϕ_n which must be known as a function of range so that the coupling coefficients may be determined. Therefore, if one is interested in the field as a function of depth at one particular range, then only the $\delta\phi_n$ corresponding to that range need be calculated with a minimal increase in computational effort.

If the field as a function of range is desired, then the computation of the $\delta\phi_n$ can become more costly in terms of effort depending on the range grid on which the field is required to be computed. One particular type of calculation using the corrected theory that requires no extra computational effort arises in the computation of the random phase propagation loss defined by

$$|\psi|^2_{RP} \sim \sum_n X_n^* X_n \Phi_n \Phi_n^* \quad .$$

Since by approximation Eq. (51) $\delta\phi_n$ is pure imaginary, Eq. (56) to first order becomes

$$|\psi|^2_{RP} \sim \sum_n X_n^* X_n \phi_n \phi_n \quad ,$$

and the $\delta\phi_n$ need not be computed at all. This could be very significant for a variety of practical applications where only an estimate of average field level is desired.

ACKNOWLEDGMENTS

The authors gratefully acknowledge useful conversations with A. O. Williams, Jr., C. T. Tindle, C. W. Horton, Sr., and E. L. Hixson.

This work was supported by the Naval Ocean Research and Development Activity and the Naval Electronic Systems Command.

APPENDIX A

This appendix is devoted to the derivation of several equations appearing in Section II.

The rate of change of power radiated through the surface of a semi-infinite cylinder was found to be, (Eq. (15)),

$$\frac{\partial P}{\partial r} = -\pi\omega r \, \mathrm{Im}\left[\rho_1 \psi_1 \dot{H}\left(\dot{\psi}_1^* - \dot{\psi}_2^*\right)\right]. \tag{A1}$$

Upon introducing the partially separated solution, Eq. (1), one has

$$\frac{\partial P}{\partial r} = -\pi\omega r \, \mathrm{Im}\left\{\sum_{m,n}\left[\rho_1 \dot{H} R_n \dot{R}_m^* \phi_n^{(1)}\left(\phi_m^{(1)} - \phi_m^{(2)}\right) + \rho_1 \dot{H} R_n R_m^* \phi_n^{(1)}\left(\dot{\phi}_m^{(1)} - \phi_m^{(2)}\right)\right]\right\}, \tag{A2}$$

or,

$$\frac{\partial P}{\partial r} = \frac{1}{2} i\pi\omega r \sum_{m,n}\left[\rho_1 \dot{H}\left(R_n \dot{R}_m^* - \dot{R}_m R_n^*\right)\phi_n^{(1)}\left(\phi_m^{(1)} - \phi_m^{(2)}\right) + \rho_1 \dot{H}\left(R_n R_m^* - R_n^* R_m\right)\phi_n^{(1)}\left(\dot{\phi}_m^{(1)} - \dot{\phi}_m^{(2)}\right)\right]. \tag{A3}$$

Now, in the second term of Eq. (A3) we introduce the notation Q_{nm} for the quantity $R_n R_m^* - R_n^* R_m$, and in the first term, after interchanging the summation indices $\{n, m\}$, one finds,

$$\frac{\partial P}{\partial r} = \frac{1}{4} i\pi\omega r \sum_{m,n}\left[\rho_1 \dot{H}\left(R_n \dot{R}_m^* - \dot{R}_m R_n^*\right)\phi_n^{(1)}\left(\phi_n^{(1)} - \phi_m^{(2)}\right) + \rho_1 \dot{H}\left(R_m \dot{R}_n^* - \dot{R}_n R_m^*\right)\phi_m^{(1)}\left(\phi_n^{(1)} - \phi_n^{(2)}\right)\right] + \frac{1}{2} i\pi\omega r \sum_{m,n}\left[\rho_1 \dot{H} Q_{nm} \phi_n^{(1)}\left(\dot{\phi}_m^{(1)} - \dot{\phi}_m^{(2)}\right)\right]. \tag{A4}$$

Upon using the continuity relation $\rho_1\phi_n^{(1)} = \rho_2\phi_n^{(2)}$, the first term in Eq. (A4) can be rewritten to obtain

$$\frac{\partial P}{\partial r} = \frac{-1}{4} i\pi\omega r \sum_{m,n}\left\{\left[\rho_1 \dot{H} \phi_n^{(1)} \phi_m^{(1)}\left(1 - \rho_1/\rho_2\right)\right] P_{nm}\right\} + \frac{1}{2} i\pi\omega r \sum_{m,n}\left\{\left[\rho_1 \dot{H} \phi_n^{(1)}\left(\dot{\phi}_m^{(1)} - \dot{\phi}_m^{(2)}\right)\right] Q_{nm}\right\}, \tag{A5}$$

where we have introduced the notation P_{nm} for the combination of radial functions appearing in Eq. (A5) (see Section II). It now remains to express the two factors in brackets, $[\cdot]$, in terms of mode coupling coefficients.

The depth functions $\phi_n(z)$ have been assumed to form a complete orthonormal set obeying $\phi_n(0)=0$, continuity of $\rho\phi_n$ and ϕ_n' at the interface $z=H(\cdot)$, and a radiation condition as $z\to\infty$. The orthogonality relation for these functions can be differentiated with respect to r to obtain

$$\frac{\partial}{\partial r}\left\{\left[\rho_1\int_0^{H(r)} dz + \rho_2\int_{H(r)}^{\infty} dz\right]\ \phi_n\ \phi_m\right\} = \frac{\partial}{\partial r}\ \delta_{nm} = 0 \quad , \tag{A6}$$

thus

$$\rho_1\ \dot{H}\ \phi_n^{(1)}\ \phi_m^{(1)} - \rho_2\ \dot{H}\ \phi_n^{(2)}\ \phi_m^{(2)} + \int_0^{\infty} dz\ \rho\left(\phi_n\ \dot{\phi}_m + \dot{\phi}_n\ \phi_m\right) = 0 \quad . \tag{A7}$$

Upon introducing the definition of the B_{nm} into Eq. (A7), and using the continuity of $\rho\phi_n$, we have

$$\rho_1\ \dot{H}\ \phi_n^{(1)}\ \phi_m^{(1)}\left(1 - \rho_1/\rho_2\right) + B_{nm} + B_{mn} = 0. \tag{A8}$$

The desired result, Eq. (20), is thus obtained at once.

$$B^S_{nm} = \frac{-1}{2}\rho_1\ \dot{H}\ \phi_n^{(1)}\ \phi_m^{(1)}\left(1 - \rho_1/\rho_2\right) . \tag{A9}$$

It should be noted that the symmetric part of B_{nm} is proportional to $\dot{H}$. Thus, in cases such as those originally considered in Refs. 1 and 2, B_{nm} is indeed antisymmetric as claimed. The symmetric part of B_{mn} is also proportional to the density discontinuity; hence, it might therefore be anticipated that for small slopes and high porosity sediments, such as clays and silts, B^S_{nm} would be small.

The corresponding expression for the second term in Eq. (A5) can be obtained by differentiating the defining equation for $B_{nm}(r)$,

$$\frac{\partial B_{nm}}{\partial r} = \frac{\partial}{\partial r}\left\{\rho_1 \int_0^H dz\ \phi_n \frac{\partial \phi_m}{\partial r} + \rho_2 \int_H^\infty dz\ \phi_n \frac{\partial \phi_m}{\partial r}\right\} , \tag{A10}$$

which yields

$$\dot{B}_{nm} = \rho_1 \dot{H}\ \phi_n^{(1)}\ \dot{\phi}_m^{(1)} - \rho_2 \dot{H}\ \phi_n^{(2)}\ \dot{\phi}_m^{(2)} + \int_0^\infty dz\ \rho\left(\dot{\phi}_n\ \dot{\phi}_m + \phi_n\ \ddot{\phi}_m\right) , \tag{A11}$$

or, after introducing the definition of A_{nm},

$$\dot{B}_{nm} = \rho_1 \dot{H}\ \phi_n^{(1)}\left(\dot{\phi}_m^{(1)} - \dot{\phi}_m^{(2)}\right) + \int_0^\infty dz\ \rho\ \dot{\phi}_n\ \dot{\phi}_m + A_{nm} . \tag{A12}$$

Thus, the matrix $\dot{B}_{nm}-A_{nm}$ is given by,

$$\dot{B}_{nm} - A_{nm} = \rho_1 \dot{H}\ \phi_n^{(1)}\left(\dot{\phi}_m^{(1)} - \dot{\phi}_m^{(2)}\right) + \int_0^\infty dz\ \rho\ \dot{\phi}_n\ \dot{\phi}_m . \tag{A13}$$

It is easily seen that the second term on the right-hand side of Eq. (A13) is completely symmetric in (m,n), and consequently the desired antisymmetric matrix is given by

$$\left(\dot{B}_{nm} - A_{nm}\right)^A = \frac{1}{2}\rho_1 \dot{H}\left[\phi_n^{(1)}\left(\dot{\phi}_m^{(1)} - \dot{\phi}_m^{(2)}\right) - \phi_m^{(1)}\left(\dot{\phi}_n^{(1)} - \dot{\phi}_n^{(2)}\right)\right] , \tag{A14}$$

which is the result previously quoted in Eq. (19).

APPENDIX B

In this appendix it is shown that the rate of radial energy flow for the field given by Eq. (50) is a constant to first order in the bottom slope $\dot{H}$.

The time averaged radial energy flux is given by

$$J_r = \frac{1}{2} \, \mathrm{Re}\left[p \, v_r^*\right] \quad , \tag{B1}$$

where p is the acoustic pressure and v_r the radial particle velocity defined by

$$\begin{aligned} p &= i\omega\rho\psi \quad , \\ v_r &= \frac{\partial\psi}{\partial r} \quad . \end{aligned} \tag{B2}$$

In the following developments it is useful to remove the $1/\sqrt{r}$ dependence from the radial functions. In this appendix the field will be assumed to have the form

$$\psi = \sum_n \frac{G_n(r)}{\sqrt{r}} \, \Phi_n(z;r) \quad , \tag{B3}$$

where the equation for G_n is obtained from Eq. (48).

$$\ddot{G}_n + \left(k_n^2 + \frac{1}{4r^2}\right) G_n = -\sum_{\substack{m \\ m \neq n}} 2B_{nm} \, \dot{G}_m \quad , \tag{B4}$$

with $G_n(r) = \sqrt{r} \, X_n(r)$.

An expression for the time averaged radial energy flux may be obtained from Eq. (B1) through Eq. (B3).

$$J_r = \frac{-\omega\rho}{2r} \, \mathrm{Im}\left\{ \sum_{m,n} \left(G_n \, \dot{G}_m^* - \frac{G_m^* \, G_n}{2r} \right) \Phi_m^* \, \Phi_n + G_m^* \, G_n \, \Phi_n \, \dot{\Phi}_m^* \right\} \quad . \tag{B5}$$

The time rate of energy flow in the radial direction is obtained from Eq. (B5) by integrating over a cylindrical surface of radius r. This procedure yields the radial rate of energy flow, P.

$$P = \int_0^\infty 2\pi r \, J_r \, dz$$

$$P = -\omega\pi \, \mathrm{Im}\left\{\sum_{m,n}\left(G_n \dot{G}_m^* - \frac{G_m^* G_n}{2r}\right)\left(\delta_{n,m} + I_{nm}^* + I_{mn}\right) + G_m^* G_n B_{nm}\right\} . \quad \text{(B6)}$$

In Eq. (B6), I_{mn} is given by Eq. (43) and terms of higher order than $\dot{H}$ were neglected. If one uses the approximation $\dot{X}_n \approx (ik_n)X_n$ in Eq. (43), $I_{nm}^* + I_{mn}$ is seen to be pure imaginary. Therefore, Eq. (B6) becomes

$$P = \frac{i\omega\pi}{2}\left\{\sum_n\left(G_n \dot{G}_n^* - G_n^* \dot{G}_n\right) + \sum_{m,n}\left(G_n \dot{G}_m^* + G_n^* \dot{G}_m\right)\left(I_{nm}^* + I_{mn}\right)\right.$$

$$\left. + \sum_{m,n}\left(G_n G_m^* - G_n^* G_m\right) B_{nm}\right\} . \quad \text{(B7)}$$

In Eq. (B7) the terms $G_m^* G_n/2r$ were neglected in comparison to $G_n \dot{G}_m^*$. If $\dot{G}_n \approx ik_n G_n + O(\dot{H})$ is used in the second and third terms of Eq. (B7), the result is

$$P = \frac{i\pi\omega}{2}\left\{\sum_n\left(G_n \dot{G}_n^* - G_n^* \dot{G}_n\right) + \sum_{m,n}\left(G_n G_m^* - G_n^* G_m\right)\left[B_{nm} - ik_m\left(I_{nm}^* + I_{mn}\right)\right]\right\} . \quad \text{(B8)}$$

In Eqs. (B6) and (B7) the approximation $\dot{X}_n = ik_n X_n$ was employed. This approximation gives an expression for $\dot{X}_n$ that is correct through terms of zero order in $\dot{H}$ and is appropriate whenever terms of first order in $\dot{H}$, such as B_{mn}, occur as multiplicative factors of $\dot{X}_n$. This approximation may be viewed as a WKB expression for the derivative of the forward going component of the adiabatic solution of the radial equation. The backscattered

component can be shown to be of order $\dot{H}$ compared to the forward going component and is ignored.

To show that P is independent of range, Eq. (B8) is differentiated with respect to range. This yields

$$\dot{P} = \frac{i\pi\omega}{2}\left\{\sum_n \frac{d}{dr}\left(G_n \dot{G}_n^* - G_n^* \dot{G}_n\right)\right.$$

$$\left. + \sum_{n,m} i\left(k_n - k_m\right)\left(G_n G_m^* + G_n^* G_m\right)\left[B_{nm} - ik_m\left(I_{nm}^* + I_{mn}\right)\right]\right\} \quad . \tag{B9}$$

In obtaining Eq. (B9) terms of order $\dot{H}$ were not differentiated since they would produce quantities of order $\dot{H}^2$. From Eq. (B4) it follows that

$$\frac{d}{dr}\left(G_n \dot{G}_n^* - G_n^* \dot{G}_n\right) = \sum_{\substack{m \\ m\neq n}} 2B_{nm}\left(G_n^* \dot{G}_m - G_n \dot{G}_m^*\right) \tag{B10}$$

Equation (B10), (B9) gives

$$\dot{J}_r = \frac{i\pi\omega}{2}\left\{\sum_{\substack{n,m \\ n\neq m}} 2B_{nm}\, ik_m\left(G_n^* G_m + G_n G_m^*\right)\right.$$

$$\left. + \sum_{n,m} i\left(k_n - k_m\right)\left[B_{nm} - ik_m\left(I_{nm}^* + I_{mn}\right)\right]\left(G_n^* G_m + G_n G_m^*\right)\right\} \quad . \tag{B11}$$

If one uses the WKB approximation in Eq. (43), $I_{nm}^* + I_{mn}$ is seen to be

$$I_{mn} + I_{nm}^* = \frac{-2i\, B_{mn}^S}{k_n - k_m} \quad . \tag{B12}$$

The use of Eq. (B12) in Eq. (B11) yields

$$\dot{J}_r = \frac{i\pi\omega}{2}\left\{\sum_{\substack{n,m \\ n\neq m}} i\left(k_n - k_m\right) B_{mn}^S \left(G_n G_m^* + G_n^* G_m\right)\right\} \quad . \tag{B13}$$

Equation (B13) vanishes by virtue of the symmetry properties of the quantity being summed. Therefore, $\dot{P}$ is zero through terms of order $\dot{H}$,

$$\dot{J}_r = 0 + O\left(\dot{H}^2\right) \quad . \tag{B14}$$

REFERENCES

[a] Based in part on a Ph.D. dissertation submitted by S. R. Rutherford to The University of Texas at Austin.

[1] A. D. Pierce, "Extension of the method of normal modes to sound propagation in an almost-stratified medium," J. Acoust. Soc. Am. 37, 19-27 (1965).

[2] D. M. Milder, "Ray and wave invariants for SOFAR channel propagation," J. Acoust. Soc. Am. 46, 1259-1263 (1969).

[3] F. S. Chwieroth, A. Nagl, H. Überall, R. D. Graves, and G. L. Zarur, "Mode coupling in a sound channel with range-dependent parabolic velocity profile," J. Acoust. Soc. Am. 64, 1105-1112 (1978).

[4] S. T. McDaniel, "Coupled power equations for cylindrically spreading waves," J. Acoust. Soc. Am. 60, 1285-1289 (1976).

[5] S. T. McDaniel, "Mode conversion in shallow-water sound propagation," J. Acoust. Soc. Am. 62, 320-325 (1977).

[6] S. T. McDaniel, "Calculation of mode conversion rates," J. Acoust. Soc. Am. 63, 1372-1374 (1978).

[7] L. B. Dozier and F. D. Tappert, "Statistics of normal mode amplitudes in a random ocean, I. Theory," J. Acoust. Soc. Am. 63, 353-365 (1978).

[8] L. B. Dozier and F. D. Tappert, "Statistics of normal mode amplitudes in a random ocean, II. Computations," J. Acoust. Soc. Am. 64, 533-547 (1978).

[9] S. R. Rutherford and K. E. Hawker, "An examination of the influence of the range dependence of the ocean bottom on the adiabatic approximation," J. Acoust. Soc. Am. 66, 1145-1151 (1979).

[10]R. D. Graves, A. Nagl, H. Überall, and G. L. Zarur, "Range-dependent normal modes in underwater sound propagation: application to the wedge-shaped ocean," J. Acoust. Soc. Am. 58, 1171-1177 (1975).

[11]A. Nagl, H. Überall, A. J. Haug, and G. L. Zarur, "Adiabatic mode theory of underwater sound propagation in a range-dependent environment," J. Acoust. Soc. Am. 63, 739-749 (1978).

[12]R. D. Graves, A. Nagl, H. Überall, and G. L. Zarur, "Normal modes in a sound channel with range dependent parabolic sound speed profile," Acustica 39, 173-181 (1978).

[13]As to the questions of units, in a solution to the inhomogeneous wave equation having a source term $-4\pi\delta(\underline{r}-\underline{r}_o)$, a constant having the units of L^3T^{-1} and unit magnitude is conventionally suppressed. Furthermore, a factor of $\rho(z_o)$ appears multiplying the normal mode solution, and this too is often ignored because sources are generally located in the water where $\rho\approx 1$. Bearing these comments in mind, the units in Eq. 10 are correct.

[14]C. Froese, "Numerical solution of the Hartree-Fock equations," Can. J. Phys. 41, 1895-1910 (1963).

[15]T. L. John, "The numerical solution of the exchange equation for slow electron collisions with hydrogen atoms," Phys. Soc., LXXVI, (July-December 1960), 532-538.

[16]S. R. Rutherford, "An examination of multipath processes in a range dependent ocean environment within the context of adiabatic mode theory," J. Acoust. Soc. Am. 66, 1482-1486 (1979).

[17]S. R. Rutherford, "An examination of coupled mode theory as applied to underwater sound propagation," Applied Research Laboratories Technical Report No. 79-44 (ARL-TR-79-44), Applied Research Laboratories, The University of Texas at Austin (1979).

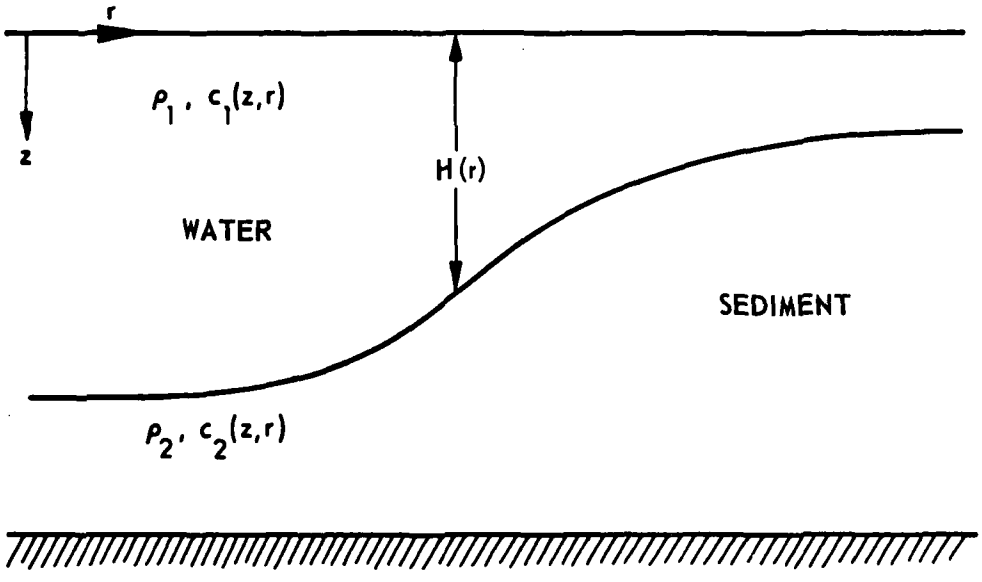

FIGURE 1
WAVEGUIDE STRUCTURE WITH SLOPING WATER-SEDIMENT INTERFACE

ARL:UT
AS-79-1949-P
SRR - GA
9 - 13 - 79

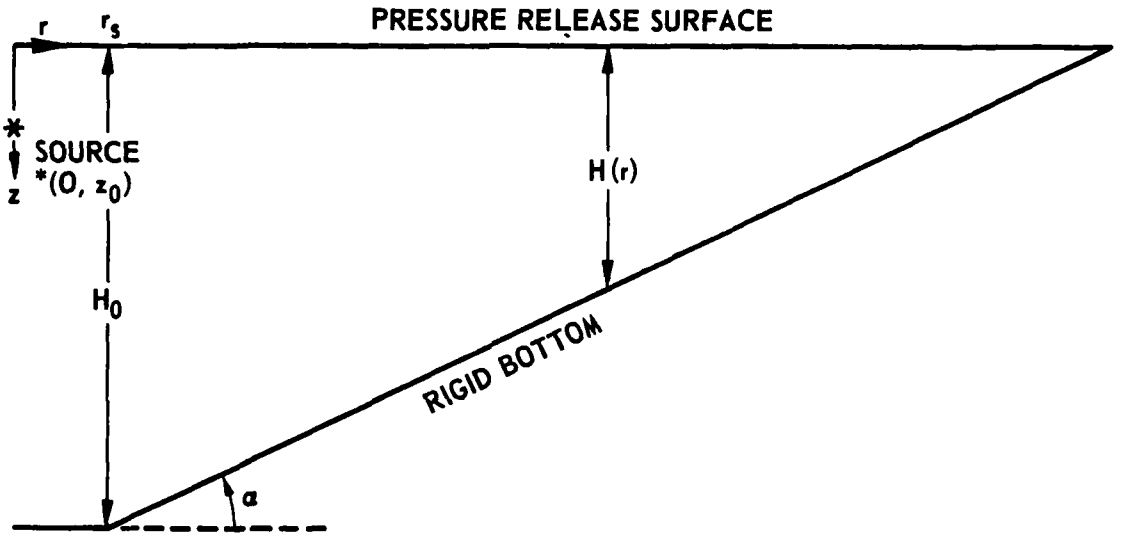

FIGURE 2
ISOVELOCITY WEDGE SHAPED WAVEGUIDE
ASSUMED FOR NUMERICAL COMPUTATIONS
c = 1500 m/sec, H_0 = 500 m

ARL:UT
AS-79-1950-P
SRR - GA
9 - 13 - 79

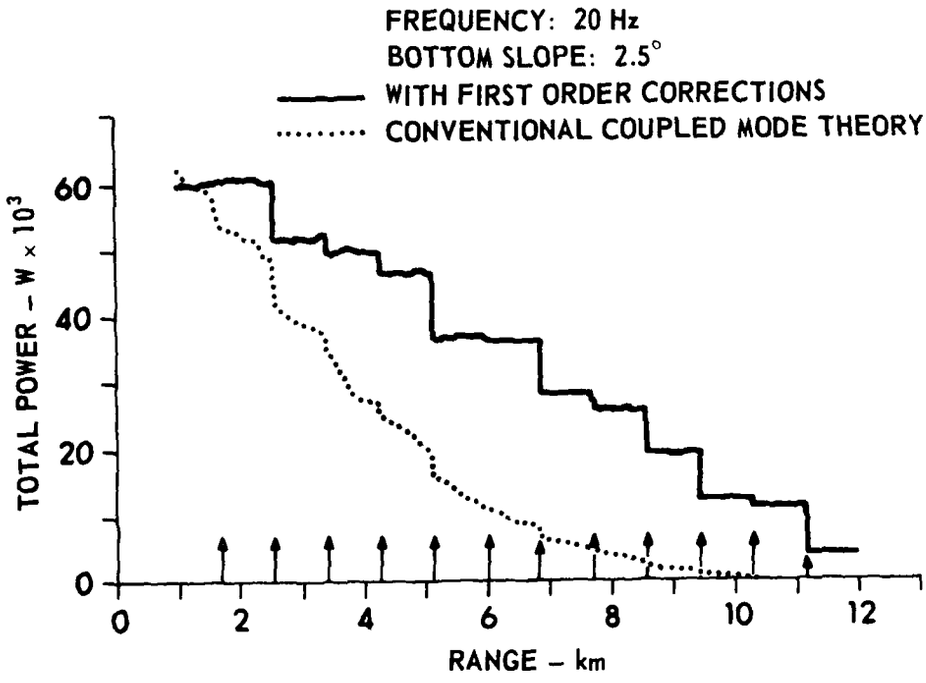

FIGURE 3

TOTAL POWER TRANSPORTED IN RADIAL DIRECTION (W) versus RANGE

THE ARROWS DENOTE MODE CUTOFF RANGES
SOURCE STRENGTH = 1 m^3/sec, SOURCE DEPTH = 200 m

ARL:UT
AS-79-1951-P
SRR - GA
9 - 13 - 79

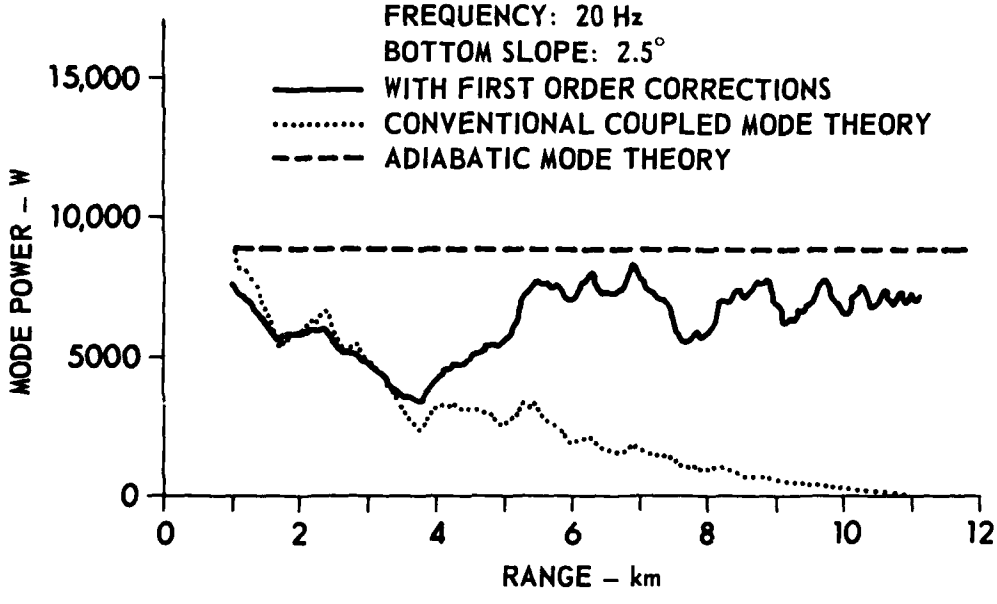

FIGURE 4
POWER TRANSPORTED BY MODE 1 (W) versus RANGE
SOURCE STRENGTH = 1 m^3/sec, SOURCE DEPTH = 200 m

ARL:UT
AS-79-1952-P
SRR- GA
9-13 -79

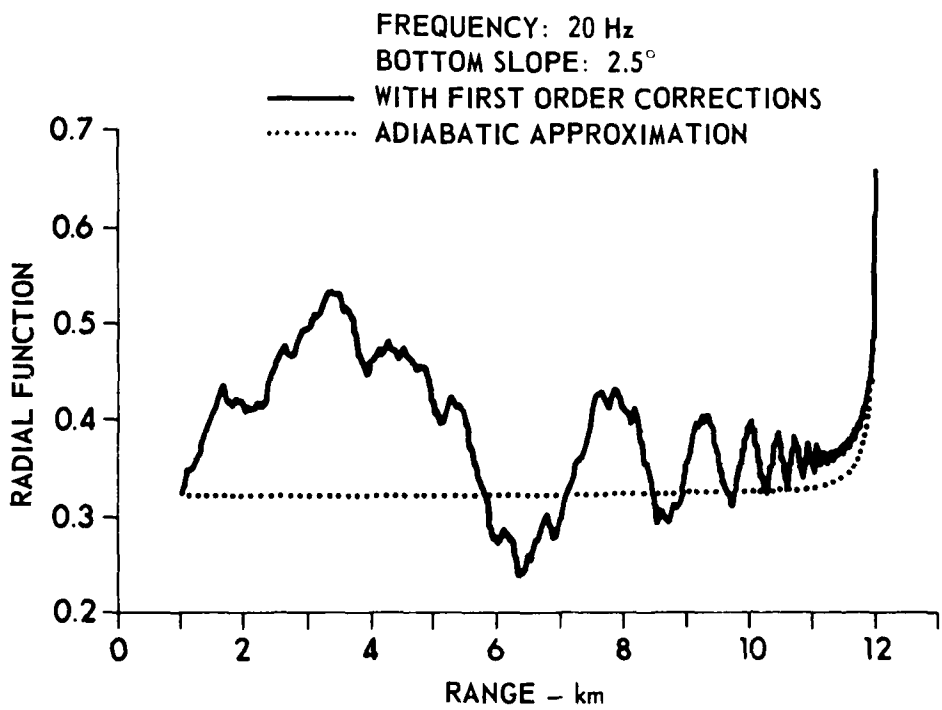

FIGURE 5
REDUCED RADIAL FUNCTION ($\sqrt{rX_n}$)
FOR MODE 0 versus RANGE
SOURCE STRENGTH 1 m^3/sec,
SOURCE DEPTH 200 m

ARL:UT
AS-79-1953-P
SRR- GA
9-13-79

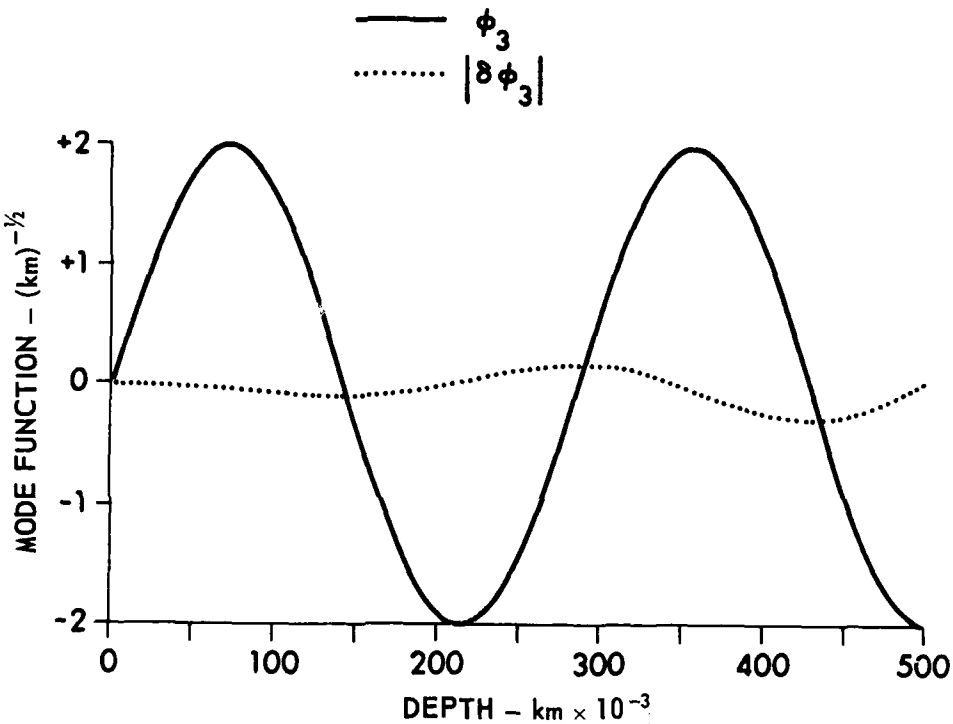

FIGURE 6
DEPTH FUNCTION AND CORRECTION
TO DEPTH FUNCTION versus DEPTH
RANGE = 1 km, FREQUENCY = 20 Hz
BOTTOM SLOPE = 2.5°

ARL:UT
AS-79-1954-P
SRR - GA
9 - 13 - 79

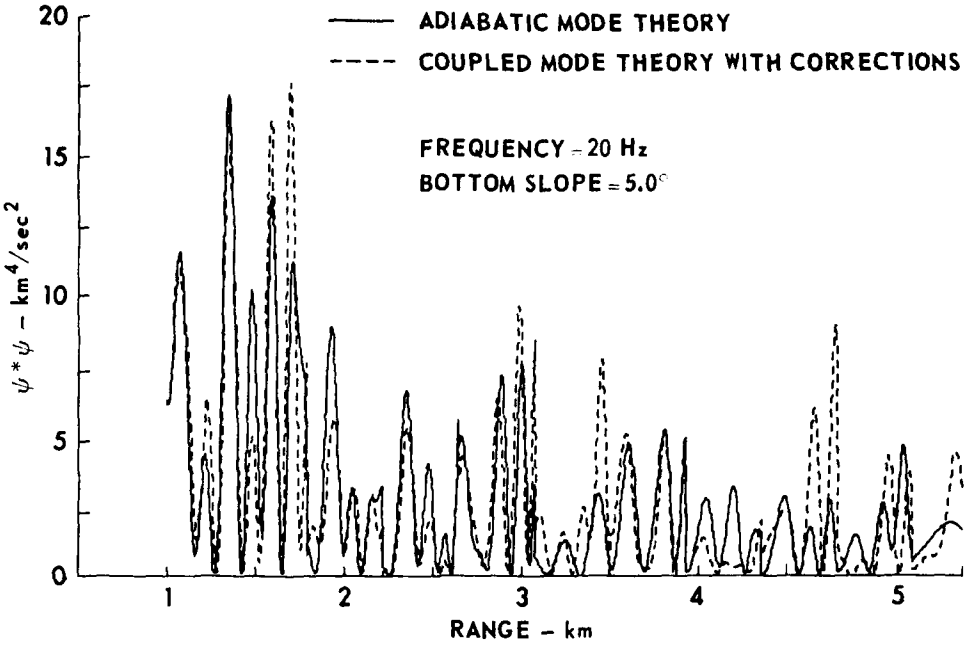

FIGURE 7
ABSOLUTE SQUARE OF VELOCITY POTENTIAL versus RANGE
SOURCE STRENGTH = 1 m^3/sec, SOURCE DEPTH = 200 m

ARL:UT
AS-79-796-P
SRR - GA
10 - 17 - 79

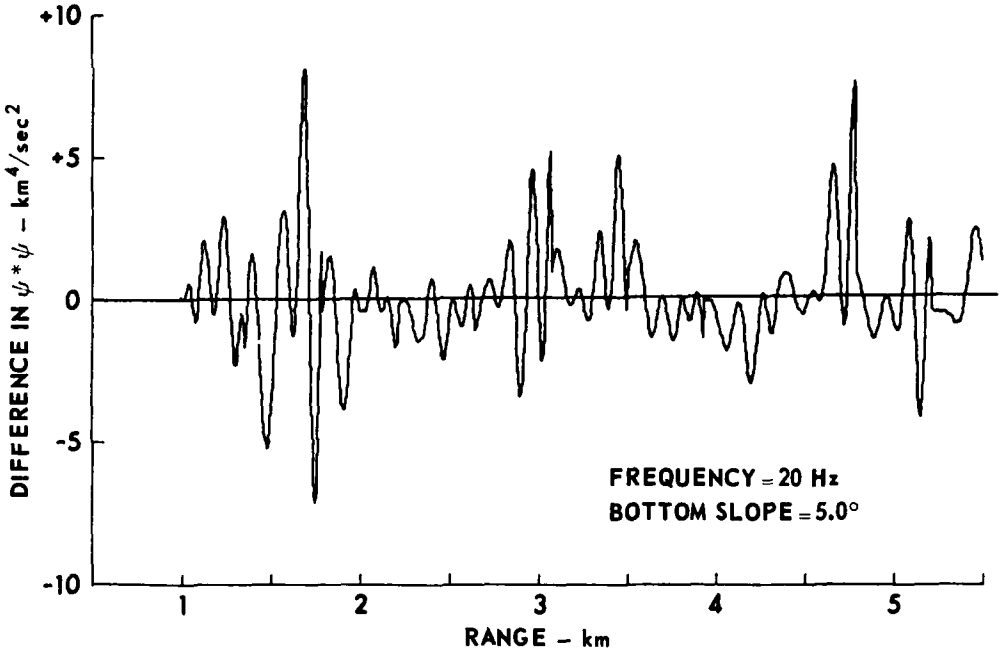

FIGURE 8
DIFFERENCE BETWEEN TWO CURVES OF Fig. 7 versus RANGE

ARL:UT
AS-79-798-P
SRR - GA
10 - 17 - 79

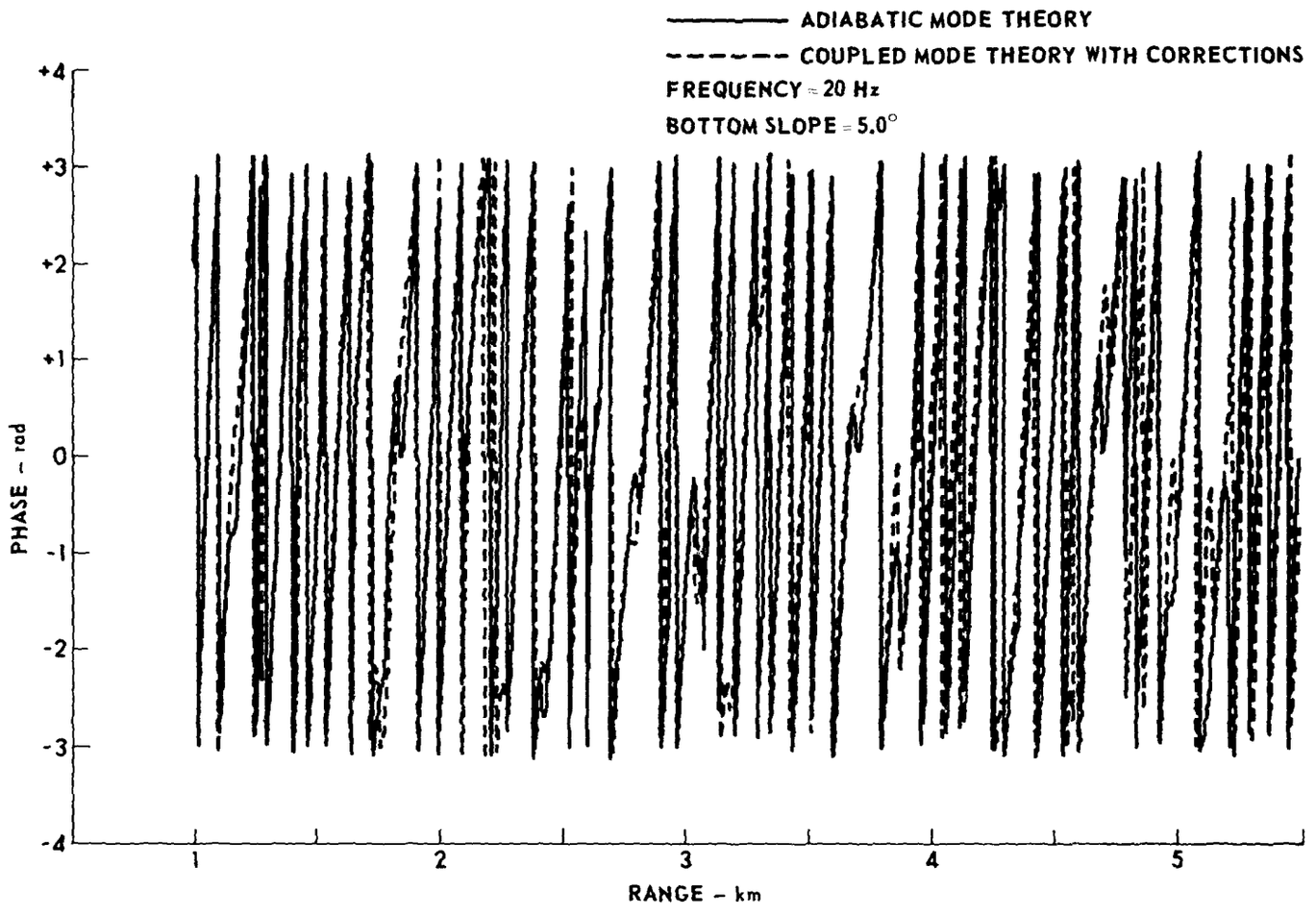

FIGURE 9
PHASE OF VELOCITY POTENTIALS USED TO PRODUCE Fig. 7 versus RANGE

APPENDIX B

THE EFFECT OF SEDIMENT RIGIDITY ON BOTTOM REFLECTION LOSS IN A TYPICAL DEEP SEA SEDIMENT

by

Paul J. Vidmar

Paper submitted to The Journal of The Acoustical Society of America for publication

The effect of sediment rigidity on bottom reflection loss in a typical deep sea sediment

Paul J. Vidmar, Applied Research Laboratories, The University of Texas at Austin, Austin, TX 78712

(Received

The effect of sediment rigidity on bottom reflection loss, RL = $-20 \log_{10}|R|$ where R is the plane wave reflection coefficient, is studied using a computational model. A single inhomogeneous turbidite layer overlying a homogeneous substrate is treated with an emphasis on low frequencies (10 to 200 Hz) and low grazing angles (0° to 45°). We find that sediment rigidity can be neglected for thick layers (~500 m) while it can produce significant increases in RL for thin layers (~36 m). The frequency dependence of RL for thin layers has a low frequency regime characterized by large peaks (~25 dB) recurring at short (~2 Hz) intervals. At high frequencies there remains a persistent increase in RL (~4 dB). The most important mechanism for sediment S wave excitation is found to be compressional wave conversion at the sediment-substrate interface.

PACS numbers: 43.20.Fn 43.30.Dr

I. INTRODUCTION

The acoustic interaction with the ocean bottom is an important factor in determining the propagation of low frequency sound waves in the oceans. Because of the long wavelengths involved, the acoustic energy penetrates into the ocean bottom and interacts with the subbottom structure. The compressional (P), shear (S), and interface waves excited in the sediment-substrate structure are important energy loss mechanisms influencing low frequency sound propagation in the oceans. A useful and traditional measure of this bottom interaction is the plane wave reflection coefficient R and its analog the reflection loss, $RL = -20 \log_{10}|R|$.

Theoretical studies for an assumed fluid sediment, using numerical models to compute R, have investigated the influence of several subbottom features on RL at low frequencies. Density gradients[1] and the roughness of the water-sediment interface[2] have a negligible effect for typical deep sea sediment types. The effect of P wave speed[3,4] and absorption[5] profiles have also been treated. Stoneley wave excitation at the interface between the (fluid) sediment and a (solid) substrate has been identified as a loss mechanism.[6,7]

The effect of sediment rigidity (shear wave propagation) on R has received little attention and is not well understood. Although included in some numerical models,[8,9] no systematic studies have been made to determine the importance of energy lost to sediment S waves. A detailed study at this time would be useful since parameter ranges can now be constrained by estimates of sediment S wave properties that have recently become available.[10-12] Such a study is important because the relatively high attenuation of sediment S waves make their excitation a potentially important energy loss mechanism. Recent work[13,14] indicates that sediment S wave excitation can be the dominant energy loss mechanism is thin sediment layers.

In this paper we investigate the effect of sediment rigidity on R for a typical deep sea subbottom structure composed of a single inhomogeneous turbidite layer overlying a homogeneous basalt substrate. Our emphasis is on, but not restricted to, low grazing angles and low frequencies. The effect of sediment rigidity is determined by comparing RL for a solid sediment and a fluid sediment. The difference between them, ΔRL, is due to sediment rigidity. We find that the dependence of ΔRL on the thickness of the sediment layer leads to an empirical classification of sediments into "thick" and "thin" categories. For a thick (518 m) layer $\Delta RL \simeq 0$ at low grazing angles and sediment rigidity can be neglected. For a thin (36 m) layer at a grazing angle of 20°, $\Delta RL \sim 20$ dB at 20 Hz and $\Delta RL \simeq 4$ dB at 200 Hz; sediment rigidity in this case is not negligible but produces significant increases in RL. The frequency dependence of RL for the 36 m thick layer reveals high and low frequency regimes with strikingly different behavior. For a grazing angle of 20°, ΔRL is about 2 dB at low frequencies with very large peaks (~25 dB) occurring at 2 Hz intervals. The peaks decrease in magnitude at higher frequencies until they entirely disappear. At high frequencies there remains a persistent 4 dB increase in RL compared to that computed for a fluid sediment. Our study suggests that the mechanism for sediment S wave excitation is primarily P wave conversion at the sediment-substrate interface. The gradient-driven P-S conversion is negligible for these sediment types for frequencies above about 3 Hz.[15] This excitation mechanism explains the classification of sediment layers into thick and thin categories. For a thick sediment the P wave has its turning point well above the sediment-substrate interface. Consequently, sediment S wave excitation is negligible and the sediment can be accurately treated as a fluid. For a thin sediment the P wave significantly interacts with

the substrate. Shear waves are excited in the sediment, and the sediment must be treated as a solid.

The separation into high and low frequency regimes in thin layers is due to interference effects related to S wave propagation within the sediment. At low frequencies sediment shear wave attenuation is small and interference effects will dominate the dependence of R on frequency. Large peaks in RL will occur with a separation in frequency related to changes in S wave phase of 2π. At higher frequencies the increased shear wave attenuation decreases the magnitude of this peak structure. At high frequencies S waves excited at the sediment-substrate interface are totally absorbed within the sediment, resulting in an almost constant additional loss compared to the RL of a fluid sediment.

The tool used in this study is a recently developed computational model[15] of R which allows sediment shear wave propagation. The model assumes horizontal stratification and treats a single sediment layer overlying a semiinfinite homogeneous substrate. The model is based on numerical integration of the depth-separated wave equations for the potentials giving rise to the compressional and shear waves in the sediment and thus includes all wave properties such as penetration beyond turning points, boundary wave excitation, etc. The use of numerical integration permits arbitrary depth variations of sediment parameters and allows them to be individually varied to determine their influence on R. The basic approximation in the model is the use of the Helmholtz equations with depth dependent wave number to describe the potentials. This is esentially a high frequency approximation in which the continuous coupling between shear and compressional waves and effects directly dependent on gradients are neglected. For parameters typical of deep sea sediments, this model is accurate for frequencies above about 10 Hz.

II. REFLECTION LOSS OF A HYPOTHETICAL TURBIDITE LAYER

In this section we consider the effect of sediment rigidity on the reflection loss from a hypothetical turbidite layer. RL is studied as a function of grazing angle θ, frequency f, and sediment layer thickness H (the grazing angle is the complement of the angle of incidence γ, i.e., $\theta = 90 - \gamma$).

The depth structure of the turbidite layer is given in Table I. These parameters were obtained from the recent work of Fryer.[9] Constant gradients are assumed between the depths given in Table I. The parameter values and gradients of this depth structure are representative deep sea turbidite layers. The attenuation is assumed to depend linearly on frequency.[11] For our computational model it was necessary to truncate Fryer's 650 m sediment layer at 518 m to produce accurate results at low grazing angles for a frequency of 20 Hz. For a significantly thicker layer (650 m) the large S wave attenuation combines with the finite computer word length to produce a loss of precision for grazing angles below about 20°.

Figure 1 shows RL as a function of θ for f = 20 Hz and H = 518 m. The three curves were obtained for different sediment-substrate configurations. The dotted line was obtained for a fluid sediment and fluid substrate (the FF case), the dashed line for a fluid sediment and solid substrate (the FS case) and the solid line for a solid sediment and solid substrate (the SS case). The remaining case of a solid sediment and a fluid substrate (the SF case) is not shown in Fig. 1. It is essentially identical to the FF case over the entire range of grazing angles, frequencies, and sediment thicknesses considered. The parameters for the fluid sediment and substrate were obtained from Table I by ignoring the S wave parameters.

A comparison of the curves of Fig. 1 shows the effect of sediment rigidity in this thick layer. Case FF has the expected small RL for small θ followed by an oscillatory structure due to interference between the wave directly reflected from the water-sediment interface and the P wave refracted in the sediment and returning to the water. Beyond the critical angle for substrate P wave propagation ($\theta_p \simeq 70°$) RL increases as energy is carried away by substrate P waves. A comparison of the FS and FF cases shows the effect of substrate rigidity alone. At both small and large grazing angles the FS and FF cases are nearly identical showing that substrate rigidity has a negligible effect at these angles. RL, however, increases between the critical angle for substrate S wave propagation, θ_s, and θ_p. Substrate S waves carry away additional energy in this angular range. Comparing the SS and FS cases shows the additional effects of sediment rigidity. Except for grazing angles between θ_s and θ_p, sediment S wave propagation has a negligible effect on RL. The major effect between the critical angles is a shift in the peak structure.

Comparison of Fig. 1 with Fryer's[9] Fig. 8 shows qualitative agreement between the corresponding FF and SS cases. Fryer obtained his result using a different computational technique and for a thicker (650 m) sediment layer. Our computation of the intermediate FS case allows us to draw the conclusion that for this particular subbottom structure sediment rigidity is negligible at low grazing angles and for a frequency of 20 Hz.

Figure 2 shows RL for a thinner sediment layer, H = 252 m, at f = 20 Hz. The FS and SS cases are shown. Comparison of the solid (SS) and dashed (FS) curves shows that the presence of sediment rigidity produces the expected shift in the oscillatory structure between the critical angles θ_s and θ_p. In addition, the SS case has an increased RL beginning at a minimum grazing

angle, $\theta_o \simeq 24°$, and extending up to about 45°. This increase in RL is entirely due to sediment rigidity. For grazing angles below θ_o the effect of sediment rigidity is negligible.

Figure 3 shows RL for the 252 m layer as a function of frequency at $\theta = 20° < \theta_o$ for the frequency range from 10 to 100 Hz. A comparison of the SS and FS cases shows that for frequencies above 15 Hz sediment rigidity is negligible. Below 15 Hz the difference between the curves may not be meaningful since this is near the low frequency limit of the validity of our computational model.

A consideration of RL as a function of θ for sediment thicknesses less than 252 m reveals a relationship between H and θ_o. As H decreases, θ_o also decreases. Thus, as sediment thickness decreases, sediment rigidity causes changes in RL at steadily lower grazing angles. In fact, sediment S wave excitation can be the dominant energy loss mechanism in thin sediment layers. This is illustrated in Fig. 4, which compares RL for the SS and FS case at H = 36 m and f = 20 Hz. The angle θ_o is 0°. Sediment S wave excitation is responsible for the dramatic 20 dB increase in RL near $\theta = 12°$.

These results lead to an empirical classification of sediments into thick and thin layers based on the effect of sediment rigidity. For thick sediments little energy is transferred to sediment S waves and the sediment can accurately be treated as a fluid at low grazing angles. For a thin sediment significant energy can appear in sediment S waves. Sediment rigidity is not negligible and the sediment must be treated as a solid.

The dependence of RL on frequency for the same 36 m layer is shown in Fig. 5. The SS and FS cases are compared from 10 to 200 Hz at $\theta = 20°$. The SS case has high and low frequency regimes with strikingly different properties. At low frequencies the effects of sediment rigidity increase

the level of RL, relative to the FS case, by about 3 dB with additional very large peaks of up to 25 dB. The peaks repeat with an almost constant separation of 2.65 Hz. The magnitude of the peaks generally decrease with increasing frequency; however, any individual peak may be higher or lower than neighboring peaks. The peaks disappear by about 90 Hz and the high frequency regime, characterized by rather broad oscillations in RL, begins. The maxima of these broad oscillations are separated in frequency by about 65.5 Hz and occur in both the SS and FS cases. In this high frequency regime, sediment S wave excitation produces an almost constant increase in RL of about 4 dB.

The large peaks in the low frequency regime of Fig. 5 are associated with interference effects due to sediment S wave propagation. This identification is made by noting that the frequency interval between peaks is related to S wave parameters. One expects interference effects to recur when the relative phase of the waves involved change by 2π. The phase of the S wave, accumulated in traveling through the sediment and back, changes by 2π for a frequency change $\Delta f \simeq v_2/2H$, where v_2 is the average sediment S wave speed (the sediment shear speed is so small that the S wave propagates nearly normal to the plane of stratification). The measured separation between peaks is within 5% of the estimated value of Δf. The corresponding quantity for P waves (including the grazing angle correction) estimates a frequency change of 65.4 Hz which is a factor of 30 too large to explain the peak separation. In addition, the decrease in peak height with frequency appears to be related to the increased attenuation of S waves with frequency. At 90 Hz the attenuation is estimated to be 23 dB for an S wave traveling one way through the sediment. This suggests that S wave interference would be negligible above 90 Hz as observed in Fig. 5.

The gentle oscillations above 90 Hz in Fig. 5 are due to P wave interference effects. This conclusion is reached because the same oscillations are observed in both the SS and FS cases. The measured separation between maxima is 65.5 Hz which agrees very well with the estimated Δf = 65.4 Hz.

Figure 6 shows that sediment rigidity is still significant in the high frequency regime. The SS and FS cases are compared at H = 36 m and f = 200 Hz. The increase in RL due to sediment S wave excitation is significant (~4 dB) between 15° and 30°. The minimum angle, θ_o, is about 5°.

Inspection of Fig. 5 near 20 Hz shows that the very large increase in RL seen in the SS case in Fig. 4 is due to the fortuitous location of one of the interference peaks at 20 Hz. For comparison with Fig. 4, RL at 21 Hz (a minimum in RL) is given in Fig. 7. The increase in RL due to sediment S wave excitation is still present at low angles but its magnitude is 2 dB rather than 20 dB. This is still an important increase in RL when compared to the RL≈0 in the fluid sediment case.

The dependence of θ_o on H gives an indication of the physical mechanism responsible for the increase in RL due to sediment rigidity. For a given grazing angle the compressional wave in the sediment has a turning point at a depth H_t. For a thick sediment layer H_t will be well above the sediment-substrate interface. As the grazing angle increases, H_t increases. At some critical angle θ_c, $H_t \approx H$ and the compressional wave interacts with the sediment-substrate interface. As the thickness of the sediment layer decreases, the angle θ_c also decreases. This is the same qualitative behavior exhibited by the angle θ_o, above which sediment rigidity causes an increase in RL. This similarity suggests that sediment shear wave excitation by compressional wave conversion at the sediment-substrate interface produces the increase in RL.

Two other observations support this identification of P wave conversion at the sediment-substrate interface as the dominant mechanism for sediment S wave excitation. One concerns the negligible influence of the water-sediment interface while the other shows the importance of the substrate interface. S wave excitation at the water-sediment interface appears to be negligible. The properties of the water interface remained constant while the sediment thickness varied and large changes in RL due to sediment rigidity occurred. This suggests the lack of a casual relationship between the constant water-sediment interface conditions and the significantly increased RL. The importance of the substrate interface is further indicated by the negligible difference between RL for the FF and SF cases and the large changes seen between the SS and FS cases. This indicates that the nature of the substrate is important. Since the substrate parameters enter our model only through the sediment-substrate interface conditions, this also indicates that sediment S waves originate at the substrate interface.

III. SUMMARY

A study of the effect of sediment rigidity on bottom reflection loss (RL) from typical deep sea sediment types shows that sediment shear (S) wave excitation is important for thin sediment layers but is negligible for thick layers. The major mechanism for S wave excitation is compressional (P) wave conversion at the sediment-substrate interface. Little energy is coupled into S waves at the water-sediment interface.

The mechanism for S wave excitation provides a means for quantifying the categories of thick and thin layers. It is the amplitude of the P wave at the substrate interface that matters. If the P wave amplitude at the substrate interface is significant, the layer is thick; if it is small, the layer is thin. In general there is a grazing angle θ_o separating

a low angle region in which the P wave turning point is well above the substrate from a high angle region in which the P wave strikes the substrate interface or has a turning point near the interface. For angles less than θ_o the layer is thick and S wave effects are negligible. For angles greater than θ_o the layer is thin and S wave effects produce significant increases in RL. For physically thick layers θ_o is large and S wave effects are negligible for all grazing angles, except for a shift in the peak structure between the critical angles for substrate S and P wave propagation. For physically thin layers θ_o can be 0° and sediment rigidity will be particularly important at low grazing angles.

For thin layers the dependence of RL on frequency shows the existence of high and low frequency regimes. The total attenuation of the S wave traveling one way through the sediment provides a means of separating these frequency regimes. For total S wave attenuation greater than 20 dB an S wave generated at the substrate interface is essentially absorbed within the sediment without striking the other interface. Since we assume attenuation is proportional to frequency, this defines a high frequency regime in which the propagation of sediment S waves can be neglected; however, their excitation is still an important loss mechanism. At low frequencies S wave attenuation is less than 20 dB across the layer and the additional interference effects due to the propagation of S waves through the sediment are important. Very large peaks in RL (>20 dB) are possible.

ACKNOWLEDGMENTS

The author has greatly benefited from numerous discussions with K. E. Hawker, S. R. Rutherford, C. T. Tindle, C. W. Horton, Sr., T. L. Foreman, and E. L. Hamilton. This work was supported by Naval Ocean Research and Development Activity and Naval Electronic Systems Command.

REFERENCES

1. S. R. Rutherford and K. E. Hawker, "The effects of density gradients on bottom reflection loss for a class of marine sediments," J. Acoust. Soc. Am. 63, 750-757 (1978).

2. S. R. Rutherford, K. E. Hawker, and S. G. Payne, "A study of the effects of ocean bottom roughness on low-frequency sound propagation," J. Acoust. Soc. Am. 65, 381-386 (1979).

3. K. E. Hawker, K. C. Focke, and A. L. Anderson, "A sensitivity study of underwater sound propagation loss and bottom loss," Applied Research Laboratories Technical Report No. 77-17 (ARL-TR-77-17), Applied Research Laboratories, The University of Texas at Austin (1977).

4. A. O. Williams, Jr., "Hidden depths: Acceptable ignorance about ocean bottoms," J. Acoust. Soc. Am. 59, 1175-1179 (1976).

5. K. E. Hawker, W. E. Williams, and T. L. Foreman, "A study of the acoustical effects of subbottom absorption profiles," J. Acoust. Soc. Am. 65, 360-367 (1979).

6. K. E. Hawker, "The influence of Stoneley waves on plane wave reflection coefficients: Characteristics of bottom reflection loss," J. Acoust. Soc. Am. 64, 548-555 (1978).

7. K. E. Hawker, "Existence of Stoneley waves as a loss mechanism in plane wave reflection problems," J. Acoust. Soc. Am. 65, 682-686 (1979).

8. H. P. Bucker, J. A. Whitney, G. S. Yee, and R. R. Gardner, "Reflection of low-frequency sonar signals from a smooth ocean bottom," J. Acoust. Soc. Am. 37, 1037-1051 (1965).

9. G. J. Fryer, "Reflectivity of the ocean bottom at low frequency," J. Acoust. Soc. Am. 63, 35-42 (1978).

10. E. L. Hamilton, "Shear-wave velocity versus depth in marine sediments: A review," Geophys. 41, 985-996 (1976).

11. E. L. Hamilton, "Attenuation of shear waves in marine sediments," J. Acoust. Soc. Am. 60, 334-338 (1976).

12. D. J. Shirley and L. D. Hampton, "Shear wave measurements in laboratory sediments," J. Acoust. Soc. Am. 63, 607-613 (1978).

13. P. J. Vidmar and T. Foreman, "The effect of sediment rigidity on the acoustic reflectivity of the ocean bottom," EOS, Trans. Am. Geophys. Union 59, 1119(A) (1978).

14. P. J. Vidmar and T. L. Foreman, "A plane-wave reflection loss model including sediment rigidity," J. Acoust. Soc. Am. 65, S43(A) (1979).

15. P. J. Vidmar and T. L. Foreman, "A plane-wave reflection loss model including sediment rigidity," to be published in The Journal of The Acoustical Society of America.

TABLE I. Acoustic parameters of the hypothetical turbidite layer: c is the compressional wave speed, v is the shear wave speed, ρ is the density, k_p is the compressional wave attenuation, k_s is the shear wave attenuation.

Depth m	c m/sec	k_p dB/m/kHz	ρ gm/cm^3	v m/sec	k_s dB/m/kHz
water	1530		1.030		
0	1510	0.065	1.530	116	8.46
36	1582	0.100	1.579	283	5.60
120	1674	0.200	1.689	391	8.60
518	1992	0.135	2.010	621	4.35
substrate	4460	0.008	2.460	2400	0.040

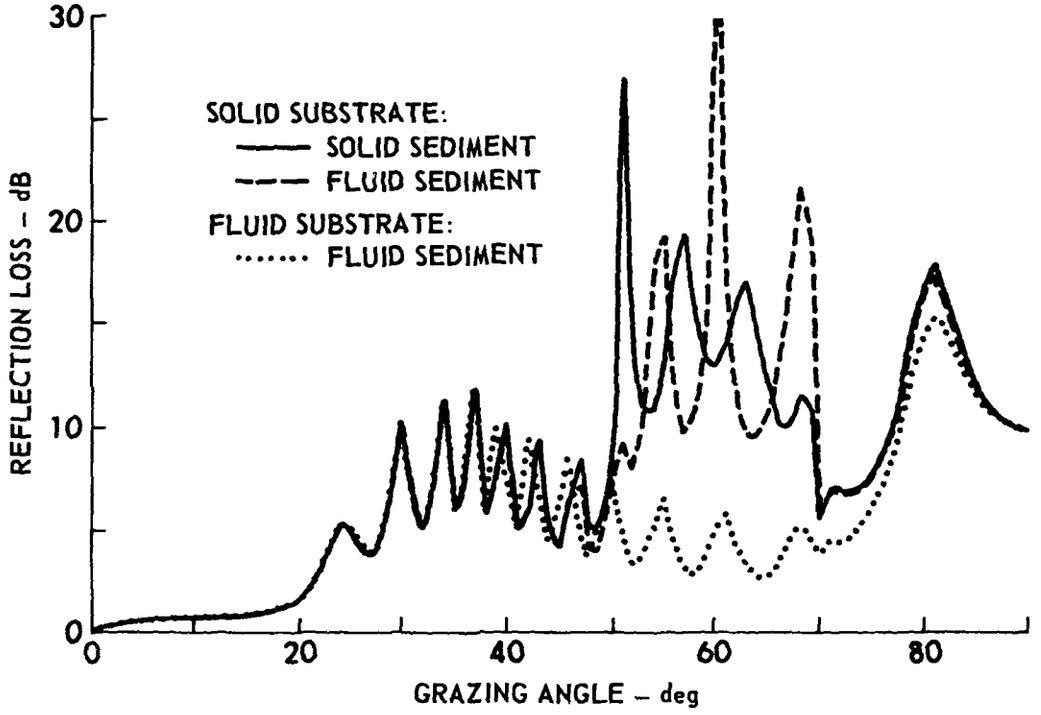

FIGURE 1
REFLECTION LOSS versus GRAZING ANGLE FOR A 518 m
THICK HYPOTHETICAL TURBIDITE LAYER AT 20 Hz

ARL:UT
AS-78-1735-S
PJV-GA
11-27-78

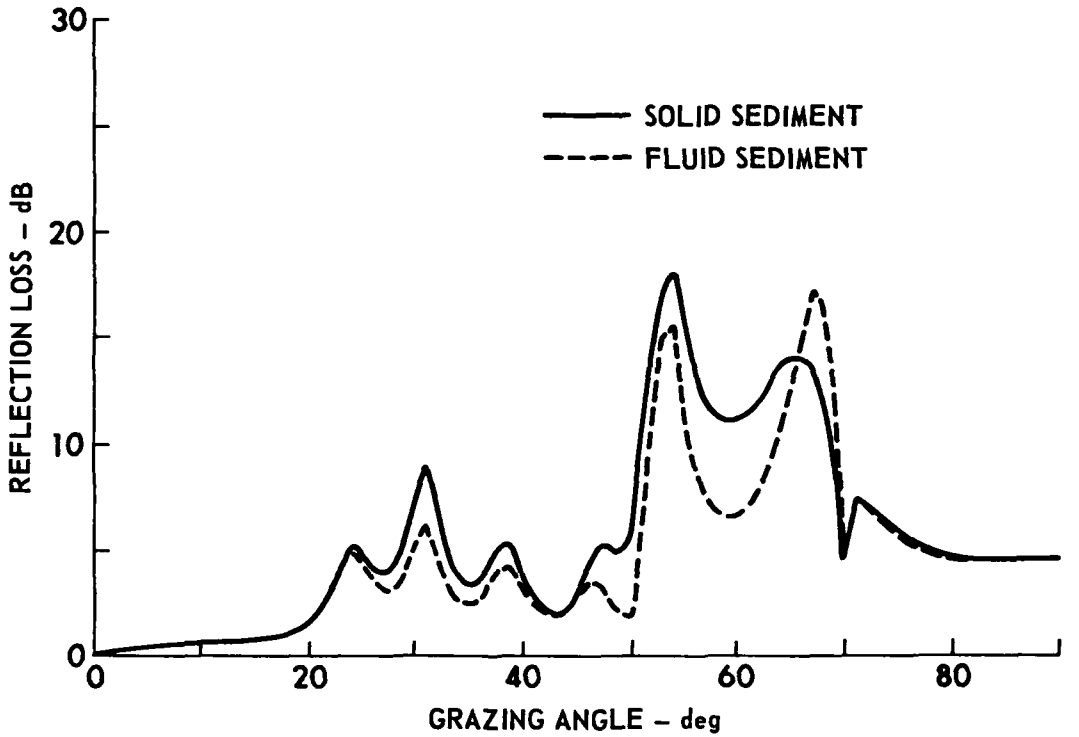

FIGURE 2
REFLECTION LOSS versus GRAZING ANGLE FOR A 252 m
THICK HYPOTHETICAL TURBIDITE LAYER AT 20 Hz

ARL:UT
AS-78-1737-S
PJV-GA
11-27-78

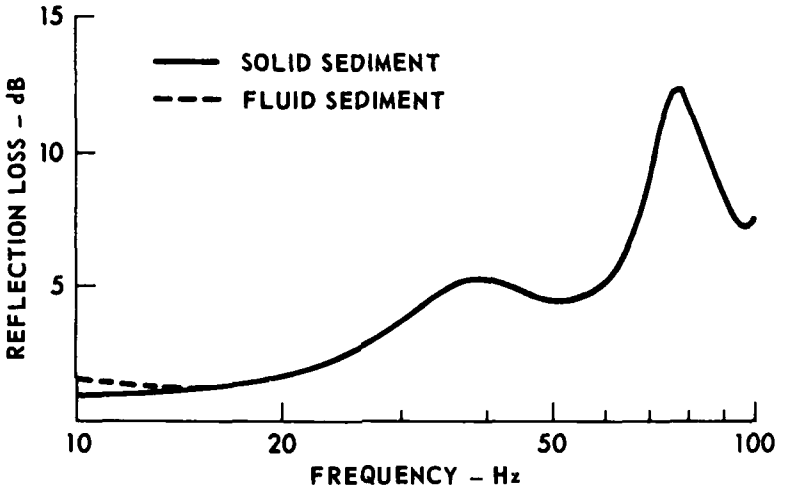

FIGURE 3
REFLECTION LOSS versus FREQUENCY FOR A 252 m
THICK HYPOTHETICAL TURBIDITE LAYER AT 20°

ARL:UT
AS-79-1815-P
PJV - GA
8 - 17 - 79

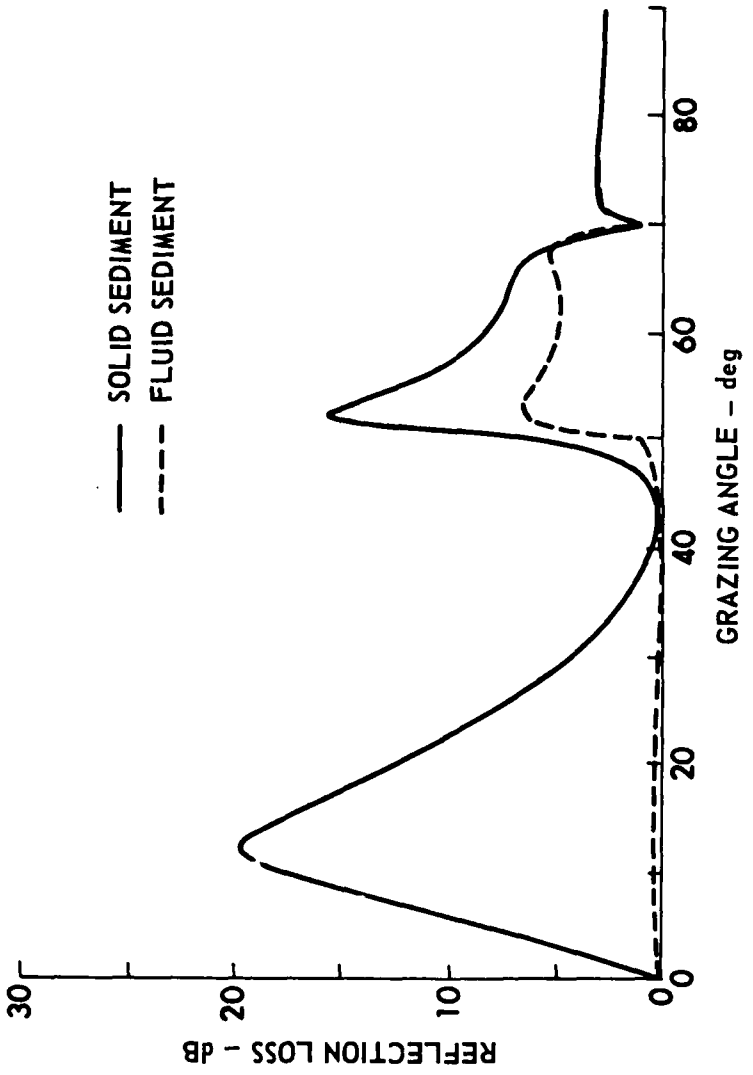

FIGURE 4
REFLECTION LOSS versus GRAZING ANGLE FOR A 36 m
THICK HYPOTHETICAL TURBIDITE LAYER AT 20 Hz

ARL:UT
AS-78-1738-S
PJV - GA
11-27-78

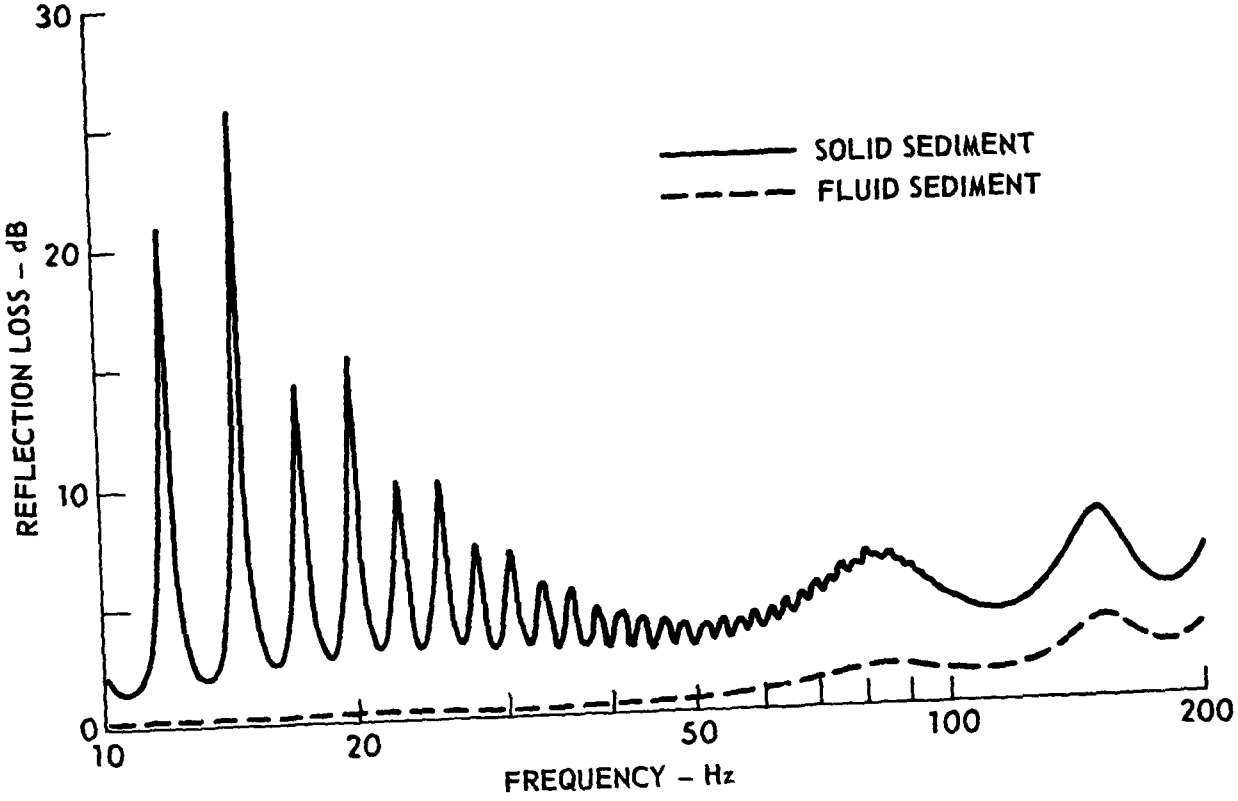

FIGURE 5
REFLECTION LOSS versus FREQUENCY FOR A 36 m
THICK HYPOTHETICAL TURBIDITE LAYER AT 20°

ARL:UT
AS-79-1123-S
PJV-GA
5-28-79

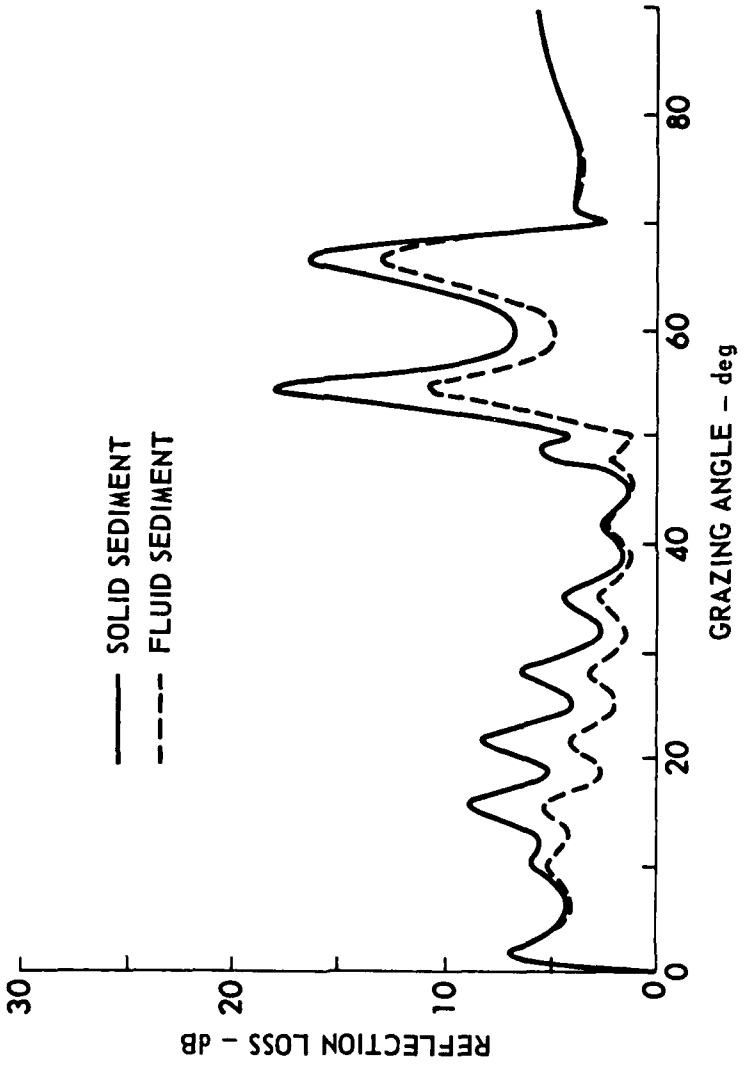

FIGURE 6
REFLECTION LOSS versus GRAZING ANGLE FOR A 36 m
THICK HYPOTHETICAL TURBIDITE LAYER AT 200 Hz

ARL:UT
AS-78-1739-S
PJV-GA
11-27-78

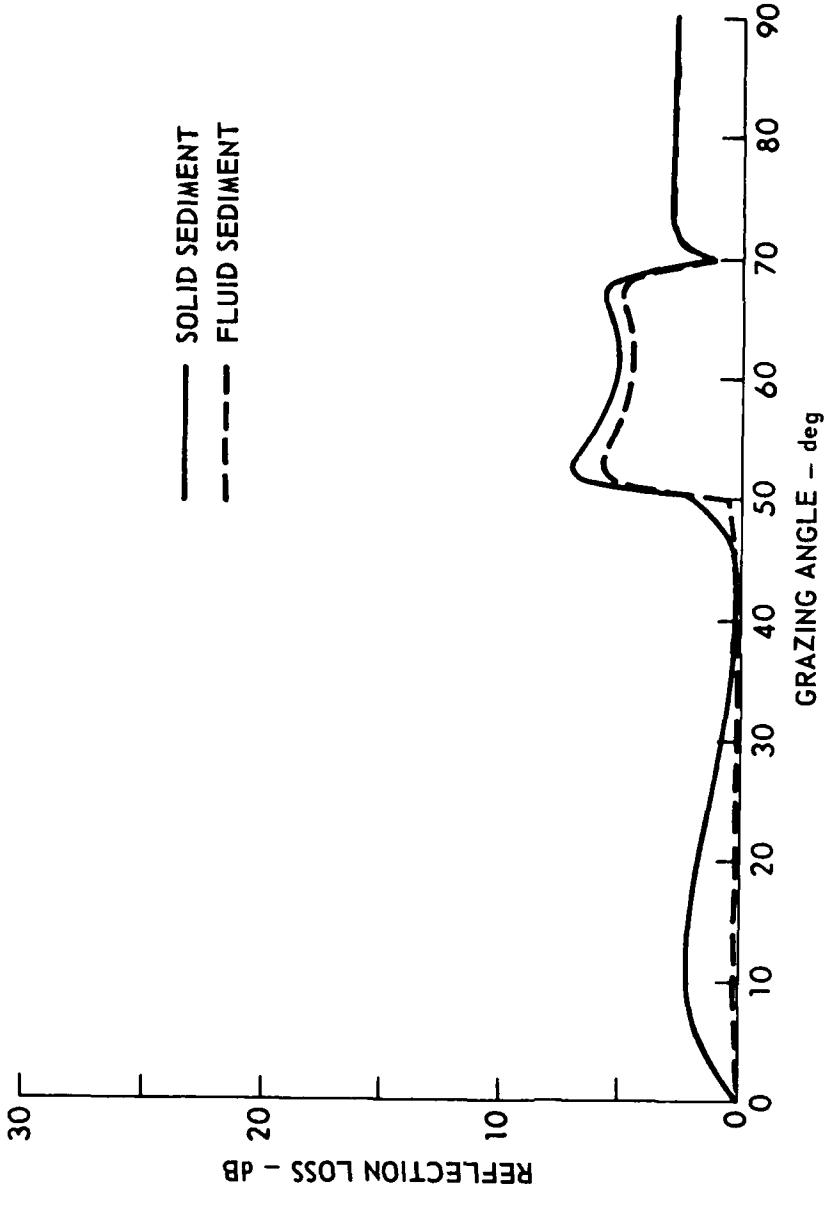

FIGURE 7
REFLECTION LOSS versus GRAZING ANGLE FOR A 36 m
THICK HYPOTHETICAL TURBIDITE LAYER AT 21 Hz

ARL:UT
AS-79-1122-S
PJV - GA
5 - 28 - 79

APPENDIX C

A RAY PATH ANALYSIS OF SEDIMENT SHEAR WAVE EFFECTS ON BOTTOM REFLECTION LOSS

by

Paul J. Vidmar

Paper submitted to The Journal of The Acoustical Society of America for publication

A ray path analysis of sediment shear wave effects on bottom reflection loss

Paul J. Vidmar

Applied Research Laboratories, The University of Texas at Austin, Austin, Texas 78712

(Received

The effect of sediment shear wave propagation on bottom reflection loss (RL) from a typical deep sea sediment layer is analyzed by means of a ray path decomposition of the acoustic field. The amplitude of each shear (S) and compressional (P) ray is obtained from the interface reflection and transmission coefficients. These coefficients are analyzed by means of an expansion in the parameter ε which is proportional to the relatively small S wave velocity of marine sediments. Ray paths with amplitudes up to order ε^2 are identified and used to develop a qualitative ray path model of RL. P wave conversion at the sediment-substrate interface is the dominant mechanism for sediment S wave excitation. To order ε^2, RL is the result of the interference of three waves in the water whose amplitudes are proportional to ε^0, ε^1, and ε^2. Comparison with RL obtained from a computational model shows that the ray path model correctly predicts the dependence of RL on frequency, S wave speed, S wave attenuation, and P wave attenuation.

PACS number: 43.20.Fn 43.20.Dk 43.30.Dr 43.30.Bp

AD-A083 127 TEXAS UNIV AT AUSTIN APPLIED RESEARCH LABS F/G 17/1
SUMMARY OF RECENT RESULTS IN ACOUSTIC BOTTOM INTERACTION.(U)
FEB 80 P J VIDMAR, S R RUTHERFORD, K E HAWKER N00014-78-C-0113
UNCLASSIFIED ARL-TR-80-6 NL

2 OF 2
AD
A083127

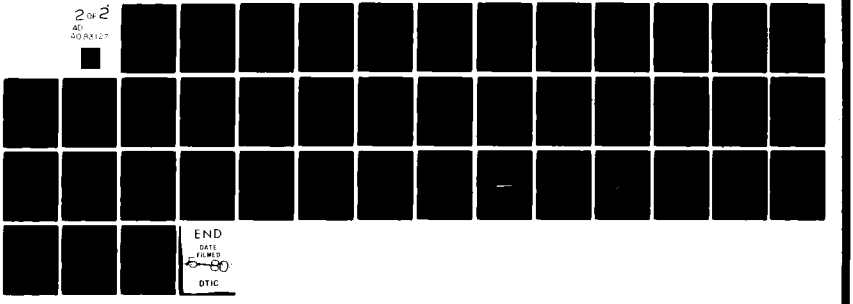

END
DATE FILMED
5-80
DTIC

I. INTRODUCTION

Recent work on the effect of sediment rigidity on bottom reflection loss, RL = $-20 \log_{10} (|R|)$, where R is the reflection coefficient of the ocean bottom, shows that sediment shear (S) wave excitation can be an important loss process influencing low frequency sound propagation in the oceans. For a typical deep sea sediment structure, a single turbidite layer overlying a basalt substrate, the sediment S wave excitation is negligible at low grazing angles for thick sediment layers.[1,2] However, for thin layers sediment S wave excitation is an important, and in some cases dominant, energy loss process.[1] The dependence of RL on frequency for thin layers has low and high frequency regimes with strikingly different properties.[1] At low frequencies RL increases a few decibels relative to the RL for a fluid sediment and also has very large peaks up to 25 dB. At high frequencies the peaks disappear, and rather broad oscillations in RL occur in both fluid and solid sediment cases with the solid sediment RL having an almost constant increase above the fluid sediment RL. Compressional (P) wave conversion at the sediment-substrate interface was suggested as the major mechanism for S wave excitation in the sediment.[1]

In this paper a ray path analysis of P and S wave propagation in a solid sediment layer is developed and used to elucidate the qualitative properties of RL described above. Basic to this approach is an understanding of the effect of sediment rigidity on the reflection and transmission coefficients at the water-sediment and sediment-substrate interfaces. An expansion of these coefficients, using a small parameter ϵ proportional to the small S wave speed in marine sediments, is used

to identify P and S wave ray paths with amplitudes up to second order in the expansion parameter. The ray path model, based on the P and S wave amplitudes, reveals the mechanism for sediment S wave excitation to be primarily P wave conversion at the sediment-substrate interface and shows that RL can be described as the result of the interference of three waves representing energy returned to the water from the sediment. The three waves have magnitudes proportional to the expansion parameter to the zero, first, and second powers. The utility of the ray model is established by comparing predictions of the dependence of RL on sediment parameters with results obtained from a numerical model[3] of RL from solid sediments.

The remainder of this paper is organized as follows. In section II the expansion theory of the reflection and transmission coefficients is developed. In section III these coefficients are used to develop the qualitative ray path model. In section IV the bottom reflection loss generated by a numerical model is used to check the predictions and applicability of the ray model. Section V discusses the mechanism for shear wave excitation in sediments. The final section summarizes our results.

II. EXPANSION THEORY OF REFLECTION AND TRANSMISSION COEFFICIENTS

The following conventions and definitions will be used in the study of the reflection and transmission coefficients. Subscripts 1, 2, and 3 identify quantities in the water, sediment, and substrate, respectively. For simplicity we assume a horizontally stratified ocean bottom with homogeneous media, and a harmonic time dependence with

angular frequency ω. Compressional wave speeds are c_j, S wave speeds are v_j, and densities are ρ_j. Wave numbers are defined as

$$K_j=\omega/c_j, \quad B_j=\omega/v_j, \quad k=K_1\cos\theta, \quad \kappa_j=\left[K_j^2-k^2\right]^{1/2}, \quad \left[\beta_j=B_j^2-k^2\right]^{1/2},$$

where θ is the grazing angle of the incident wave in the water. Subscripts p and s will identify reflection and transmission coefficients for P and S waves respectively. The water-sediment interface will be denoted by W-S and the sediment-substrate interface by S-S.

The basis of our study of the reflection and transmission coefficients is an expansion in the small parameter $\varepsilon=v_2/c_1$. This is an excellent expansion parameter at the W-S interface where the surficial shear wave velocities[4] are between 50 m/sec and 200 m/sec giving $0.03<\varepsilon<0.15$. The expansion parameter is not as good at the S-S interface because of the larger S wave velocity due to positive shear speed gradients[4] in realistic sediments. For a typical turbidite layer[4] ε varies from 0.076 at the W-S interface to 0.185 at 36 m, 0.256 at 120 m, and 0.406 at 518 m. Even at 518 m the second order terms contribute only 15% corrections compared to the 40% corrections due to first order terms. Only the lowest order corrections in ε will be retained in our expansion.

The z axis increases downward from the water into the sediment. The displacement $\underline{u}_j$ is defined in terms of a scalar potential, $\Phi_j=\phi_j(z)\, e^{i(kx-\omega t)}$, and a vector potential, $\underline{\tilde{\psi}}_j=\hat{y}X_j(z)\, e^{i(kx-\omega t)}$, by $\underline{u}_j=\underline{\nabla}\Phi_j+\underline{\nabla}\times\underline{\tilde{\psi}}_j$, where $\hat{y}$ is a unit vector along the y axis. The depth dependencies are given by

$$\phi_j = W_j^- e^{i\kappa_j z} + W_j^+ e^{-i\kappa_j z} \quad , \text{ and}$$

$$X_j = V_j^- e^{i\beta_j z} + V_j^+ e^{-i\beta_j z} \quad ,$$

where W_j^- and V_j^- are the amplitudes of the downward propagating waves and W_j^+ and V_j^+ are the amplitudes of the upgoing plane waves.

Beginning at the W-S interface with a unity amplitude sound wave incident from the water, $\phi_1 = e^{i\kappa_1 z} + R_{p12} e^{-i\kappa_1 z} e^{i(kx-\omega t)}$ and, following the procedure given in the appendix, we obtain

$$R_{p12} = R_{12}^{(o)} - 2\varepsilon^2 T_{12}^{(o)} T_{21}^{(o)} \cos^2\theta \quad , \tag{1}$$

$$T_{p12} = T_{12}^{(o)} + 2\varepsilon^2 T_{12}^{(o)} R_{21}^{(o)} \cos^2\theta \quad , \tag{2}$$

$$T_{s12} = 2\varepsilon^2 T_{12}^{(o)} (\kappa_2/k) \cos^2\theta \quad , \tag{3}$$

where $R_{ij}^{(o)} = (\kappa_i\rho_j - \kappa_j\rho_i)/(\kappa_i\rho_j + \kappa_j\rho_i)$ and $T_{ij}^{(o)} = 2\kappa_i\rho_i/(\kappa_i\rho_j + \kappa_j\rho_i)$ are the zero order reflection and transmission coefficients obtained for a fluid sediment with the P wave incident from medium i.[5]

Equations (1) through (3) show that, as far as the incident sound wave is concerned, the sediment can be accurately treated as a fluid. Equations (1) and (2) show that sediment rigidity produces only second order ε^2 corrections to the fluid-fluid interface reflection and transmission coefficients. Equation (3) shows that the excited sediment shear wave amplitude is of order ε^2 and thus contains little of the incident energy.

The downward propagating P and S waves next strike the S-S interface. For the incident P wave we find

$$R_{p23} = R_{p23}^{(o)} - \varepsilon\Gamma_p\eta\cos\theta \quad , \tag{4}$$

$$T_{p23} = T_{p23}^{(o)} - \varepsilon\Gamma_p\tau_p\cos\theta \quad , \tag{5}$$

$$R_{s23} = -2\varepsilon\Gamma_p\cos\theta \quad , \tag{6}$$

$$T_{s23} = T_{s23}^{(o)} - \varepsilon\Gamma_p\tau_s\cos\theta \quad . \tag{7}$$

For an incident S wave we have

$$r_{p23} = \eta(1-\varepsilon\Gamma_s\cos\theta) \quad , \tag{8}$$

$$t_{p23} = \tau_p(1-\varepsilon\Gamma_s\cos\theta) \quad , \tag{9}$$

$$r_{s23} = 1 - 2\varepsilon\Gamma_s\cos\theta \quad , \tag{10}$$

and

$$t_{s23} = \tau_s(1-\varepsilon\Gamma_s\cos\theta) \quad . \tag{11}$$

In Eqs. (4) through (11) we have used the quantities

$$\Gamma_s = \frac{\left(R_{p23}^{(o)} - T_{p23}^{(o)} + \beta_3 T_{s23}^{(o)}/k\right)}{2} \quad , \tag{12}$$

$$\Gamma_p = \Gamma_s + 1/2 \quad , \tag{13}$$

$$\eta = 2k\Gamma_p/\kappa_2 \quad , \tag{14}$$

$$\tau_p = \frac{-k}{\kappa_1}\left[\frac{\left(1-R_{p23}^{(o)}\right)\rho_2\kappa_2}{\rho_3\kappa_3} - T_{p23}^{(o)} + \frac{T_{s23}^{(o)}\kappa_2\beta_3}{\kappa_3 k}\right] \quad , \tag{15}$$

$$\tau_s = \frac{\left(1-R_{p23}^{(o)}\right)\rho_2}{\rho_3} + \frac{T_{s23}^{(o)}k}{\kappa_2} + T_{p23}^{(o)} \quad , \tag{16}$$

and the zero order reflection and transmission coefficients for a P wave, with horizontal wave number k, incident from a fluid sediment:[5,6]

$$R_{p23}^{(o)} = \left\{\rho_3\kappa_2\left[(1-2a^2)^2 + 4a^4\kappa_2\beta_3/k^2\right] - \rho_2\kappa_3\right\}/D \quad , \tag{17}$$

$$T_{p23}^{(o)} = 2\rho_2\kappa_2(1-2a^2)/D \quad , \tag{18}$$

$$T_{s23}^{(o)} = 4\rho_2\kappa_2 a^2\kappa_3/kD \quad , \tag{19}$$

where $a=(v_2/c_1)\cos\theta$ and

$$D = \rho_3\kappa_2\left[(1-2a^2)^2 + 4a^4\kappa_2\beta_3/k^2\right] + \rho_2\kappa_3 \quad . \tag{20}$$

Equations (4) through (11) show that sediment rigidity can be important at the S-S interface. According to Eq. (6) the P wave incident upon the S-S interface excites a first order (ε^1) S wave in the sediment. Equations (4), (5), and (7) show that the reflected P wave and P and S waves transmitted into the substrate also have first order corrections to their amplitudes. Recall that the S wave excited at the W-S interface is of order ε^2 [Eq. (3)]. Equations (8) through (10) show that the reflected and transmitted waves due to it are at most of order ε^2 and are small compared to the larger, order ε^1, corrections due to P wave conversion at the S-S interface. The presence of gradients will increase the relative effectiveness of the S-S interface by increasing the value of ε.

Equations (8) through (11) show an apparent inconsistency. The incident S wave is perfectly reflected to order ε^o and yet sets up other

reflected and transmitted waves whose amplitudes are also of order ε^0. A consideration of the total energy flux resolves this inconsistency. Recalling that the energy flux is proportional to the inverse of the wave speed,[5] the incident and reflected S waves in the sediment have an energy flux proportional to ε^{-1} while the energy flux of the other waves is to lowest order proportional to ε^0. The S waves, then, carry one order higher energy flux than the other waves even though all the amplitudes are of the same order. To order ε^{-1}, the incident and reflected S waves conserve energy flux. To the next order, ε^0, the part of the S wave energy that is not perfectly reflected (ε^1 corrections to the amplitude) provides some order ε^0 energy which appears in the lowest order energy flux of the other waves.

We next consider incident S and P waves in the sediment striking the W-S interface. The computed reflection and transmission coefficients are

$$R_{p21} = R_{21}^{(o)} + 2\varepsilon^2 T_{12}^{(o)} T_{21}^{(o)} \cos^2\theta \quad , \tag{21}$$

$$T_{p21} = T_{21}^{(o)} + 2\varepsilon^2 T_{21}^{(o)} R_{12}^{(o)} \cos^2\theta \quad , \tag{22}$$

$$R_{s21} = 2\varepsilon^2 T_{21}^{(o)} (\kappa_1/k) \cos^2\theta \quad , \tag{23}$$

for an incident P wave, and

$$r_{p21} = -2\varepsilon\left(1-R_{21}^{(o)}\right)\cos\theta \quad , \tag{24}$$

$$t_{p21} = 2\varepsilon T_{21}^{(o)} \cos\theta \quad , \tag{25}$$

$$r_{s21} = -1 \quad , \tag{26}$$

for an incident S wave. The lowest order corrections to Eq. (26) are of order ε^3.

Equations (21) through (23) give the same qualitative results as Eqs. (1) through (3). Both sets of equations show that the corrections due to sediment rigidity are of order ε^2 at the W-S interface when a P wave is incident, i.e., the sediment can be accurately treated as a fluid at the W-S interface whenever a P wave is incident. Recalling that the incident S wave is at most order ε [Eqs. (3), (6), (10)], the corrections to P wave amplitudes due to S wave conversion are at most of order ε^2 [Eqs. (24), (25)]. This leads to the conclusion that, as far as P waves are concerned, the sediment at the W-S interface can be accurately treated as a fluid.

III. RAY PATH MODEL AND PREDICTIONS

The transmission and reflection coefficients derived above will now be used to develop a ray path model of the qualitative effects of sediment rigidity in a single homogeneous sediment layer. The reflection and transmission coefficients of the previous section will be used to determine the wave amplitudes associated with the ray paths at each interface. Subscripts U or L will identify the values of the expansion parameters at the W-S or S-S interfaces, respectively. The corrections due to sediment rigidity at each interface can then be identified and the qualitative effect of the shear speed gradient treated by setting $\varepsilon_L > \varepsilon_u$. To allow for $\varepsilon_L > \varepsilon_u$, corrections of order ε_L^2 will be retained while those of the order ε_u^2 will be neglected compared to one.

The ray path model is shown schematically in Figs. 1, 2, and 3. The solid lines are ray paths for P waves and the dashed lines are those

for S waves. Each ray path is labeled with the amplitude of the wave associated with that path. The positions at which the rays strike the interfaces are labeled a, b, c, and d for identification purposes. Figure 1 shows the ray paths excited when the S wave attenuation is high enough for the S wave to be totally absorbed before crossing the layer. Figure 2 shows the additional ray paths resulting from the first reflection of the sediment S waves, and Fig. 3 shows those due to the second reflection. Since the S wave speed in marine sediments is so small compared to the sound speed in water, the S wave ray paths are almost normal to the plane of stratification.

In Fig. 1 the S wave attenuation is high enough for an S wave to be completely absorbed in traveling one way through the sediment. At position a, the incoming wave in the water reflects from the W-S interface with negligible corrections [Eq. (1)] due to sediment rigidity. The corrections to the transmitted P wave are also negligible [Eq. (2)]. A small amplitude S wave of order ϵ_u^2 is also excited [Eq. (3)]. At position b the transmitted P wave strikes the S-S interface where an order $\epsilon_L+\epsilon_L^2$ S wave is excited [Eq. (6)]. The reflected P wave and the substrate P and S waves suffer order $\epsilon_L+\epsilon_L^2$ corrections [Eqs. (4), (5), and (7)]. The reflected P wave carries its corrected amplitude back through the sediment to the W-S interface at position c. Here a small order ϵ_u^2 S wave is excited [Eq. (23)]. The transmitted wave in the water has $\epsilon_L+\epsilon_L^2$ corrections [Eq. (22)]. The reflected P wave carries corrections of the order $\epsilon_L+\epsilon_L^2$ [Eq. (21)] back down through the sediment where it again interacts with the S-S interface at position d, and the process repeats.

Figure 2 shows the additional rays set up when the S wave attenuation is reduced to allow the sediment S waves to strike one interface before being absorbed. The order ϵ_u^2 S wave ray originating at the W-S interface (position a in Fig. 1) is totally reflected from the substrate at position a [Eq. (10)] and retains its ϵ_u^2 magnitude (corrections of order $\epsilon_u^2\epsilon_L$ are neglected). Order ϵ_u^2 P and S waves are also excited in the substrate at position a [Eqs. (9) and (11)] and a reflected P wave of order ϵ_u^2 in the sediment [Eq. (8)]. At position b the P wave from position a transmits its ϵ_u^2 magnitude into the water and also into the reflected P wave at the W-S interface [Eqs. (21) and (22)]. The reflected S wave is of order ϵ_u^4 and is neglected [Eq. (23)]. At position c the downward propagating P wave strikes the S-S interface where it sets up order ϵ_u^2 waves in the substrate and an order ϵ_u^2 reflected P wave [Eqs. (4), (5), and (7)]. No significant S wave is excited in the sediment [Eq. (6)]. The upgoing P wave then continues to position d where the process begun at position b repeats.

Figure 2 also contains ray paths coming from the S wave originating at the substrate interface (position b in Fig. 1). At position b this S wave is totally reflected from the W-S interface [Eq. (26)] and retains its order $\epsilon_L+\epsilon_L^2$ magnitude. A reflected P wave of order $\epsilon_u\epsilon_L$ is excited [Eq. (24)] along with a wave of amplitude $\epsilon_u\epsilon_L$ in the water [Eq. (25)]. The reflected P wave carries its magnitude through a reflection at the S-S interface at position c [Eq. (4)] where it also excites P and S waves of order $\epsilon_u\epsilon_L$ in the substrate [Eqs. (5) and (7)]. No significant sediment S wave is set up [Eq. (6)]. The upward traveling P wave is again reflected from the W-S interface at position d. The reflected

sediment P wave and the transmitted wave in the water carry an order $\epsilon_u\epsilon_L$ magnitude [Eqs. (21) and (22)]. No significant S wave is excited [Eq. (23)]. The order $\epsilon_u\epsilon_L$ P wave moving downward from the position d then continues the process.

Figure 3 shows the situation for an attenuation small enough for the sediment S waves to reflect a second time before being absorbed. The S waves originating at the W-S interface (positions a and c in Fig. 1) produce negligible effects when they strike the W-S interface at positions a and c. The reflected S waves retain their order ϵ_u^2 magnitudes and no significant P waves are excited [Eqs. (24), (25), and (26)]. The S wave originating at the S-S interface (position b in Fig. 1), however, does produce additional corrections to the energy returned to the water. On striking the S-S interface at position b it reflects with its order $\epsilon_L+\epsilon_L^2$ magnitude [Eq. (10)]. It also excites P and S waves in the substrate and a reflected P wave in the sediment, all of order $\epsilon_L+\epsilon_L^2$ [Eqs. (8), (9), and (11)]. The P wave travels through the sediment to the water interface where it reflects at position c, retaining its order $\epsilon_L+\epsilon_L^2$ magnitude, and is transmitted into the water with magnitude $\epsilon_L+\epsilon_L^2$ [Eqs. (21) and (22)]. It does not excite a significant S wave [Eq. (23)]. At position d, the downward propagating P wave reflects from the substrate interface retaining its $\epsilon_L+\epsilon_L^2$ magnitude, and sets up order $\epsilon_L+\epsilon_L^2$ waves in the substrate [Eqs. (4), (5), and (7)]. The reflected P wave then continues the process.

Figure 3 also contains an S wave of order ϵ_L^2 excited in the sediment at position d [Eq. (6)]. This S wave produces no further effects since it is absorbed before reaching the W-S interface, as can be seen by

recalling that the magnitude of this S wave is proportional to the amplitude of the P wave which struck the S-S interface. The magnitude of the P wave is in turn proportional to the magnitude of the S wave which originated at the S-S interface and has traveled up and back through the sediment. The maximum amplitude of the newly excited S wave then corresponds to the amplitude of the twice reflected shear wave. By hypothesis (in this example) an S wave is absorbed before its third reflection. Hence, the new S wave will be absorbed before it reaches the W-S interface.

For still lower S wave attenuation additional reflections from the interfaces are important. New ray paths similar to those of Figs. 2 and 3 are generated. The lower S wave attenuation means that the ray paths of a particular type (for example those of order $\epsilon_L+\epsilon_L^2$ similar to those of Fig. 3) have comparable amplitude but differ in phase because of the additional path lengths traveled by the S waves.

For a homogeneous layer ($\epsilon_u=\epsilon_L=\epsilon$) Figs. 1 through 3 show that there are three types of waves emerging from the W-S interface. Figure 1 shows the largest of these. The directly reflected ray and the series of rays carrying a magnitude of order $1+\epsilon+\epsilon^2$ combine to form a single wave, the A_o wave. For a fluid sediment ($\epsilon=0$) the A_o wave still exists and in fact produces the usual fluid sediment RL. For $\epsilon\neq 0$ the A_o wave contains a correction to its magnitude of order $\epsilon+\epsilon^2$ due to the S wave excited at the substrate interface by the P wave. The phase of the A_o wave does not, however, depend on S wave propagation. The second type of wave, the A_1 wave, is formed by the series of rays of order $\epsilon+\epsilon^2$ shown in Fig. 3. It is the most important correction to the A_o

wave. Its magnitude is proportional to ϵ^1, to lowest order, while its phase contains the two-way S wave phase $\phi_2=2\omega H/v_2$. The third type of wave, the A_2 wave, is formed by the series of rays of order ϵ^2 in Fig. 2. Since its magnitude is of order ϵ^2 it produces only small corrections compared to those due to the A_1 wave. The phase of the A_2 wave contains the one-way S wave phase, $\phi_1=\omega H/v_2$.

The ray path model predicts the dependence of the magnitudes of the A_1 and A_2 wave on shear wave attenuation. Figures 2 and 3 show that the magnitude of these waves depends on the attenuation suffered by the S wave in traveling through the sediment. The A_1 wave (Fig. 3) depends on the two-way attenuation while the A_2 wave (Fig. 2) depends only on the one-way attenuation. As S wave attenuation increases, the A_1 wave will decrease in magnitude more rapidly than the A_2 wave.

For low S wave attenuation, powerful interference effects are possible between the many ray paths of a particular type (for example, additional ϵ^2 paths) returning energy to the water. These interference effects will modify the dependence of the A_1 and A_2 waves on S wave attenuation. The magnitude of A_o is also affected since essentially all of the energy converted from P to S must return to the water.

Finally, the ray path model shows the importance of S wave excitation by P wave conversion at the substrate interface. All corrections of order ϵ occur because of the initial interaction of the P wave with the substrate shown in Fig. 1. The order ϵ corrections in the A_o wave are clearly due to this interaction (Fig. 1). The A_1 wave is excited by S waves set up by the initial P wave interaction (Fig. 3).

Part of the second order corrections, the $\epsilon_u \epsilon_L$ contribution in Fig. 2, is also due to this initial P wave. The remaining part of A_2, that labeled ϵ_u^2 in Fig. 2, while basically set up by P wave conversion at the water interface, also depends on the P wave traveling through the sediment layer. The same P wave conditions which would make the $\epsilon_u \epsilon_L$ wave unimportant would also affect this contribution to A_2 in the same manner. Thus, it is crucial for the P wave amplitude at the S-S interface to be significant if sediment rigidity is going to have an important effect on RL.

IV. COMPARISON OF RAY PATH MODEL PREDICTIONS WITH COMPUTED BOTTOM REFLECTION LOSS

In this section a computational model, described in detail elsewhere,[3] will be used to test some of the predictions of the ray path model. The dependence of R on frequency that is produced by the computational model will be used to extract the magnitudes of the A_o, A_1, and A_2 waves. Homogeneous layers will be treated at frequencies near 14 Hz and a grazing angle of 20°. The acoustic parameters used in the numerical calculations are: $\rho_1 = 1.053$ g/cm^3, $c_1 = 1540$ m/sec, $\rho_2 = 1.27$ g/cm^3, $c_2 = 1525$ m/sec, $v_2 = 70$ m/sec, $\rho_3 = 2.8$ g/cm^3, $c_3 = 5700$ m/sec, and $v_3 = 2900$ m/sec. The P wave attenuations are: $k_{p2} = 0.115$ dB/m/kHz, $k_{p3} = 0.152$ dB/m/kHz. The S wave attenuations are: $k_{s2} = 10.0$ dB/m/kHz, $k_{s3} = 0.90$ dB/m/kHz. The layer thickness is H = 40 m. Individual parameters will be varied to illustrate the features of the ray path model. The range of the parameters does not necessarily represent values attained in marine sediments.

The different phases of the A_o, A_1, and A_2 waves make it possible to extract their amplitudes from the interference structure seen in the dependence of RL on frequency. The ray path model shows that the magnitude of the reflection coefficient can be written approximately as

$$|R| = A_o + A_1 \cos\phi_2 + A_2 \cos(\phi_1+\mu) \quad , \tag{27}$$

where A_o, A_1, and A_2 are the amplitudes of the A_o (order $1+\varepsilon$), A_1 (order ε^1) and A_2 (order ε^2) waves, and μ is a frequency independent phase difference between the A_1 and A_2 waves. This form for $|R|$ assumes that $\phi_1=\omega H/v_2$ and $\phi_2=\omega 2H/v_2$ contain the major frequency dependence of the phases. This is true in our case since the frequency range will be limited so that the phase shifts due to P wave propagation and the interface continuity conditions are small compared to those due to S wave propagation. The major interference pattern in $|R|$ will be due to a superposition of the A_o and A_1 waves. The smaller magnitude A_2 wave will add a modulation to this structure.

A typical reflection coefficient is shown in Fig. 4. Four of the maxima and minima are labeled by letters. The basic oscillatory structure is due to the interference of the A_o and A_1 waves. The maxima (or minima) recur when ϕ_2 changes by 2π. The difference in height of peaks b and d clearly shows the effect of the modulation produced by A_2. The unknown amplitudes and the relative phase in Eq. (27) are obtained by setting: $\phi_1=\phi_2=0$ at peak a; $\phi_1=\pi/2$, $\phi_2=\pi$ at valley b; $\phi_1=\pi$, $\phi_2=2\pi$ at peak c; $\phi_1=3\pi/2$, $\phi_2=3\pi$ at valley d. This generates a set of four equations:

$$R_a = A_o + A_1 + A_2 \cos\mu \quad , \tag{28}$$

$$R_b = A_o - A_1 - A_2 \sin\mu \quad , \tag{29}$$

$$R_c = A_o + A_1 - A_2 \cos\phi \quad , \tag{30}$$

$$R_d = A_o - A_1 + A_2 \sin\phi \quad , \tag{31}$$

where R_a, R_b, R_c, and R_d are the measured values of $|R|$ at a, b, c, and d. These four equations can be easily solved for the four unknowns.

The magnitudes of A_o, A_1, and A_2 obtained from Eqs. (28) through (31) are not sufficiently accurate for the purposes of this section. The reason for this inaccuracy is an inconsistency in Eqs. (28)-(31); the frequency dependence of A_o, A_1, and A_2 has not been included, while R_a, R_b, R_c, and R_d were measured at different frequencies. In practice it is easier to correct the procedure for measuring $|R|$ than to modify Eqs. (28)-(31). A more accurate procedure for measuring $|R|$ is also illustrated in Fig. 4. Peaks corresponding to similar interference maxima (or minima) are joined by straight lines: a a', b b', and d d'. The values of R_a, R_b, and R_d are then estimated at the frequency of maxima c by obtaining their magnitudes from the intersection of a vertical line through maxima c with lines aa', bb', and dd'. The resulting values for R_a, R_b, R_c, and R_d now have the major frequency dependence removed and can be used in Eqs. (28)-(31) to obtain more accurate values of the magnitudes of A_o, A_1, and A_2. This more accurate procedure was used to obtain the results of this section.

The first parameter we will investigate is the sediment shear speed v_2. Figure 5 shows the computed RL for 3 different shear speeds: 150 m/sec, 70 m/sec, and a fluid case, v_2=0 m/sec. The results are in qualitative agreement with the ray model predictions. The RL generally increases with sediment shear speed. The rapid oscillatory structure, due to the interference of the A_o and A_1 waves, increases in magnitude

and spreads out in frequency as v_2 increases. The modulation due to the small A_2 wave is clearly evident in the v_2 = 150 m/sec curve. A similar oscillatory structure was observed in the low frequency regime of dependence of RL on frequency computed for a hypothetical turbidite layer.[1]

Figure 6 shows the dependence of the frequency interval between adjacent maxima of RL, Δf, on sediment shear speed. The line is the ray path model prediction, $\Delta f = v_2/2H$. The agreement is excellent.

Figure 7 shows the dependence of the amplitudes of the A_1 and A_2 waves on sediment shear speed. The third set of points shows the change of A_o due to sediment rigidity, i.e., $\Delta A_o(\varepsilon) = A_o(0) - A_o(\varepsilon)$. For reference, v_2 = 150 m/sec corresponds to $\varepsilon \simeq 0.10$. In agreement with the ray path model predictions, A_1 and $\sqrt{A_2}$ are proportional to v_2 at small shear speeds. The increase in ΔA_o is consistent with an increase in RL, which the ray path model predicts will be proportional to ε to lowest order. All three sets of points show the effect of higher order corrections at larger ε. The magnitude of A_2 is much smaller than that of A_1, in agreement with the ray path model predictions. The lines in Fig. 7 are drawn to illustrate the proportionality to ε; the slopes do not reflect theoretical predictions.

Figures 2 and 3, and the previous discussion of the ray path model, show that the magnitude of the A_1 and A_2 waves have different dependencies on the S wave attenuation, i.e., $A_1 \propto \exp(-2k_{is}H)$ and $A_2 \propto \exp(-ik_{is}H)$, where k_{is} is the imaginary part of the S wave wave number. Figure 1 shows that the magnitude of the A_o wave is independent of S wave attenuation. The dependence of A_o, A_1, and A_2 on the sediment shear wave attenuation

is shown in Fig. 8. The abscissa in Fig. 8 is k_s, the S wave attenuation in dB/m/kHz. Since we assume a linear dependence of k_{is} on frequency, k_s is related to k_{is} by $k_{is}=k_s f/8686$. The values of k_s greater than 10 attenuate the S wave by about 6 dB in a distance H. This effectively eliminates any waves other than those shown in Figs. 1 through 3 and permits the ray model to predict a clean exponential dependence on k_s for the magnitudes of the A_1 and A_2 waves. The lines in Fig. 8 are "eyeball" fits to the data obtained from the computed reflection coefficients. The slopes are 0.0285 for the A_2 wave and 0.0569 for the A_1 wave, and they differ by a factor of 2 as predicted by the ray theory and agree very well with the predicted slopes of 0.028 and 0.056. The change in A_o due to S waves ΔA_o is seen to be independent of k_s as expected.

The ray path model also predicts that ΔA_o, A_1, and A_2 depend on the attenuation of the P wave in the sediment. Figures 1 through 3 can be used to deduce this dependence for large P wave attenuations. Figure 1 shows that ΔA_o is carried by a P wave traveling down and back through the sediment, $\Delta A_o \propto \exp(-2k_{ip}H)$. Figure 2 shows that $A_2 \propto \exp(-2k_{ip}H)$ also. The ε_u^2 part of A_2 clearly has this dependence. The $\varepsilon_u \varepsilon_L$ part has the same dependence since it comes from the initial P wave striking the substrate interface at position b in Fig. 1. Figure 3 combined with Fig. 1 shows that $A_1 \propto \exp(-2k_{ip}H)$. These relations apply at higher P wave attenuations where only a single ray path returning to the water has a significant amplitude.

Figure 9 shows the dependence of ΔA_o, A_1, and A_2 on P wave attenuation. The abscissa in Fig. 9 is k_p, the P wave attenuation, in

dB/m/kHz. The values of k_p were computed from the actual imaginary part of the wave number, including corrections due to grazing angle. For this study the sediment thickness is H = 80 m. The values of k_p above 5 attenuate the P wave by more than 6 dB in a distance H. This effectively eliminates all but the first ray returning from the sediment to the water in Figs. 1 through 3. The ray path model then predicts the exponential dependence given above. The lines are again "eyeball" fits to the calculated magnitudes. The slopes of the lines are 0.059 for A_2, 0.123 for A_1, and 0.133 for ΔA_o. The A_1 and A_o slopes are approximately equal and are nearly double the slope of the A_2 wave in agreement with the ray model. The values of the slopes also agree well with the predicted values of 0.056 and 0.112.

The ray path model strictly predicts no important S wave effects if the sediment P wave speed is larger than the sound speed in water. The incoming wave in the water is specularly reflected with only order ϵ^2 corrections. The computational model, based on wave theory, allows the penetration of the P wave into the sediment where it becomes evanescent and decays exponentially. Generalizing the ray path model prediction for the case of P wave attenuation to the case of the evanescent P wave, one obtains the same predictions with k_{ip}, now given by

$$k_{ip} = 2\pi f \left[(c_2 \cos\theta / c_1)^2 - 1 \right]^{1/2} / c_2 \quad .$$

Since this exponential decay constant is proportional to frequency, it can be written in terms of a frequency independent decay constant, k'_p, in units of dB/m/kHz, i.e., $k_{ip} = k'_p f/8686$.

Figure 10 shows the dependence of ΔA_o, A_1, and A_2 on k_p'. For this study H = 100 m. For k_p'=8 the P wave amplitude decays by about 11 dB in a distance H. The parameter actually varied in this case was the P wave velocity in the sediment. The lines are "eyeball" fits to the calculated magnitudes. The measured slopes are: 0.162 for ΔA_o, 0.162 for A_1, and 0.072 for A_2. The slope of the A_2 line is approximately half that of the slopes of the ΔA_o and A_1 lines in agreement with the ray path model predictions. The magnitude of the slopes also agrees well with the predicted values of 0.070 and 0.140.

The qualitative effects of a gradient in shear speed can be deduced from Figs. 1 through 3. The gradient causes ε_L to be larger than ε_u, and Figs. 1 and 3 show that the larger ε_L increases the effect of sediment rigidity on the A_o and A_1 waves. Since these two waves dominate the structure of the reflection loss, the increase in RL due to sediment rigidity will be larger in layers with a shear speed gradient than in a homogeneous layer. Figure 2 shows that a larger ε_L also increases the $\varepsilon_u\varepsilon_L$ part of the A_2 wave, making it possible for the shear speed at the W-S interface to slightly influence RL; this would occur at low frequencies where the interference of the A_2 wave with the A_o and A_1 waves is important.

The use of the actual reflection and transmission coefficients given above could be used to develop a quantitative ray path model. The procedure would be analogous to the local plane wave approach used recently[7] to develop a quantitative ray path model of fluid sediments.

VI. MECHANISM FOR SHEAR WAVE EXCITATION IN DEEP SEA SEDIMENTS

Compressional wave conversion at the sediment-substrate interface has been proposed as the major mechanism for shear wave excitation in a typical deep sea sediment.[1] The expansion theory of the reflection and transmission coefficients and the ray path model developed here support this conclusion. The generality of the assumptions of the expansion theory and ray path analysis shows that this mechanism in fact applies to a large class of marine sediments. The only restrictions are that the sediment be a single, inhomogeneous layer and that gradient-driven P-S coupling be negligible. For layered rather than continuous sediment structures, additional conversion at interfaces within the sediment may also be important. For sand type sediments, important in shallow water continental shelf environments, the large near-surface gradients[4,8] may make the gradient-driven P-S coupling near the water-sediment interface an important additional mechanism at low frequencies.[9] For typical deep sea sediments, the gradient-driven P-S conversion is probably negligible above about 3 Hz.[3]

For typical deep sea sediment types, the mechanism for sediment S wave excitation to lowest order in ε can be deduced from the combined action of the reflection and transmission coefficients. As far as P waves are concerned the sediment is a fluid at the water-sediment interface, and negligible energy is transferred into S waves. An order ε S wave is excited in the sediment by the P wave striking the sediment-substrate interface. This sediment S wave has no further effect; it is essentially perfectly reflected from the water-sediment and sediment-substrate interfaces and produces, at most, order ε^2 corrections to the P wave returned

to the water column. The P wave reflected from the sediment-substrate interface does, however, have an important role to play; its amplitude picks up an order ϵ correction at the sediment-substrate interface. This correction travels through the water-sediment interface and affects the energy returned to the water.

The following picture emerges. Sediment rigidity affects bottom reflection loss by means of energy transferred to sediment shear waves at the sediment-substrate interface. Sediment compressional waves play a major role; they excite the shear wave at the sediment-substrate interface and are responsible for carrying the influence of the shear wave back through the sediment and into the water. The major effect of sediment rigidity is then to provide an energy sink at the sediment-substrate interface.

The empirical classification of sediments into thick and thin categories based on the effect of sediment shear waves can now be understood and quantified. For a thick sediment layer, the P wave has its turning point well above the sediment-substrate interface and it does not significantly interact with the sediment-substrate interface. Since only order ϵ^2 corrections are possible due to the refracted P waves at the water-sediment interface, sediment rigidity has a negligible effect on bottom reflection loss. In this case the sediment can be accurately treated as a fluid. For a thin sediment layer, the P wave interacts significantly with the sediment-substrate interface where sediment S waves are excited, and the sediment must be treated as a solid. Whether a sediment layer is thick or thin is then translated into the more easily quantified question of whether the P wave interacts with the sediment-

substrate interface (thick) or not (thin). The answer to this question depends on frequency (through P wave attenuation) and grazing angle (because of P wave evanescence).

An additional important conclusion of this paper is that sediment rigidity can be neglected at the water-sediment interface. The ray model predicts that the lowest order effects depending on the S wave velocity at the water-sediment interface are contained in the ε_u^2 and $\varepsilon_u \varepsilon_L$ waves seen in Fig. 2. Since $\varepsilon \sim 0.1$ these are small corrections compared to the ε_L corrections seen in Figs. 1 and 3 due to P wave conversion at the sediment-substrate interface.

The mechanism for sediment S wave excitation also leads to a generalization of the "hidden depths" concept[10] of fluid sediment theory. According to this concept there is a depth below which the subbottom structure has a negligible effect on the acoustic field in the water. This depth is essentially a few wavelengths below the turning point of the P wave in the subbottom. Below this turning point the P wave decays exponentially. The acoustic energy interacting with the structure below the hidden depth is a very small fraction of the total energy. Hence, the structure below the hidden depth is acoustically negligible. Since sediment S waves originate principally by means of the sediment P wave interacting with the sediment-substrate interface, the hidden depth criterion also applies to sediment S wave effects. If the sediment-substrate interface is in the hidden depths, the P wave amplitude is negligible at the sediment-substrate interface and sediment S wave effects are negligible. For solid sediments, the structure in the hidden depths is still negligible and, in addition, if the substrate interface is in

the hidden depths, the effect of sediment S waves is also negligible and the sediment can be accurately treated as a fluid.

Figure 11 illustrates the relative insensitivity of R to the sediment S wave velocity at the water-sediment interface (v_{2u}) compared to that at the sediment-substrate interface (v_{2L}). Figures 11(a) and 11(b) use the computational model to follow the development of $|R|$ starting with a homogeneous layer having v_2 = 100 m/sec and ending with v_2 = 300 m/sec. To eliminate interference effects a high frequency (S wave heavily attenuated) was chosen. In Fig. 11(a) v_{2u} is constant while v_{2L} increases. A constant gradient is used which has the value of 5 sec^{-1} when v_{2L} = 300 m/sec. Three grazing angles are shown. The $|R|$ decreases almost linearly with v_{2L} at each grazing angle. The decrease is significant, 30% at θ=30° and 50% at θ=10°. Figure 11(b) shows the additional change in $|R|$ which occurs when v_{2L} is held constant at 300 m/sec, v_{2U} is increased to form a homogeneous layer, and with v_2 = 300 m/sec. As expected, the factor of 3 increase in v_{2L} now produces only small changes in $|R|$ compared to those produced by changing v_{2L}. This result reinforces the conclusion that RL is relatively insensitive to the surficial S wave velocity. In fact, fairly accurate values of $|R|$ can be obtained at high frequencies by ignoring the S wave velocity gradient and assuming a homogeneous layer with v_2 given by the S wave velocity at the sediment-substrate interface. For the same gradients used in Fig. 11(a), the error in $|R|$ is less than 12% over the entire range of gradients and for grazing angles less than

50°. This leads to the conclusion that v_{2L} is the important S wave parameter at high frequencies.

VI. SUMMARY

A theoretical treatment of the reflection and transmission coefficients at the water and substrate interfaces, using an expansion in the small sediment S wave velocity, provides a basis for developing a ray model of the effect of sediment rigidity on bottom reflection loss. The basic mechanism for S wave excitation emerges as P wave conversion at the sediment-substrate interface. The dependence of RL on S wave velocity and attenuation, and P wave attenuation, are predicted by the ray model and verified in detail by results obtained from a computational model. The bottom reflection loss is found to be due to the interference of three waves: the A_o wave, similar to that generated by a fluid sediment, the A_1 wave, whose amplitude depends on the S wave velocity to the first power, and the A_2 wave, whose amplitude depends on the S wave velocity to the second power.

ACKNOWLEDGMENTS

The author has greatly benefited from numerous discussions with K. E. Hawker, S. R. Rutherford, T. L. Foreman, and E. L. Hamilton. This work was supported by Naval Ocean Research and Development Activity and Naval Electronic Systems Command.

APPENDIX

The procedure for calculating the reflection and transmission coefficients to any order in ε is illustrated in this appendix. The results obtained for a P wave incident upon the S-S interface will be used as an example. (The notation of section II is used.)

The continuity of the horizontal and normal components of displacement and the normal and shear stress can be written in matrix form as

$$\underline{\underline{M}}\underline{x} = \underline{y} \quad , \tag{A-1}$$

where $\underline{x}=\left(W_2^+,\ W_3^-,\ V_2^+,\ V_3^-\right)^T$ contains the reflected and transmitted potential amplitude; $\underline{y}=\left[-\rho_2\left(1-2a_2^2\right),-\kappa_2,2\rho_2 a_2^2\kappa_2/k,-k/\beta_2\right]^T$, the stress-displacement vector due to the incident unity amplitude P wave; and

$$\underline{\underline{M}} = \begin{pmatrix} \rho_2\left(1-2a_2^2\right) & -\rho_3\left(1-2a_3^2\right) & 2\rho_2 a_2^2\beta_2/k & 2\rho_3 a_3^2\beta_3/k \\ -\kappa_2 & -\kappa_3 & k & -k \\ 2\rho_2 a_2^2\kappa_2/k & 2\rho_3 a_3^2\kappa_3/k & \rho_2\left(1-2a_2^2\right) & -\rho_3\left(1-2a_3^2\right) \\ k/\beta_2 & -k/\beta_2 & 1 & \beta_3/\beta_2 \end{pmatrix} , \tag{A-2}$$

in which $a_j=(v_j/c_1)\cos\theta$. The superscript T denotes the transpose of the row vector. The quantities β_2 and a_2 in $\underline{\underline{M}}$ and $\underline{y}$ contain the expansion parameter $\varepsilon=v_2/c_1$. The rows of $\underline{\underline{M}}$ correspond to the normal stress, normal displacement, shear stress, and horizontal displacement, respectively.

The vectors $\underline{x}$ and $\underline{y}$ and the Matrix $\underline{\underline{M}}$ are now expressed as a series in ε as

$$\underline{x} = \underline{x}_o + \varepsilon\underline{x}_1 + \varepsilon^2\underline{x}_2 + \ldots + \quad , \tag{A-3}$$

$$\underline{y} = \underline{y}_o + \varepsilon\underline{y}_1 + \varepsilon^2\underline{y}_2 + \ldots + \quad , \tag{A-4}$$

$$\underline{\underline{M}} = \underline{\underline{M}}_o + \varepsilon\underline{\underline{M}}_1 + \varepsilon^2\underline{\underline{M}}_2 + \ldots + \quad , \tag{A-5}$$

Substituting Eqs. (A-3)-(A-5) into Eq. (A-1) and equating quantities of the same order in ε yields a sequence of equations;

$$\underline{\underline{M}}_o\underline{x}_o = \underline{y}_o \quad , \tag{A-6}$$

$$\underline{\underline{M}}_o\underline{x}_1 = \underline{y}_1 - \underline{\underline{M}}_1\underline{x}_o \quad , \tag{A-7}$$

$$\underline{\underline{M}}_o\underline{x}_2 = \underline{y}_2 - \underline{\underline{M}}_2\underline{x}_o - \underline{\underline{M}}_1\underline{x}_1 \quad . \tag{A-8}$$

These equations can be solved in sequence: Eq. (A-6) yields $\underline{x}_o$, Eq. (A-7) and $\underline{x}_o$ yield $\underline{x}_1$, Eq. (A-8) along with $\underline{x}_o$ and $\underline{x}_1$ yields $\underline{x}_2$. The quantities in $\underline{\underline{M}}$ and $\underline{y}$ that depend on ε are $a_2=\varepsilon\cos\theta$, and $k/\beta_2=\varepsilon\cos\theta-\varepsilon^3\cos^3\theta/2+\ldots+$. The quantities in Eqs. (A-6)-(A-8) are then:

$$\underline{\underline{M}}_o = \begin{pmatrix} \rho_2 & -\rho_3(1+a_3^2) & 0 & -2\rho_3 a_3^2\beta_3/k \\ -\kappa_2 & -\kappa_2 & k & -k \\ 0 & 2\rho_3 a_3^2\kappa_3/k & \rho_2 & -\rho_3(1-a_3^2) \\ 0 & 0 & 1 & 0 \end{pmatrix} , \tag{A-9}$$

$$\underline{y}_o = (-\rho_2, -\kappa_2, 0, 0)^T \quad . \tag{A-10}$$

$$\underline{\underline{M}}_1 = \cos\theta \begin{pmatrix} 0 & 0 & -2\rho_2 & 0 \\ 0 & 0 & 0 & 0 \\ 0 & 0 & 0 & 0 \\ 1 & -1 & 0 & \beta_3/k \end{pmatrix} . \tag{A-11}$$

$$y_1 = -\cos\theta(0,\ 0,\ 0,\ 1)^T \quad . \tag{A-12}$$

$$\underline{\underline{M}}_2 = -2\rho_2\cos^2\theta \begin{pmatrix} 1 & 0 & 0 & 0 \\ 0 & 0 & 0 & 0 \\ -\kappa_2/k & 0 & 1 & 0 \\ 0 & 0 & 0 & 0 \end{pmatrix} \quad . \tag{A-13}$$

$$y_2 = 2\rho_2\cos^2\theta(1,\ 0,\ \kappa_2/k,\ 0)^T \quad . \tag{A-14}$$

The solution of Eqs. (A-6)-(A-8) using Eqs. (A-9)-(A-14) is straightforward and yields Eqs. (4)-(7) in section II. The process can be continued to any order in ε.

REFERENCES

[1]P. J. Vidmar, "The effect of sediment rigidity on bottom reflection loss in typical deep-sea sediments," submitted for publication in The Journal of the Acoustical Society of America.

[2]G. J. Fryer, "Reflectivity of the ocean bottom at low frequency," J. Acoust. Soc. Am. 63, 35-42 (1978).

[3]P. J. Vidmar and T. L. Foreman, "A plane-wave reflection loss model including sediment rigidity," J. Acoust. Soc. Am. 66, 1830-1835 (1979).

[4]E. L. Hamilton, "Shear-wave velocity versus depth in marine sediments: a review," Geophys. 41, 985-996 (1976).

[5]L. M. Brekhovskikh, Waves in Layered Media, (Academic Press, New York, 1960).

[6]Our z axis increases downward while that in Ref. 5 increases upward. This results in the difference in sign between our Eq. (19) and the result in Ref. 5.

[7]S. K. Mitchell and J. J. Lemmon,"A ray theory model of acoustic interaction with the ocean bottom," J. Acoust. Soc. Am. 66, 855-861 (1979).

[8]E. L. Hamilton, "Sound velocity gradients in marine sediments," J. Acoust. Soc. Am. 65, 909-922 (1979).

[9]P. G. Richards, "Weakly coupled potentials for high-frequency elastic waves in continuously stratified media," Bull. Seismol. Soc. Am. 64, 1575-1588 (1974).

[10]A. O. Williams, Jr., "Hidden depths: acceptable ignorance about ocean bottoms," J. Acoust. Soc. Am. 59, 1175-1179 (1976).

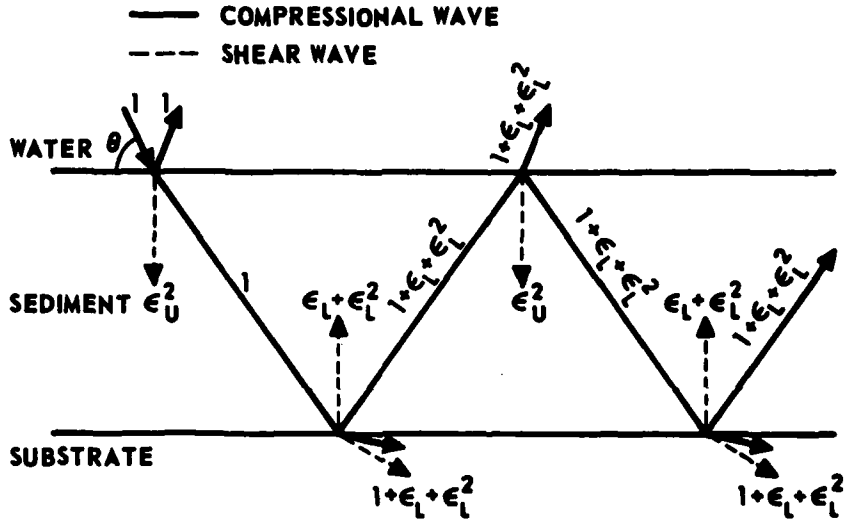

FIGURE 1
RAY PATHS EXCITED WHEN THE SEDIMENT SHEAR WAVE
IS ABSORBED BEFORE REFLECTION

ARL:UT
AS-79-1816-P
PJV- GA
8- 17- 79

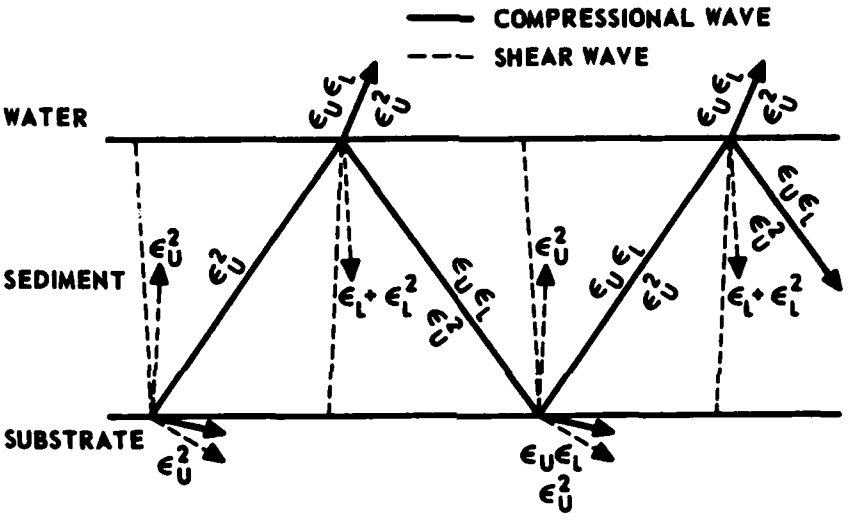

FIGURE 2
ADDITIONAL RAY PATHS DUE TO THE FIRST REFLECTION
OF THE SEDIMENT SHEAR WAVES

ARL:UT
AS-79-1817-P
PJV- GA
8-17-79

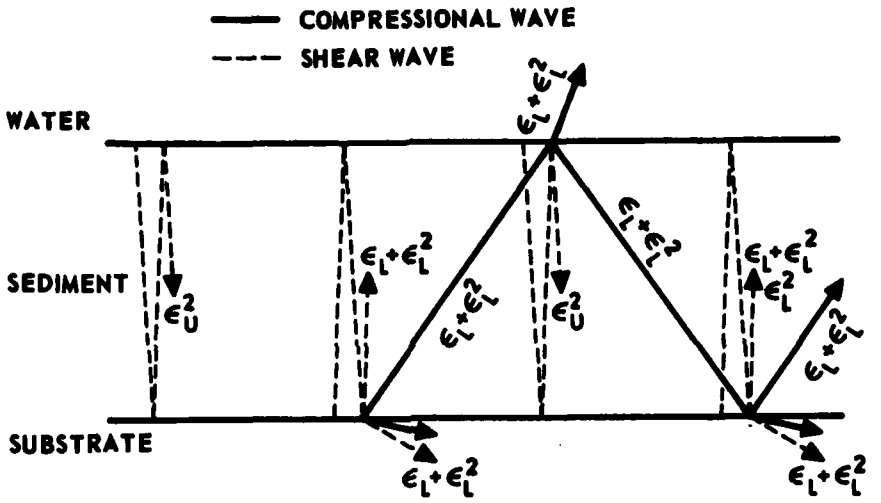

FIGURE 3
ADDITIONAL RAY PATHS DUE TO THE SECOND REFLECTION
OF THE SEDIMENT SHEAR WAVES

ARL:UT
AS-79-1818-P
PJV-GA
8-17-79

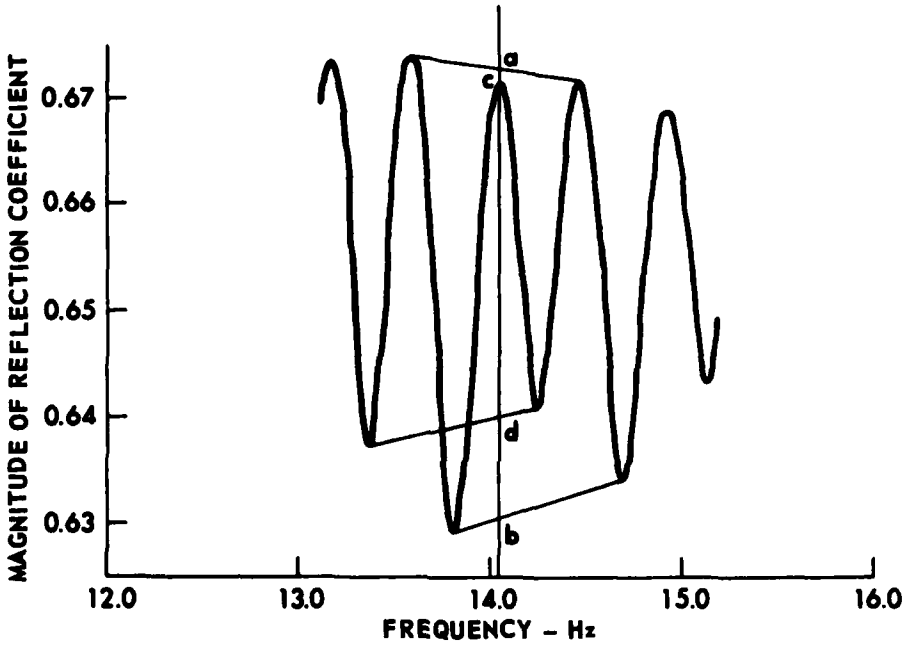

FIGURE 4
EXAMPLE OF THE DEPENDENCE OF THE MAGNITUDE
OF THE REFLECTION COEFFICIENT ON FREQUENCY

ARL:UT
AS-79-1819-P
PJV - GA
8-17-79

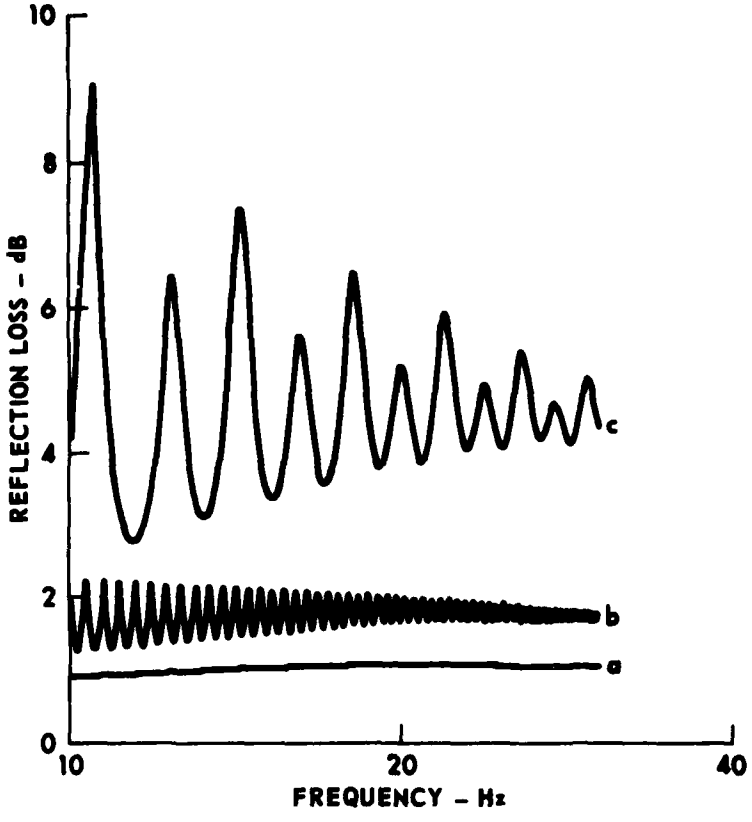

FIGURE 5
REFLECTION LOSS versus FREQUENCY FOR A 40 m THICK HOMOGENEOUS LAYER WITH SEDIMENT SHEAR SPEED AS A PARAMETER
FOR CURVE (a) v_2 = 0 m/sec; (b) v_2 = 30 m/sec; (c) v_2 = 150 m/sec

ARL:UT
AS-79-1820-P
PJV - GA
8 - 17 - 79

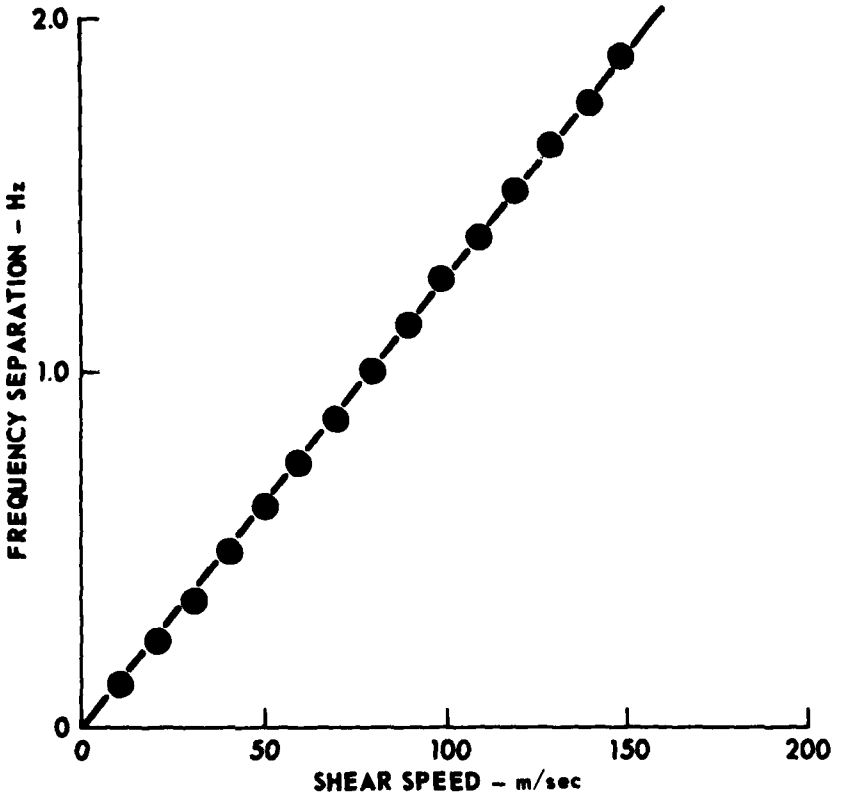

FIGURE 6
THE DEPENDENCE OF THE FREQUENCY INTERVAL BETWEEN THE ADJACENT MAXIMA OF RL ON SEDIMENT SHEAR SPEED

ARL:UT
AS-79-1821-P
PJV-GA
8-17-79

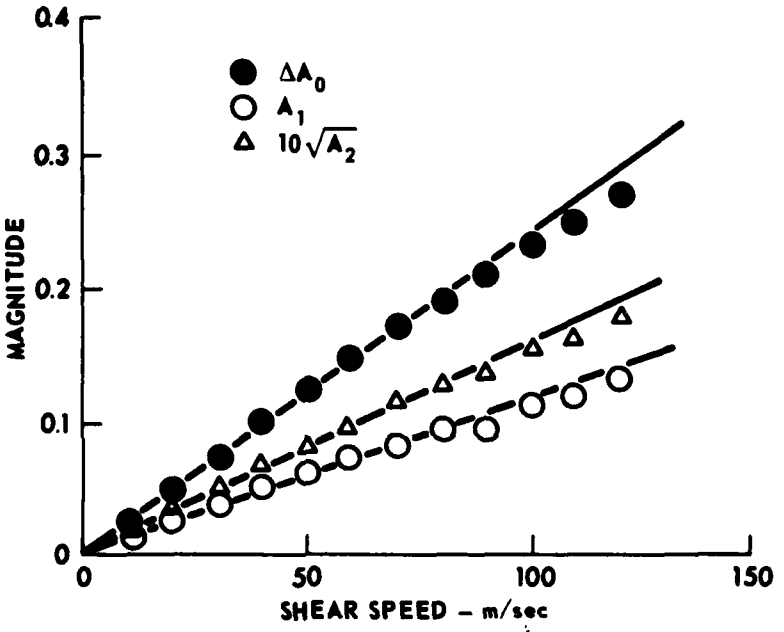

FIGURE 7
THE DEPENDENCE OF THE MAGNITUDES OF ΔA_0, A_1, AND A_2 ON SEDIMENT SHEAR SPEED

ARL:UT
AS-79-1822-P
PJV- GA
8-17-79

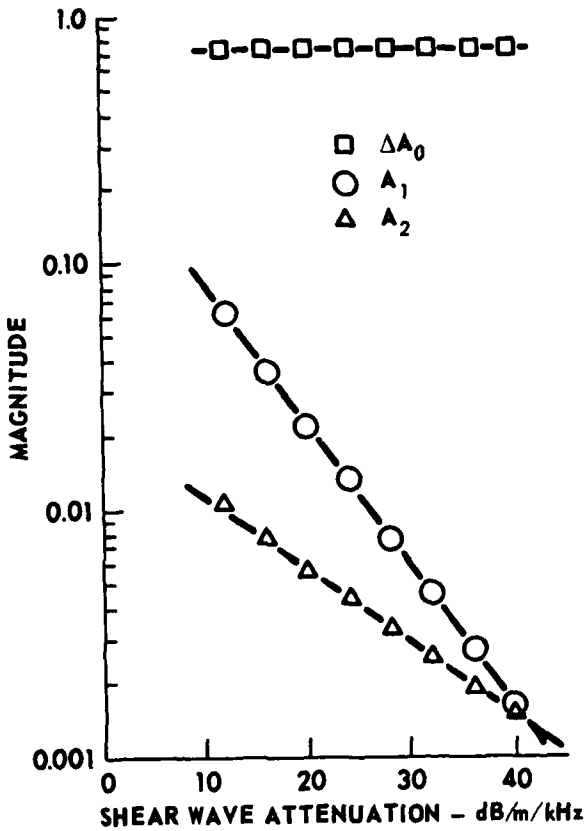

FIGURE 8
THE DEPENDENCE OF THE MAGNITUDES OF ΔA_0, A_1, AND A_2 ON THE ATTENUATION COEFFICIENT OF THE SEDIMENT SHEAR WAVE, k_s

ARL:UT
AS-79-1823-P
PJV - GA
8 - 17 - 79

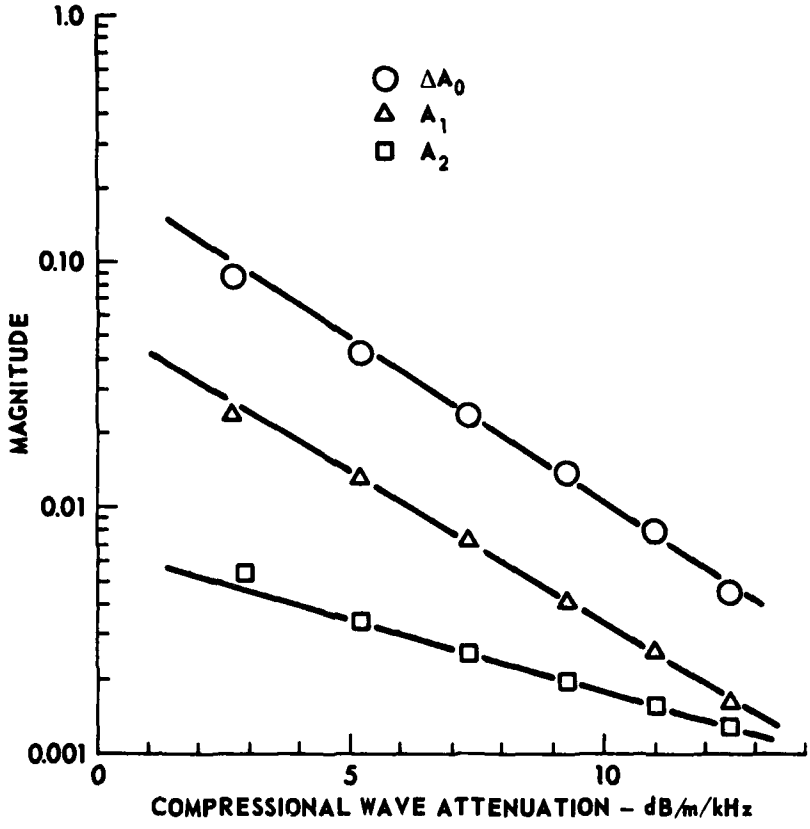

FIGURE 9
THE DEPENDENCE OF THE MAGNITUDES OF ΔA_0, A_1, AND A_2 ON THE ATTENUATION COEFFICIENT OF THE SEDIMENT COMPRESSIONAL WAVE, k_p

ARL:UT
AS-79-1824-P
PJV - GA
8 - 17 - 79

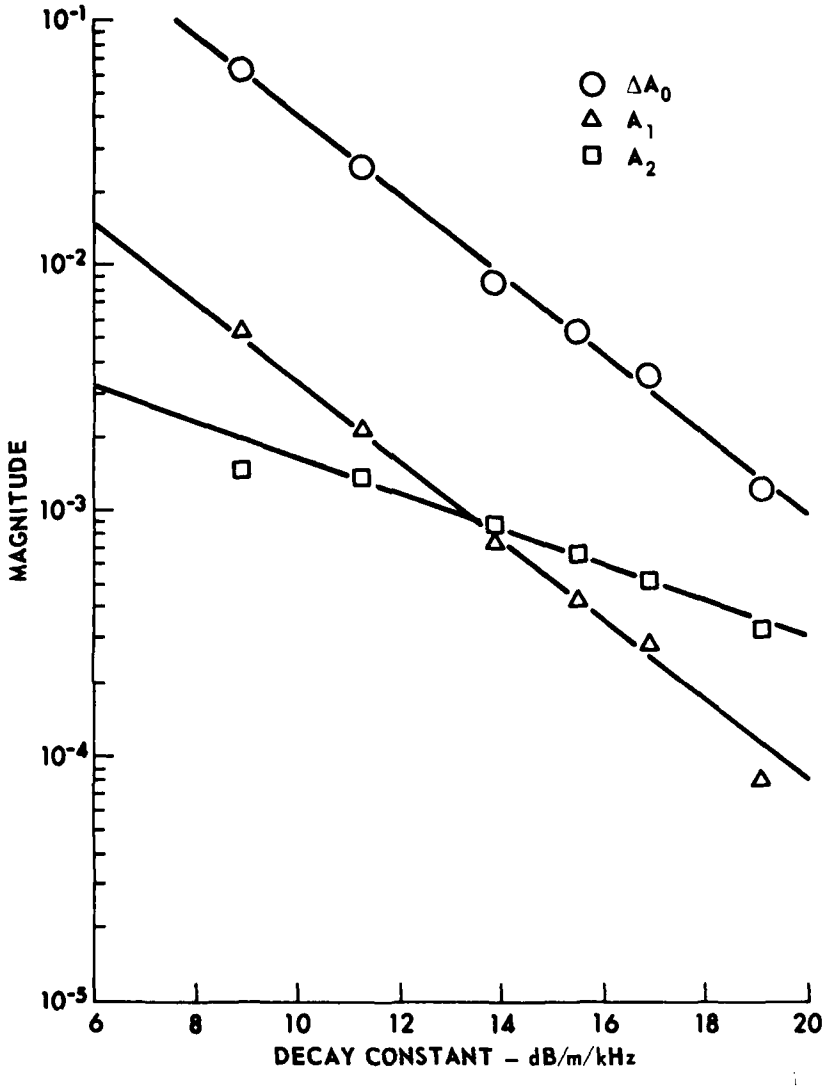

FIGURE 10
THE DEPENDENCE OF THE MAGNITUDES OF ΔA_0, A_1, AND A_2 ON THE DECAY CONSTANT OF THE EVANESCENT SEDIMENT COMPRESSIONAL WAVE, k_p'

ARL:UT
AS-79-1825-P
PJV - GA
8 - 17 - 79

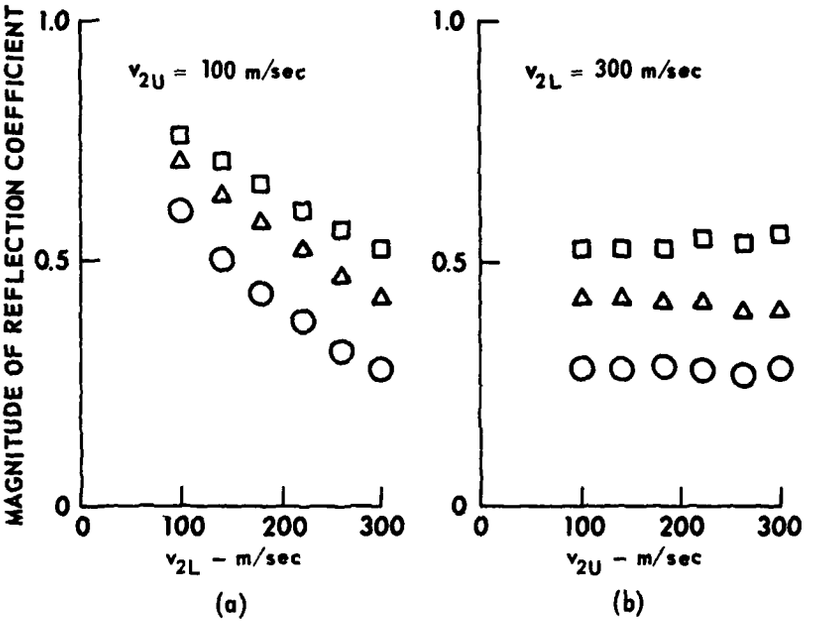

FIGURE 11

THE DEPENDENCE OF THE MAGNITUDE OF THE REFLECTION COEFFICIENT ON THE SEDIMENT SHEAR WAVE SPEED AT INTERFACES FOR GRAZING ANGLES OF 10° (CIRCLES), 20° (TRIANGLES), AND 30° (SQUARES)

(a) v_{2u} CONSTANT, (b) v_{2L} CONSTANT

ARL:UT
AS-79-1826-P
PJV - GA
8 - 17 - 79

19 February 1980

DISTRIBUTION LIST FOR

ARL-TR-80-6

UNDER CONTRACT N00014-78-C-0113

Copy No.	
	Commanding Officer Naval Ocean Research and Development Activity NSTL Station, MS 39529
1	Attn: CDR J. Paquin (Code 500)
2	J. Matthews (Code 360)
3	G. Morris (Code 340)
4	Office of Naval Research Branch Office Chicago Department of the Navy 536 South Clark Street Chicago, IL 60605
5	Commanding Officer Naval Electronic Systems Command Washington, DC 20360 Attn: J. Sinsky (Code 320)
	Commanding Officer Naval Ocean Systems Center Department of the Navy San Diego, CA 92152
6 - 7	Attn: E. L. Hamilton
8	H. P. Bucker
9	Chief of Naval Operations Department of the Navy Washington, DC 20350 Attn: R. S. Winokur (OP952D9)
10	Chief of Naval Material Department of the Navy Washington, DC 20360 Attn: CAPT E. Young (Code 08T24)
11 - 22	Commanding Officer and Director Defense Technical Information Center Cameron Station, Building 5 5010 Duke Street Alexandria, VA 22314

Dist. List for ARL-TR-80-6 under Contract N00014-79-C-0113, Cont'd

Copy No.	
23	Science Applications, Inc. 8400 Westpark Drive McLean, VA 22101 Attn: C. Spofford
24	Office of Naval Research Resident Representative Room No. 582, Federal Bldg. Austin, TX 78701
25	Glen E. Ellis, ARL:UT
26	Loyd Hampton, ARL:UT
27	Kenneth E. Hawker, ARL:UT
28	Stephen K. Mitchell, ARL:UT
29	Clark S. Penrod, ARL:UT
30	Paul J. Vidmar, ARL:UT
31	Reuben H. Wallace, ARL:UT
32	Library, ARL:UT
33 - 37	Reserve, ARL:UT